

Characterization of aberrant mTOR signaling pathway in U87MG glioblastoma cell line
by quantitative phosphoproteomics



A Dissertation Submitted in Partial Fulfillment of the Requirements
for the Degree of Doctor of Philosophy in Biomedical Sciences

Inter-Department of Biomedical Sciences

GRADUATE SCHOOL

Chulalongkorn University

Academic Year 2021

Copyright of Chulalongkorn University

การศึกษาฟอสโฟโปรตีนไอมิกส์เชิงปริมาณต่อความผิดปกติของวิถีสัญญาณ mTOR ในเซลล์มะเร็ง
สมองเพาะเลี้ยง U87MG glioblastoma



วิทยานิพนธ์นี้เป็นส่วนหนึ่งของการศึกษาตามหลักสูตรปริญญาวิทยาศาสตรดุษฎีบัณฑิต
สาขาวิชาชีวเวชศาสตร์ (สหสาขาวิชา) สหสาขาวิชาชีวเวชศาสตร์
บัณฑิตวิทยาลัย จุฬาลงกรณ์มหาวิทยาลัย
ปีการศึกษา 2564
ลิขสิทธิ์ของจุฬาลงกรณ์มหาวิทยาลัย

นัฐธิญา กาลพงษ์นุกุล : การศึกษาฟอสโฟโปรตีนไอมิกส์เชิงปริมาณต่อความผิดปกติของวิถีสัญญาณ mTOR ในเซลล์มะเร็งสมองเพาะเลี้ยง U87MG glioblastoma. (Characterization of aberrant mTOR signaling pathway in U87MG glioblastoma cell line by quantitative phosphoproteomics) อ.ที่ปรึกษาหลัก : อ. ดร.นพต จันทรวินุต

Glioblastoma multiforme หรือ Glioblastoma (GBM) เป็นมะเร็งสมองที่เกิดจากเซลล์เกลีย (Glia cell) เช่น astrocytes oligodendrocytes และ ependymal cells ของระบบประสาทที่มีความรุนแรงและตรวจพบได้ยาก โดยมะเร็งสมองชนิด GBM นี้เกี่ยวข้องกับความผิดปกติของวิถีสัญญาณ mTOR ซึ่งมีกลุ่มโปรตีน mTOR ทำหน้าที่เป็นเอนไซม์ kinase แบ่งออกเป็น 2 กลุ่มหลัก คือ mTOR complex 1 (mTORC1) และ mTOR complex 2 (mTORC2) โดยมีบทบาทในการควบคุมกิจกรรมต่างๆในเซลล์ เช่น การเจริญเติบโตและการอยู่รอดของเซลล์ การเคลื่อนที่และการแพร่กระจาย การเกิด actin cytoskeleton reorganization และกาตอบสนองต่อความผิดปกติของดีเอ็นเอ แต่อย่างไรก็ตามหน้าที่ของ mTORC2 ยังไม่ทราบแน่ชัด การศึกษาที่สนใจศึกษาความผิดปกติของวิถีสัญญาณ mTORC2 ในเซลล์มะเร็งสมองชนิด GBM โดยใช้เทคนิคติดฉลากด้วย dimethyl isotope และการเพิ่มปริมาณฟอสโฟเปปไทด์ด้วย TiO_2 ร่วมกับการวิเคราะห์ฟอสโฟเปปไทด์ทั้งหมดด้วยเทคนิคแมสสเปคโตรเมทรี (LCMS/MS) เพื่อวิเคราะห์ฟอสโฟเปปไทด์ทั้งหมดเชิงปริมาณ ที่ถูกทดสอบด้วยยา AZD8055 ที่ยับยั้ง mTORC1/2 และยา Rapamycin ที่ยับยั้ง mTORC1 โดยทำการเปรียบเทียบระดับของเปปไทด์ที่ถูกเติมฟอสเฟตแล้วลดระดับลงเมื่อได้รับเฉพาะยา AZD8055 พบว่ามีจำนวนฟอสโฟโปรตีนจำนวนมากที่สัมพันธ์กับ mTORC2 จึงได้ศึกษาถึงบทบาทหน้าที่ของฟอสโฟโปรตีนกลุ่มนี้ พบว่า การยับยั้ง mTORC2 อาจเกี่ยวข้องกับ การซ่อมแซมดีเอ็นเอ (double-strand break) และจึงศึกษาต่อถึงลักษณะของความสัมพันธ์ระหว่าง mTORC2 และ BABAM1 หรือ MERIT40 ซึ่งเป็นโปรตีนที่มีความสำคัญต่อการซ่อมแซมดีเอ็นเอที่ถูกทำลาย (DNA damage repair) พบว่า การเกิดฟอสโฟรีเลชันของ BABAM1 ที่ตำแหน่งกรดอะมิโน ser29 ถูกควบคุมด้วย mTORC2 ทำให้เกิดการกระตุ้นการตอบสนองของการทำลายดีเอ็นเอ (DNA damage response) ส่งผลให้มีการซ่อมแซมดีเอ็นเอ และเพิ่มความอยู่รอดของเซลล์มะเร็ง ดังนั้นการยับยั้งการกระตุ้นของ mTORC2 ทำให้ฟอสโฟรีเลชันที่ ser29 ของ BABAM1 ลดลงอย่างมีนัยสำคัญ ส่งผลให้เกิดการซ่อมดีเอ็นเอในนิวเคลียสลดลง นำไปสู่กระตุ้นให้เกิดการตายของเซลล์มะเร็ง (Apoptosis) นอกจากนี้ผู้วิจัยยังพบว่าการเกิดฟอสโฟรีเลชันของ γ H2AX ที่ตำแหน่ง ser139 เกี่ยวข้องกับ mTORC2 และ BABAM1 ด้วยเช่นกัน การศึกษาวิจัยนี้จึงทำให้เข้าใจหน้าที่ของ mTORC2 ต่อการตอบสนองต่อการทำลาย DNA ในเซลล์มะเร็งมากยิ่งขึ้น และอาจนำไปสู่การพัฒนาการรักษาด้วยยา mTORC2 แบบจำเพาะในการรักษาผู้ป่วยมะเร็งสมอง

สาขาวิชา ชีวเวชศาสตร์ (สหสาขาวิชา)

ลายมือชื่อนิสิต

ปีการศึกษา 2564

ลายมือชื่อ อ.ที่ปรึกษาหลัก

6087775820 : MAJOR BIOMEDICAL SCIENCES

KEYWORD: Phosphoproteomics, Glioblastoma, GBM, DNA damage, mTORC2, BABAM1

Nuttiya Kalpongkukul : Characterization of aberrant mTOR signaling pathway in U87MG glioblastoma cell line by quantitative phosphoproteomics. Advisor: Naphat Chantaravisoot, Ph.D.

Glioblastoma (GBM) is one of the most damaging primary brain tumors with a poor prognosis. GBM is associated with an abnormality of the mTOR signaling pathway, consisting of two distinct kinase complexes: mTORC1 and mTORC2. The protein complexes play critical roles in cellular metabolism, proliferation, cell survival, cell migration through the cytoskeletal organization, and DNA damage response in cancers. Nevertheless, the functions of mTORC2 are less unraveled. This study investigated the aberrant mTORC2 signaling pathway in glioblastoma cells using stable isotope labeling, phosphopeptide enrichment, and LC-MS/MS. We performed the quantitative phosphoproteomic analysis of U87MG grade IV glioma cells treated with the mTORC1/2 inhibitor AZD8055 and the mTORC1 inhibitor rapamycin. By comparing the level of phosphorylated peptides decreased when cells were treated by AZD8055 but not rapamycin, numerous phosphoproteins were identified as mTORC2 downstream target candidates. Interestingly, a functional analysis of phosphoproteome revealed that mTORC2 inhibition might be involved in double-strand break (DSB) repair. We further characterized the relationship between mTORC2 and BABAM1 (also known as MERIT40), a protein with an essential role in DNA damage repair. We demonstrated that pBABAM1 at Ser29 is one of the phosphorylation sites regulated by mTORC2. This phosphorylation event has been shown to promote DNA damage response, which contributes to DNA repair and cancer cell survival. Accordingly, the inactivation of mTORC2 significantly ablated pBABAM1 (Ser29), reduced DNA repair activities in the nucleus, and promoted apoptosis of the cancer cells. Furthermore, we also recognized and showed that γ H2AX phosphorylation at Ser139 could potentially be downstream of mTORC2 in association with BABAM1 to repair the double-strand breaks. This investigation provided a better understanding of mTORC2 function in oncogenic DNA damage response and might lead to the development of specific mTORC2 treatments for brain cancer patients in the future.

Field of Study: Biomedical Sciences

Student's Signature

Academic Year: 2021

Advisor's Signature

ACKNOWLEDGEMENTS

- The 100th Anniversary Chulalongkorn University for Doctoral Scholarship
- Ratchadapiseksompotch Funds, Faculty of Medicine, Chulalongkorn University, grant number RA62/075
- National Research Council of Thailand (NRCT)
- GRADUATE THESIS GRANT
- Interdisciplinary Program of Biomedical Sciences, Graduate School, Chulalongkorn University, Bangkok, Thailand.
- Center of Excellence in Systems Biology, Chulalongkorn University (CUSB)

Nuttiya Kalpongkul

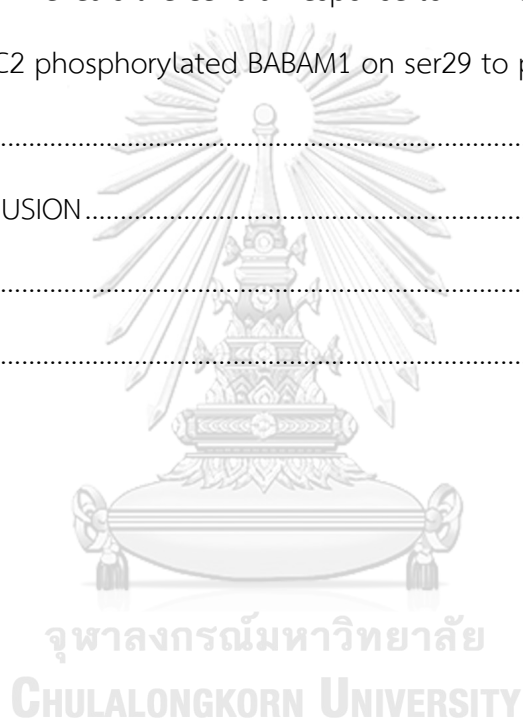


TABLE OF CONTENTS

	Page
ABSTRACT (THAI).....	iii
ABSTRACT (ENGLISH).....	iv
ACKNOWLEDGEMENTS.....	v
TABLE OF CONTENTS.....	vi
LIST OF TABLES.....	ix
LIST OF FIGURES.....	x
LIST OF ABBRIVATIONS.....	1
CHAPTER I INTRODUCTION.....	2
1.1 Rationale.....	2
1.2 Hypothesis.....	5
1.3 Research questions.....	5
1.4 Objectives.....	5
1.5 Expected outcomes.....	5
1.6 Conceptual framework.....	6
1.7 Work flow.....	7
CHAPTER II BACKGROUND AND LITERATURE REVIEWS.....	8
2.1 Background of Brain cancer.....	8
2.2 Glioblastoma multiforme (GBM).....	9
2.3 mTOR signaling pathway.....	11
2.4 mTOR in cancer.....	13
2.5 mTOR inhibitor drug with cancers.....	15

2.6 mTORC2 an essential role in DNA damage and repair.....	16
2.7 Quantitative Phosphoproteomics	18
CHAPTER III METHODOLOGY	21
3.1 Cell culture.....	21
3.2 Quantitative Phosphoproteome sample preparation	21
3.2.1 Protein Extraction and Tryptic Digestion.....	21
3.2.2 Dimethyl labeling.....	22
3.2.3 Phosphopeptide Enrichment.....	22
3.2.4 Peptide Fractionation.....	23
3.3 LC-MS/MS Analysis	24
3.4 Immunofluorescence analysis.....	25
3.5 Co-immunoprecipitation and immunoblotting.....	25
3.6 Cell viability assay.....	26
3.7 Apoptosis assay	26
3.8 <i>RICTOR</i> knockdown by siRNA and CRISPR-Cas9-mediated <i>RICTOR</i> knockdown stable cell line generation.....	26
3.9 <i>RICTOR</i> overexpression.....	27
3.10 Site-directed mutagenesis of BABAM1 (S29A mutation).....	27
CHAPTER IV RESULTS AND DISCUSSION	28
4.1 Results	28
4.1.1 The characteristics of quantitative proteomics	28
4.1.2 Development of phosphoproteomic techniques	30
4.1.3 Development of phosphopeptide fractionation	31

4.1.4 Quantitative phosphoproteome profiling by mTORC1 and mTORC1/2 and inhibitor.....	33
4.1.5 Functional analysis of phosphoproteome reveals phosphoprotein clustering related in mTOR signaling.	45
4.1.6 The potential targets in the mTORC2 signaling pathway.....	53
4.1.7 Effect of mTOR inhibitors on BABAM1 activity.....	60
4.1.8 mTORC2 reveals the cellular response to DNA damage.....	64
4.1.9 mTORC2 phosphorylated BABAM1 on ser29 to promotes DNA repair.....	71
4.2 Discussion.....	77
CHAPTER V CONCLUSION.....	80
REFERENCES	82
VITA.....	90



LIST OF TABLES

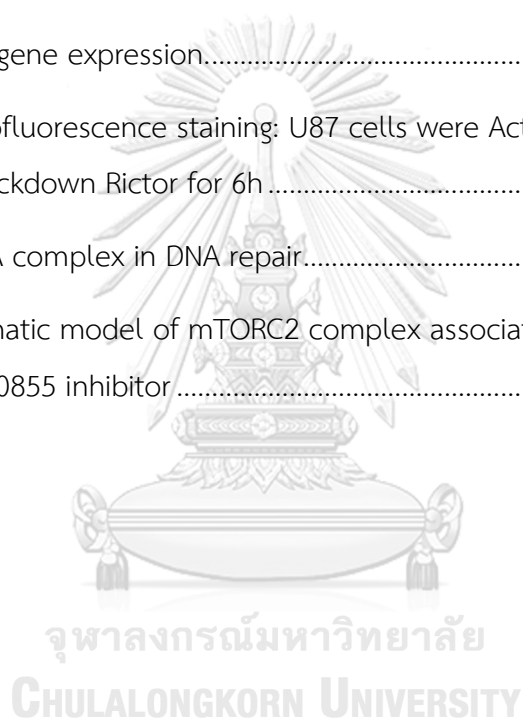
	Page
Table 1 The generation of mTOR inhibitor drug with cancers.....	16
Table 2 The characteristics of the protein ratio between Activated/Normal and Treated/Normal in mTOR signaling.....	29
Table 3 phosphopeptide enrichment efficiency	30
Table 4 The 3 set difference of phosphopeptide fractionation.....	32
Table 5 The Number of protein and peptide in 3 difference set.....	33
Table 6. Summary of the quantified phosphoproteome and proteome.....	34
Table 7 Characteristics of phosphorylation sites of AZD/ACT and.....	43
Table 8 Characteristics of phosphorylation sites of AZD/ACT and.....	45
Table 9 The upregulated phosphopeptides in AZD/ACT compared with downregulated RAP/ACT group (1h).....	49
Table 10 The upregulated phosphopeptides in AZD/ACT compared with downregulated RAP/ACT group (1h).....	50
Table 11 Characteristics of the 18 major phosphorylation sites in AZD8055 inhibition at 4 time points.....	58
Table 12 The associated proteins from BABAM1 IP to involved in DNA damage response and repair	73
Table 13 RICTOR gene sequence.....	75

LIST OF FIGURES

	Page
Figure 1 mTOR signaling pathway	11
Figure 2 Activation of mTOR signaling.....	12
Figure 3 mTOR complex1 (mTORC1) and mTOR complex 2 (mTORC2).....	13
Figure 4 Functions of mTORC2 and downstream targets.....	14
Figure 5 The effect of Rapamycin (RAP) inhibits the kinase activity of mTORC1.....	15
Figure 6 AKT promoted in homologous recombination repair (HRR) or non-homologous end-joining (NHEJ).....	17
Figure 7 mTOR and DNA damage repair response	18
Figure 8 The phosphopeptide enrichment technique	19
Figure 9 Summary of proteomic quantification	28
Figure 10 Volcano plot of Activated/Normal and Treated/Normal.....	30
Figure 11 Venn diagram of TiO2 compared with IMAC	31
Figure 12 The Number of peptides in each fraction.....	33
Figure 13 The number of proteins, phosphopeptides, and phosphosites.....	34
Figure 14 The phosphorylation site expression in the phosphoproteomic dataset ...	35
Figure 15 The overlap of phosphopeptides in.....	36
Figure 16 Phosphopeptides profiling in RAP/ ACT and AZD/ACT.....	37
Figure 17 The distributions of phosphopeptide ratio and p-value.....	38
Figure 18 The distributions of phosphopeptide ratio and p-value.....	39
Figure 19 The distributions of phosphopeptide ratio and p-value.....	40
Figure 20 The distributions of phosphopeptide ratio and p-value.....	41

Figure 21 Upstream and downstream target of mTOR signaling pathway	42
Figure 22 the downregulated phosphopeptides in AZD/ACT group	46
Figure 23 The downregulated phosphopeptides in RAP/ACT group	47
Figure 24 The upregulated phosphopeptides in AZD/ACT group	51
Figure 25 the Classification of the functionally related phosphopeptides and phosphoprotein interactions involved in the mTOR pathway.....	52
Figure 26 The distributions of phosphosite ratio and p-value of AZD/ACT group and RAP/ACT group for 1h.....	54
Figure 27 Heatmap of log 2 ratio of phosphosites significant (p-value < 0.05).....	55
Figure 28 Average Log ₂ fold change of the phosphorylation sites in AZD8055 inhibition at 4 time points.	56
Figure 29 Functional annotations of more than 2 fold of downregulated AZD/ACT with upregulated Rap/ACT at 1 h and 24h.	59
Figure 30 The classification of phosphoprotein interactions	59
Figure 31 U87 cells were activated with 10% FBS, treated with 2 μ M AZD8055 and 0.1 μ M Rapamycin for 1, 6, 24 and 48 hours, respectively.....	61
Figure 32 RICTOR siRNA and RICTOR overexpression.....	62
Figure 33 The log ₂ fold change of pBABAM1 and The intensity of pBABAM1 and BABAM1.....	63
Figure 34 The percentage of Cell viability in different condition.....	64
Figure 35 The flow cytometry measurement of apoptosis in AZD 24h	65
Figure 36 Western blotting analysis of BABAM1 overexpression in U87MG cells	66
Figure 37 Cell viability of U87MG-overexpressing BABAM1	66
Figure 38 Percentages of early and late apoptotic cells in U87MG	67
Figure 39 The flow cytometry measurement of apoptosis in BABAM1	68

Figure 40 The co-localization of BABAM1, Rap80, and γ H2AX in serum activated and AZD8055 treatment for 1 and 24h.....	69
Figure 41 The co-localization of pBABAM1 (s29), BRCA1, and γ H2AX in serum activated and AZD8055 treatment	70
Figure 42 Co-immunoprecipitation of BABAM1	71
Figure 43 Co-immunoprecipitation of Rap80.....	74
Figure 44 Figure Vectors of stable RICTOR knockdown gene.....	75
Figure 45 RICTOR gene expression.....	76
Figure 46 Immunofluorescence staining: U87 cells were Activated with serum, 2 μ M AZD8055, and knockdown Rictor for 6h	76
Figure 47 BRCA1-A complex in DNA repair.....	78
Figure 48 A schematic model of mTORC2 complex associated with DNA damage response by AZD80855 inhibitor	79



LIST OF ABBRIVATIONS

GBM	glioblastoma multiforme
mTORC1	mechanistic target of rapamycin complex 1
mTORC2	mechanistic target of rapamycin complex 2
S6K1	ribosomal protein S6 kinase beta-1
4EBP1	eukaryotic initiation factor 4E-binding protein 1
AKT	RAC-alpha serine/threonine-protein kinase
PKC- α	protein kinase C alpha
BABAM1	BRISC and BRCA1-A complex member 1
RICTOR	Rapamycin-insensitive companion of mTOR
γ H2AX	Phosphorylation of the Ser-139 residue of the histone variant H2AX
DSBs	double-strand breaks
DDR	DNA damage response
Co-IP	Co-immunoprecipitation
LC-MS	liquid chromatography-mass spectrometry
PTMs	posttranslational modifications

CHAPTER I

INTRODUCTION

1.1 Rationale

Brain malignancy is one of the most deleterious cancers among all forms. Medical centers worldwide have raised the importance of brain tumor disease because the brain plays a central role in the homeostasis. The growth of brain tumors can cause patients to have a wide variety of painful and life-altering symptoms including weakness, difficulty in walking, dizziness, seizures, headaches, vomiting and blurry vision (1). Most of the brain cancers are highly invasive, and they can spread to other parts of the body beyond the brain. Nowadays cancers of the brain can happen both adults and children, and come in several different forms. The cause of these cancers has not yet been well understood, and functions at tumor sites within the brain itself also have not been known. These lead to limitations in early diagnosis and the successful therapies (2, 3).

Glioblastoma multiforme (GBM) formed from astrocytes, is the most dangerous and aggressive form of brain cancer. GBM patients typically have short life expectancy after diagnosis. More than two-thirds of adults diagnosed with glioblastoma will die within two years (4). Glioblastoma consists of 2 subtypes, which are primary glioblastoma and secondary glioblastoma, and both can affect patients of different ages and develop through different genetic pathways. The majority of cases (>90%) are primary glioblastomas that develop rapidly *de novo*, without clinical or histological evidence of a less malignant precursor lesion. Secondary glioblastomas develop through the progression from low-grade diffuse astrocytoma or anaplastic astrocytoma and manifest in younger patients. Glioblastoma spreads out and grows rapidly to the other parts of the brain. It exhibits a high rate of recurrence and poor prognosis due to the invasive nature of the tumor. As of now, there is still no specific cure for GBM. Furthermore, genetic, epigenetic, and microenvironmental cues can influence cellular programs and drive glioblastoma heterogeneity (5, 6).

Dysregulation of cellular signal transduction pathways, that allows cells to over proliferate and escapes regulating mechanisms, normally controls their survival and migration. Many signaling pathways, which control cell growth, cell division, cell death, and cell motility, can be distortions of wider signaling networks that lead to cancer progression. Mutations of oncogenes can cause hyperactivation of these signaling pathways, whereas inactivation of tumor suppressors eliminates critical negative regulators of signaling (7).

One of the most frequently altered pathways in human cancers is the mTOR signaling pathway. Abnormal mTOR signaling can produce various key characteristics of several types of tumor cells, including brain tumors. The mTOR protein is serine/threonine kinase that presents in two distinct complexes called mTOR complex 1(mTORC1) and mTOR complex 2 (mTORC2). While mTORC1 regulates cell growth and metabolic processes including proteins synthesis, lipids synthesis and autophagy, mTORC2 participates in the control of cytoskeleton reorganization, migration and invasion (8).

Aberrant mTOR plays an essential role in tumorigenesis and development. Overactivation of mTOR signaling is can lead to several key features such as cells growth, metastasis, and invasion of different types of cancer cells (9). In breast cancer, activating the mTORC1-SREBP pathway is a crucial mechanism through a motivated lipogenic program to promote abnormal growth and proliferation (10). Loss of critical ubiquitination residues in G β L leads to raised mTORC2 formation and down-regulation of mTORC1 expression (11). Similarly, hyperactivation of mTORC1-S6K signaling and decreases RNF168 expression connects cell growth signaling to genome stability control caused by the defeat of LKB1, resulting in defects in the DNA damage response (12).

The regulation and functions of mTORC1, its many upstream regulators, cellular functions, and the availability of Rapamycin as an inhibitor are well known, and this complex has been thoroughly investigated. On the other hand, mTORC2 may play an unexpectedly important role in carcinogenesis, tumor growth promotion, and chemotherapy resistance in glioblastoma cells (13). Multiple of study present that mTORC2 is a potential target for molecular therapeutics in GBM. The

mTOR inhibitor PP242 effectively targets both mTORC1 and mTORC2 activation and reduces cell proliferation, migration, invasiveness, and stemness properties in GBM (14). mTORC2 drives GBM growth by promoter histone acetylation and nuclear translocation (15). Likewise, mTORC2 is able to regulate YAP independent of Hippo signaling in GBM patient samples (16).

Moreover, the role of mTORC2 is far less elucidated. Its complex functions are not well defined, and the little information about the biology of mTORC2 is due to the fact that there is no mTORC2-specific inhibitor (17). This problem is one of the difficulties in the study of this protein complex. In recent years, mTORC2 has been shown to play a key role in several biological processes of cancer cells, including cell survival, metabolism, proliferation, and cytoskeletal reorganization (18). However, it has been associated with metabolic reprogramming in GBM, including glycolytic metabolism, glutaminolysis, lipogenesis, and nucleotide and ROS metabolism (19).

Phosphoproteomics technology plays a major role in understanding molecular mechanisms in human cancers. Quantitative phosphoproteomics profiling allows researchers to investigate aberrantly activated signaling pathways, discover therapeutic targets in cancers, and also elucidate insight proteins that are important for the regulation of essential signaling pathways and cellular processes (20, 21). Recently, phosphoproteomic analysis was used to identify ATP-citrate lyase (ACLY) and Acetyl-CoA synthetase 2 (ACSS2) as key targets of mTORC2-sensitive AKT substrate in brown adipocytes. These fills an important gap in understanding of this more secret mTOR complex and may be relevant to understanding mTORC2 activity in other diseases (22).

However, knowledge about mTORC2 biological functions and relationship with other signaling pathways need to be further clarified in glioblastoma cells. Therefore, an examination into more insights of the mechanisms controlling cancer cell progression is required for better understandings of brain cancer metastasis process. The novel basic knowledge gained from this research will increase the understandings of how tumor cells become resistant leading to cancer recurrence. This will eventually result in better predictions, appropriated treatments, and personalized targeted drug selection for patients.

1.2 Hypothesis

- Quantitative phosphoproteomics can determine changes in phosphorylation patterns affected by the aberration of mTOR signaling pathway, and associated with brain cancer progression.
- Dysregulation of some phosphorylated proteins important for glioblastoma invasiveness can be an effect of mTOR complex 2 (mTORC2) hyperactivation.
-

1.3 Research questions

- How does the aberration of mTOR signaling pathway affect phosphorylation patterns of proteins and promote brain cancer progression?
- How does abnormal mTORC2 signaling regulate the phosphorylation of proteins resulting in glioblastoma aggressive properties?

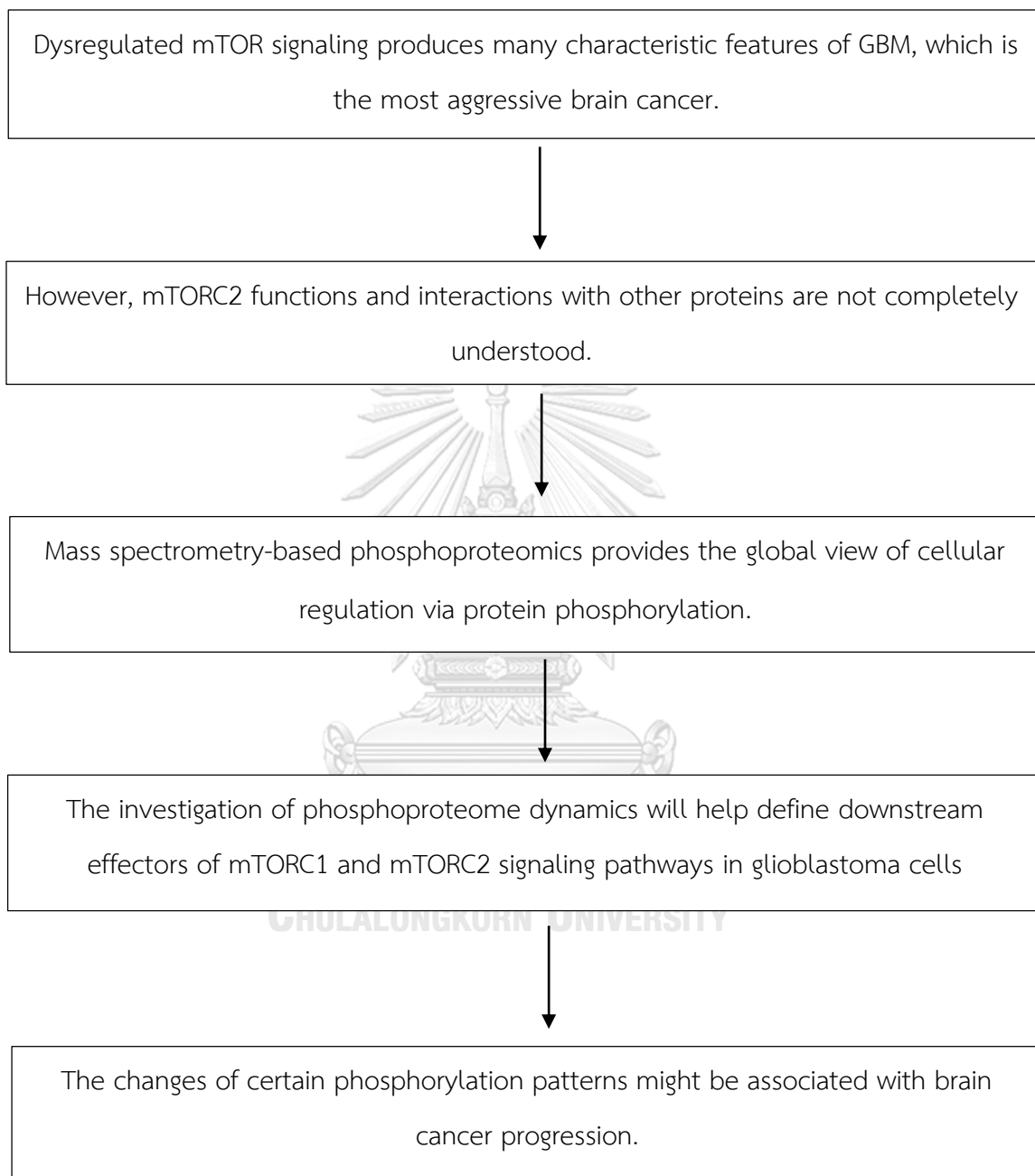
1.4 Objectives

- To investigate the phosphorylation patterns of proteins in glioblastoma cells under mTOR activation and inhibition conditions using quantitative phosphoproteomics.
- To investigate the relationships between mTOR protein complexes and the downstream associated proteins.
- To investigate novel mTORC2-associated proteins and their roles in promoting highly aggressive characteristics of high-grade glioma cells.

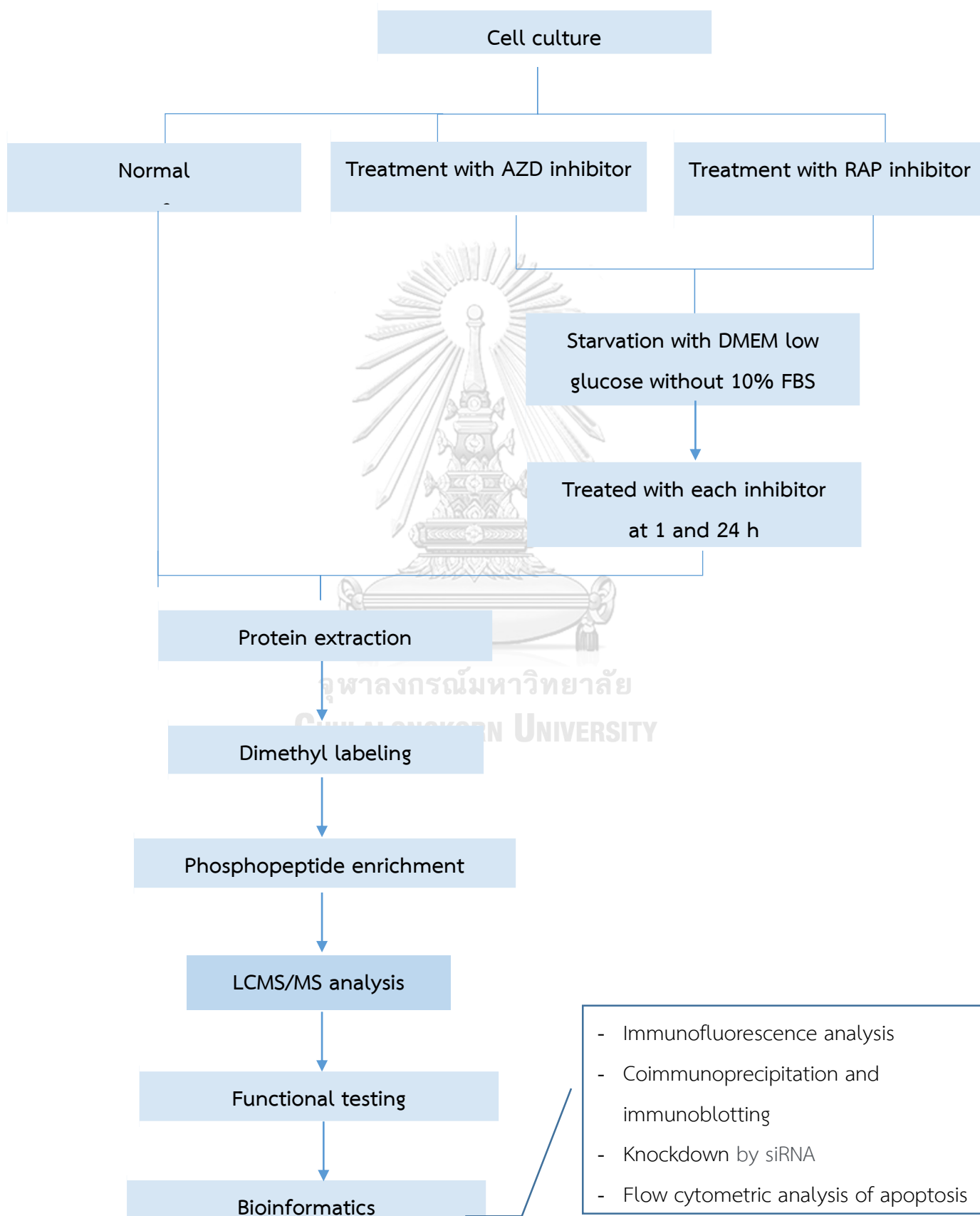
1.5 Expected outcomes

- Elucidation of the mechanism and components of the mTOR pathway which might be potential targets to inhibit the metastasis of glioblastoma.
- This knowledge might lead to better prediction, appropriated treatment and selecting more specific drug candidates for patients.

1.6 Conceptual framework



1.7 Work flow



CHAPTER II

BACKGROUND AND LITERATURE REVIEWS

2.1 Background of Brain cancer

Nowadays, cancer is considered as a major health concern. There are a lot of interests in finding the causes of the disease and developing novel drugs. Although chemotherapy is the standard treatment to kill fast-growing cancer cells, it has many side effects. For example, normal cells are also killed because the drug is non-specific, patient's immune system is weakened, and infection occurs easily (23). Furthermore, one of the limitations to acquire successful outcomes of the therapies is drug resistance, which may lead to cancer recurrence. Medical advances help improve cancer treatment strategies to become more targeted, developed, and personalized than in the past. The researchers have attempted to solve these problems for a long time and have reported many successful studies. For example, the discovery of targeted proteins in breast cancer, leukaemia, and lung cancer leads to the development of many antibody drugs such as bevacizumab and rituximab. Bevacizumab is a humanized immunoglobulin G monoclonal antibody that binds to VEGF with high specificity, thereby blocking VEGF-mediated signaling pathways and angiogenesis(24). Rituximab binds CD20 and stabilizes the CD20 molecules on lipid rafts. It promotes antibody-dependent cellular cytotoxicity and complement-dependent cytotoxicity activities in patients with diffuse large B-cell lymphoma (25). Combination of these drugs with standard chemotherapy in cancer patients has been reported to elevate efficacy, reduce side effects and improve survival (24, 25).

However, several studies reported that many types of cancer cells gain adaptive behaviors to promote migration and resistance to anticancer drugs. The specific mechanisms underlying these processes are specific to each cancer type(26). Thus, the understanding of molecular, cellular, and tissue biology is essential to help provide guidance to appropriate treatments for patients. Although the improvement in medical molecular biology additionally leads to the discovery of novel cancer biomarkers that have major roles in signal transduction important for cell growth and

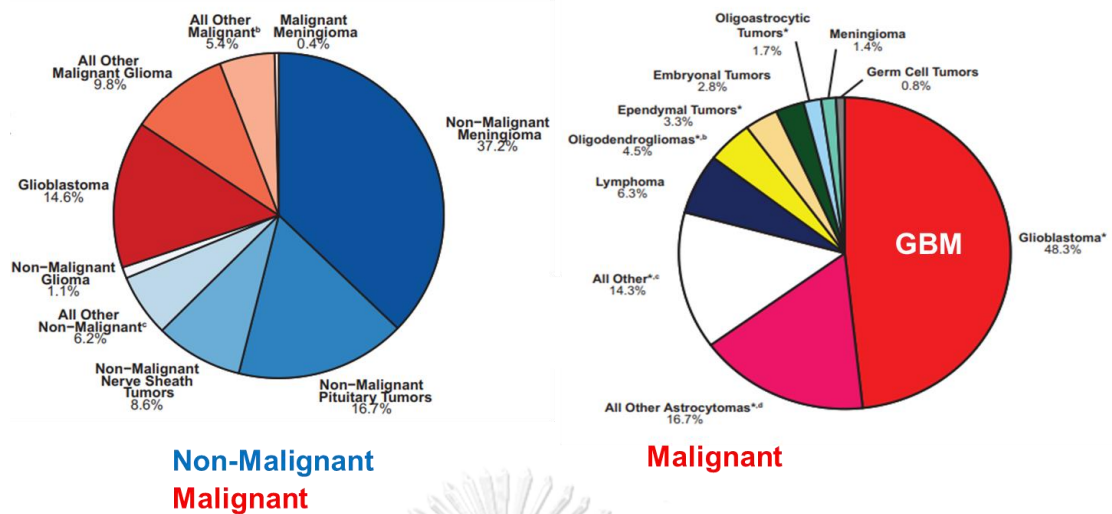
proliferation, protein synthesis, apoptosis, survival under stress conditions, cellular metabolism, and cell motility and metastasis (27), overcoming brain cancers is still not successful. The reason for this might be that the causes of brain cancers are still not completely known. Also, there is currently no specific and effective treatment. In addition, brain tumors constitute the most frequent solid malignancy in children since the limitation of basic knowledge and functions at tumor sites within the brain is not known (3). These issues lead to limitations in the success of the therapies and promote recurrence in patients.

2.2 Glioblastoma multiforme (GBM)

Glioma is a type of brain tumors formed from abnormal supportive cells of the brain called glial cells that include astrocytes, oligodendrocytes, and ependymal cells. The World Health Organization (WHO) classifies glioma into 4 grade. Grade I and II tumors are slowly growing, while high-grade gliomas (of grade III and IV) are malignant tumors with high proliferation rates (28).

- Grade I Pilocytic astrocytoma
- Grade II Oligodendroglioma, Astrocytoma
- Grade III Anaplastic oligodendroglioma/astrocytoma/oligoastrocytoma
- Grade IV Glioblastoma

Glioblastoma multiforme (GBM) is a primary brain tumor that originates from astrocytes. It is the most common brain cancer accounting for over 50 percent of all brain cancers with the worst prognosis (29). GBMs grow quicker and faster than low-grade astrocytomas. They invade nearby tissues and primarily occur in the cerebrum. The huge majority of grade IV gliomas presents as primary GBM in adults, while secondary GBM that progresses from lower-grade gliomas can be found more frequently in children (30). Although the primary and secondary GBMs display the same histopathologic features, they have different underlying genetic mutations and molecular characteristics (31).



Incidence Rates of Primary Brain and Other CNS Tumors by Year per 100,000 Population. Approximately 30.2% of all brain is a malignant and 69.8% is non-malignant. The most common malignant brain is glioblastoma, found 48.3%. Incidence peaks between ages 55 to 60, and the prevalence is higher in males, with a relative sex ratio of 1.66 in England and 1.56 in the USA. Median survival for GBM has been reported as 6.1 months with 1, 2 and 5-year survivals estimated as 28.4%, 11.5% and 3.4%, respectively

Statistics showed that brain cancer infrequently occurs in 1.4% of all new cancer patients every year. It is developed in about 23,770 new people per year with about 16,050 deaths as estimated by the National Cancer Institute (NCI) and the American Cancer Society. Only about 5% of brain tumors may inherit from hereditary genetic conditions such as neurofibromatosis, tuberous sclerosis, and a few others. Glioblastoma multiforme (GBM) has an incidence of 3.19 cases per 100,000 person-years and remarkably poor prognosis showing a 5-year survival rate of 4-5%. Moreover, it has only 26-33% 2-year survival rate in clinical trials (32). The prevalence of brain tumors in Thailand referred from the National Health Security Office (NHSO) database was 12.79/100,000 populations in 2005 and increased to 25.04/100,000 populations in 2014. Benign tumors were more frequently founded than malignant tumors (13.8 benign tumors compared to 11.9 malignant tumors per 100,000 populations in 2014). Brain and other CNS tumors are accounted for 56% of the total brain tumors following by cerebral metastasis and meningioma (33).

2.3 mTOR signaling pathway

Signal transduction is essential for most eukaryotic cellular activities. In a common case of cell signaling mediated by growth factor, binding of the hormone to its receptor initiates a process that starts with the auto- or cross-phosphorylation of the receptor. The activating signal is then propagated through intracellular signaling pathways to the nucleus, resulting in alterations in gene expression, change enzyme activity or ion-channel activity (2).

One of the most frequently altered pathways in human is the mechanistic Target of Rapamycin (mTOR) signaling pathway. It integrates both intracellular and extracellular signals and serves as a central regulator of cell metabolism, growth, proliferation and survival. The central component of the pathway, the mTOR protein kinase, nucleates two distinct multi-protein complexes, mTOR complex 1 (mTORC1) and mTOR complex 2 (mTORC2). The mTOR complex 1 (mTORC1) consists of mTOR, raptor and mLST8. It regulates cell growth, protein synthesis and autophagy through downstream effectors such as ribosomal protein S6 kinase beta-1 (S6K1) and eukaryotic initiation factor 4E-binding protein 1 (4EBP1). In contrast, the mTOR complex 2 (mTORC2) containing mTOR, RICTOR, mSIN1 and mLST8, regulates cytoskeleton organization through protein kinase C alpha (PKC- α) (8).

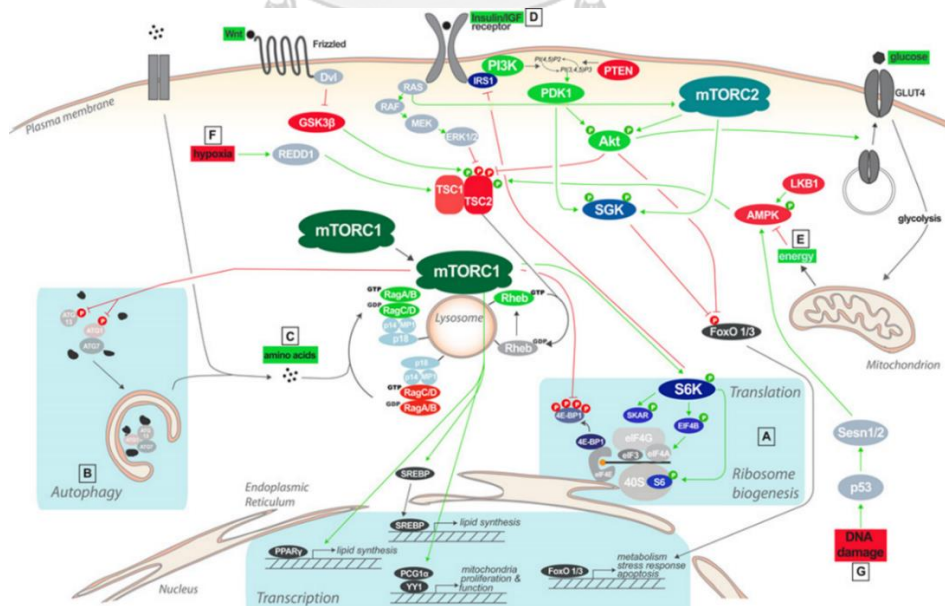


Figure 1 mTOR signaling pathway

(34)

The mTOR complex 1 (mTORC1) has unique protein is raptor. the mTOR complex 2 (mTORC2) has unique accessory protein is RICTOR. The activation of mTORC1 is dependent on nutrients and growth factors. In response to nutrients including arginine, leucine, glutamine, mTORC1 translocates from the cytoplasm to the lysosomal surface via the RAS-related GTP binding proteins (RAGs). bind RAPTOR to activate mTORC1

In contrast, growth factor signaling alone is sufficient to activate mTORC2, for example, insulin, promote activation of PI3K and production of phosphatidylinositol-(3,4,5)-triphosphate (PIP₃), which binds mSIN1 to activates mTORC2.

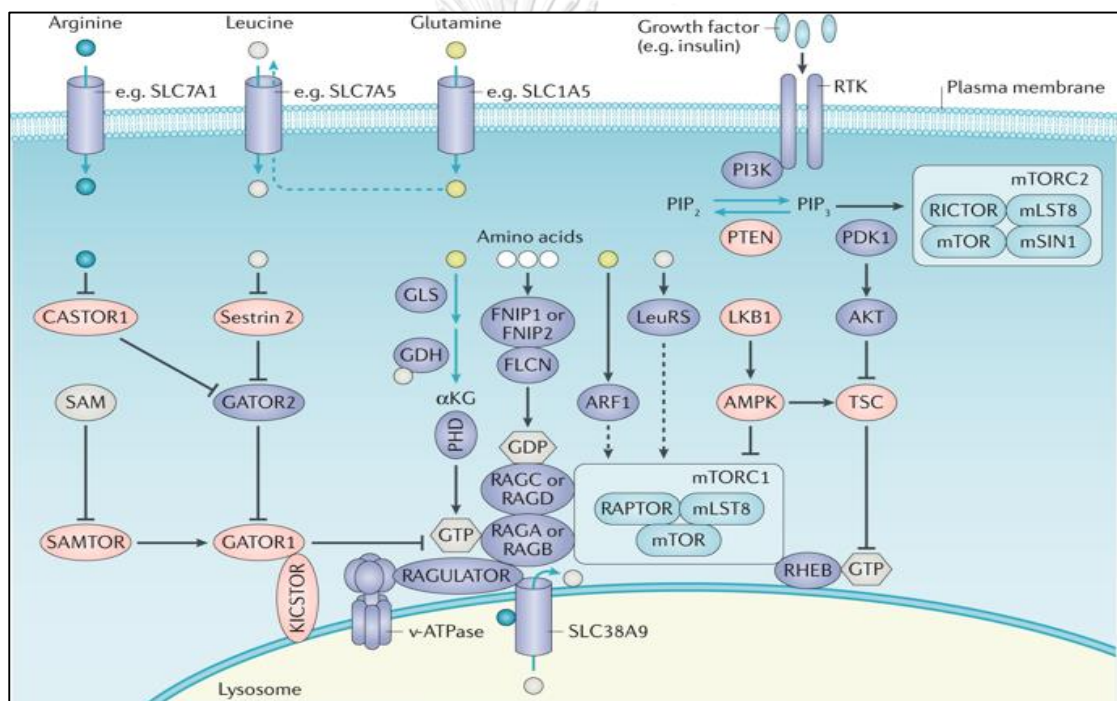


Figure 2 Activation of mTOR signaling

(35)

mTORC1 regulates cell growth and metabolic processes, consist of proteins synthesis, lipids synthesis and autophagy through phosphorylation. The last few years, it has been demonstrated that mTORC2 plays an important role in various biological processes, including cell survival, proliferation and cytoskeleton organization.

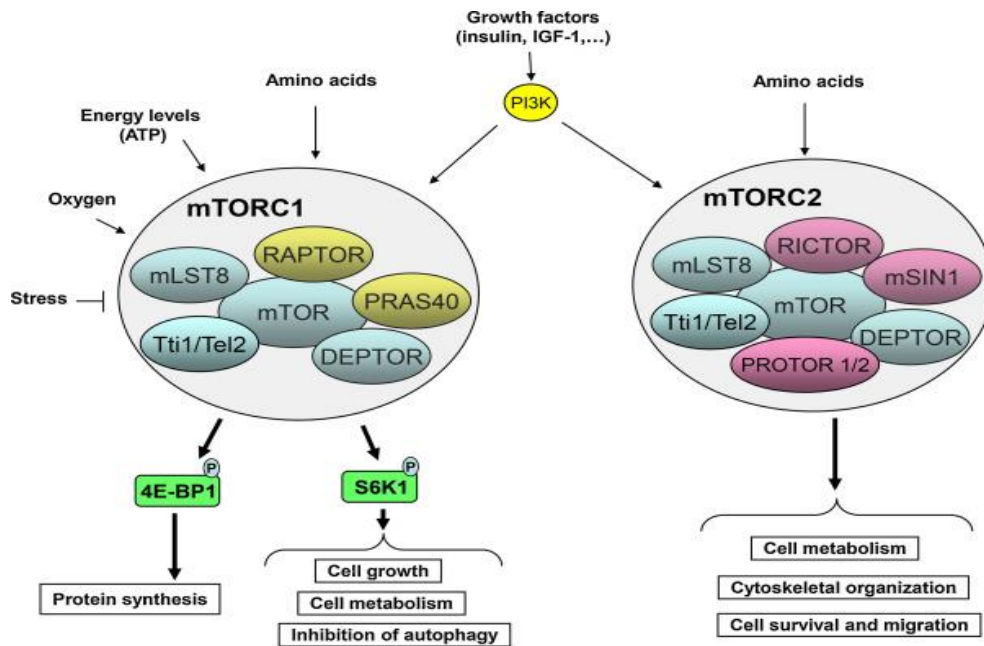


Figure 3 mTOR complex1 (mTORC1) and mTOR complex 2 (mTORC2)
(36)

2.4 mTOR in cancer

Defects of multiple elements of the mTOR pathway such as PI3K amplification or mutation, PTEN loss of function, AKT overexpression, and S6K1, 4EBP1 and eIF4E overexpression have been reported in nervous system diseases, and neurodegenerative disorders (Alzheimer's disease, Parkinson's disease, and Huntington's disease) including highly aggressive types of cancers such as glioblastoma multiforme (GBM), hepatocellular carcinoma (HCC), breast cancer, and non-small cell lung cancer (NSCLC) (37, 38). The mTOR pathway is involved in a variety of cellular functions and often contributed to oncogenesis and cancer progression. This pathway is highly activated in central nervous system cancers of adults and children, especially malignant gliomas (39).

With a lot of knowledge in the regulation and functions of mTORC1, many upstream regulators, cellular functions, and availability of rapamycin as its inhibitor, this complex has been thoroughly studied. On the other hand, the roles of mTORC2 were much less elucidated. The complex functions have not been well defined and less information about mTORC2 biology is caused by the fact that there is no

mTORC2-specific inhibitor (13). This issue becomes one of the difficulties to study this protein complex. During the last few years, it has been demonstrated that mTORC2 plays key roles in various biological processes of cancer cells, including cell survival, metabolism, proliferation and cytoskeleton reorganization (17). In addition, mTORC2 regulates cell motility and invasion of GBM through the association with Filamin A (FLNA), a widely expressed protein that regulates reorganization of the actin cytoskeleton (8).

Nonetheless, mTORC2 is a downstream effector of many cancer-causing mutations in metabolic reprogramming and several cancer drug resistances in glioblastoma (GBM). mTORC2 has been considered to be insensitive to nutrient levels but responsive to growth factor signaling and to function mainly through activating AKT by phosphorylating it on Ser473 (40). mTORC2 may have unexpectedly important roles in cancer pathogenesis, tumor growth promotion and chemotherapy resistance in glioblastoma cells (40).

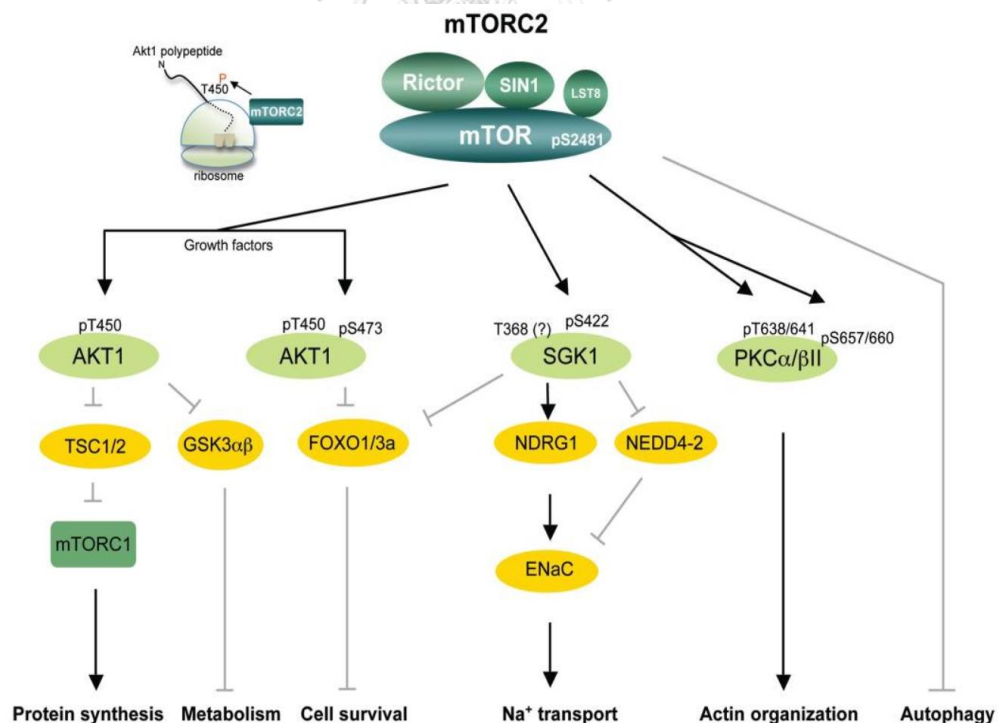


Figure 4 Functions of mTORC2 and downstream targets

(17)

2.5 mTOR inhibitor drug with cancers

Although various studies have been performed so far, there is no effective treatment for patients with glioblastoma. Conventional therapy for GBM is treatment with temozolomide (TMZ) in combination with radiation therapy. However, in most cases, the therapy is usually followed by acquired resistance to TMZ, resulting in complications and failure of treatment (41). The mTOR pathway is highly activated in GBMs, and one of the most studied inhibitors of mTOR is Rapamycin (RAP). RAP binds to the intracellular protein FKBP12 to generate a drug-receptor complex that binds to and inhibits the kinase activity of mTORC1. Most of the researches on the mTOR signaling pathway of GBM in the past has been focusing on the use of rapamycin, which blocks mainly mTORC1 activity but not mTORC2.

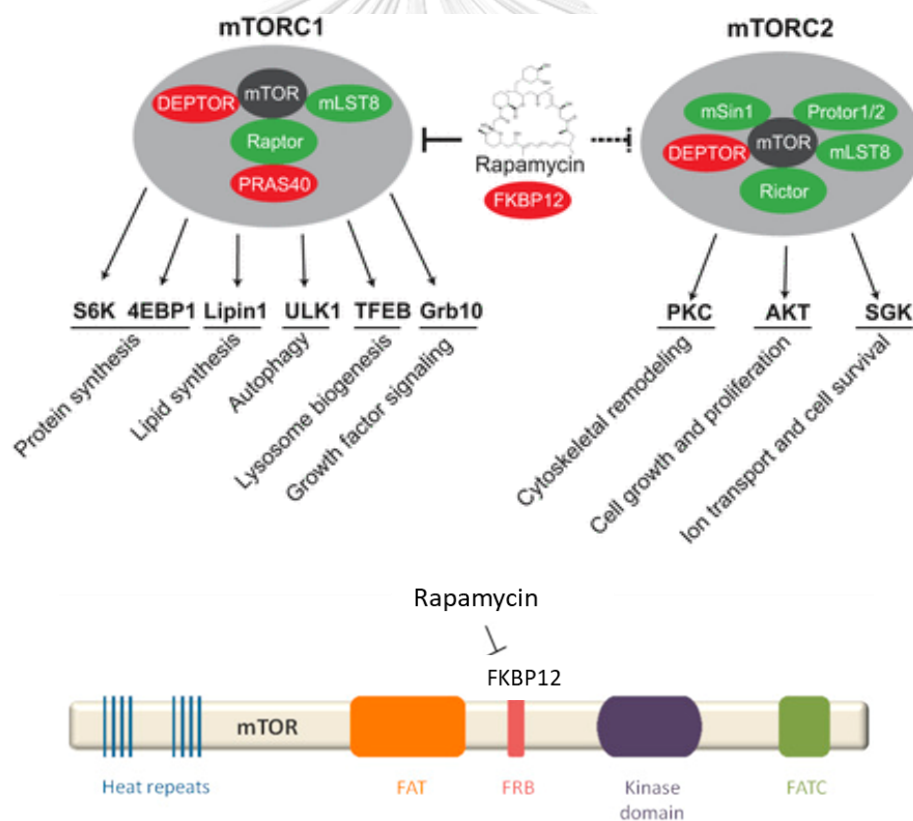


Figure 5 The effect of Rapamycin (RAP) inhibits the kinase activity of mTORC1 (42) (43)

Therefore, the resistance of mTORC2 downstream target phosphorylation to rapamycin likely contributes to poor efficiency of rapamycin in this type of cancer.

Another confounding factor is that rapamycin can promote growth factor signaling by increasing hyperactivity of mTORC2 and AKT via the negative feedback loop and crosstalk between signaling pathways. The development of novel mTOR kinase inhibitors (TORKinibs) that inhibit mTORC1 and mTORC2 was expected to provide more effective results (44, 45).

AZD8055 is a potent small molecule ATP-competitive inhibitor. *In vivo*, AZD8055 reduced S6 and AKT phosphorylation, thereby leading to the reduction of tumor growth. It is implicated that AZD8055 may provide a more promising therapeutic strategy than rapamycin and its analogues. Currently, AZD8055 has been studied in phase I clinical trials (42).



Generation	Compound name	Approved year or current phase	Developer	Examples of indications in completed clinical trials
1st	Rapamycin (sirolimus)	1999	Wyeth-Ayerst	Acute renal allograft rejection/restenosis
1st	RAD001 (everolimus)	2003–2011	Novartis	Allograft rejection/advanced kidney cancer/ tuberous sclerosis/advanced RCC/pNET/neurofibromatosis
1st	CCI-779 (temsirolimus)	2007–2008	Wyeth-Ayerst/Pfizer	Advanced RCC/mantle cell lymphoma
DI	NVP-BEZ235 (dactolisib)	Phase I/II (22)	Novartis	MBC/pNET
DI	GSK2126458	Phase I/II (3)	GlaxoSmithKline	Advanced solid tumors, lymphoma
DI	XL765	Phase I/II (5)	Sanofi-Aventis, Exelixis	Glioblastoma multiforme/NSCLC/ MBC
2nd	AZD8055	Phase I/II (5)	AstraZeneca	Advanced solid tumors/glioma/HCC
2nd	INK128/MLN0128	Phase I/II (25)	Intellikine	Advanced solid tumors/multiple myeloma/Waldenstrom macroglobulinemia
2nd	OSI027	Phase I/II (1)	OSI Pharmaceuticals	Advanced solid tumors/lymphoma
3rd	RapaLinks	Developed in 2016	Rodrik-Outmezguine <i>et al.</i>	Tested in rapamycin- and AZD8055-resistant cell lines and mouse xenografts

Table 1 The generation of mTOR inhibitor drug with cancers

(44)

2.6 mTORC2 an essential role in DNA damage and repair

Recently, mTORC2 was also reported to play a new important role in DNA damage response (DDR) and repair. Inhibitors of DNA damage response (DDR) have a high potential for radiosensitization of various cancers, including glioblastoma (GBM). Interestingly, the global transcriptional and translational response to DNA damage

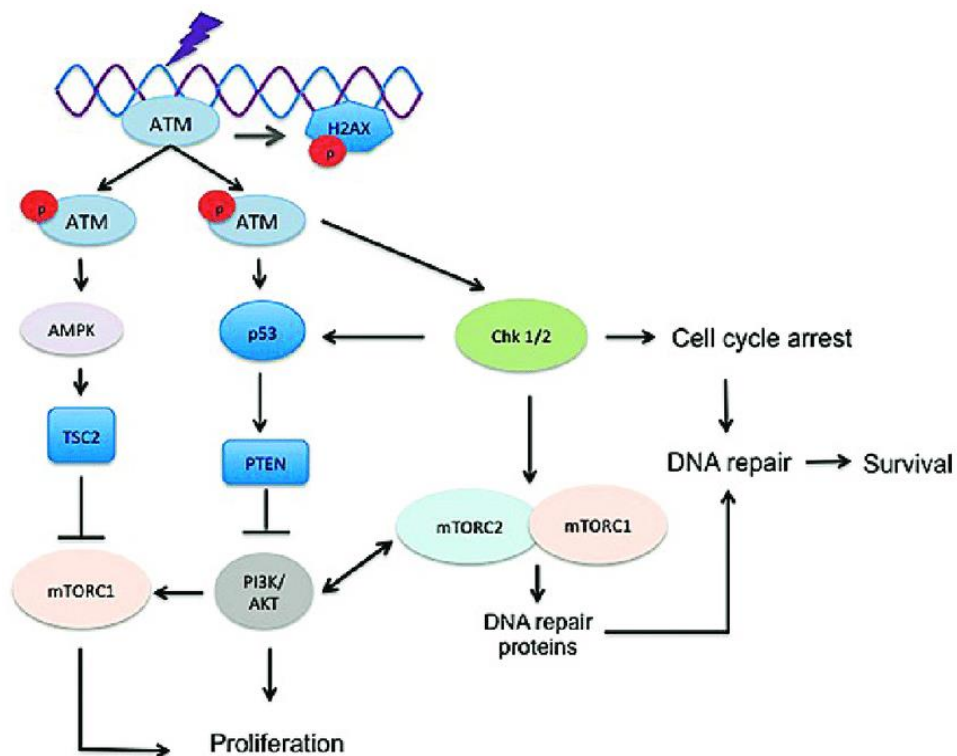


Figure 7 mTOR and DNA damage repair response

(56)

2.7 Quantitative Phosphoproteomics

Signal transduction system transmits cellular information into the nucleus in response to external stimuli via posttranslational modifications (PTMs) and plays critical roles in regulating fundamental biological events such as cell growth, proliferation, and differentiation. Reversible phosphorylation events are widely recognized as a central player in tumor growth. Several studies have identified the phosphopeptidome and localized the phosphorylation sites associated with cancer cells using mass spectrometry-based phosphoproteomics. Also, quantitative phosphoproteome profiling allows researchers to study abnormally activated signaling pathways, discover therapeutic targets in cancer, and also identify proteins important in regulating essential signaling pathways and cellular processes (20) (21). Recently, phosphoproteomic analyzes identified ATP citrate lyase (ACLY) and Acetyl-CoA synthetase 2 (ACSS2) as important targets of the mTORC2-sensitive AKT substrate in brown adipocytes (57). Inhibition of Wee 1 resulted in decreased CDK1

Y15 phosphorylation and increased DNA damage and apoptosis in glioblastomas (58). Increasing phosphorylated proteins in glioblastoma cells and extracellular vesicles (EVs) was associated with the EGFR-signaling cascade and included EGFR, AKT2, MAPK8 SMG1, MAP3K7, DYRK1A, RPS6KA3 and PAK4 kinases (59). Besides, phosphoproteomic studies show that DYRK1A induces degradation of cyclin B by phosphorylating CDC23 of cell cycle arrest (60).

Although phosphorylation events in cancer cell signaling have largely been studied in numerous biological backgrounds for many years, network-wide description of each signaling dynamics is essentially needed to define signaling machinery at the system level (61). Recently, mass spectrometry-based proteomics technology enables us to identify and quantify thousands of proteins based on shotgun strategies using labeling technique and phosphopeptide enrichment by strong cation exchange (SCX) and titanium dioxide (TiO_2) chromatography providing a global view of cellular regulation via phosphorylation (62).

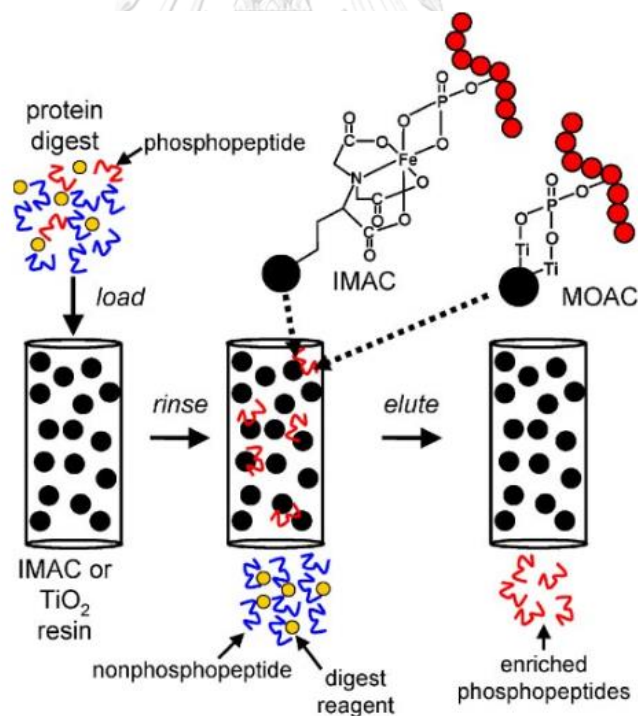


Figure 8 The phosphopeptide enrichment technique

(62)

Several studies have identified the phosphopeptidome and localized the phosphorylation sites associated with cancer cells using mass-spectrometry-based phosphoproteomics. For example, the aberrant phosphorylation patterns of two kinases RAF1, PAK2 and MEF2D in MAPK pathway promoted proliferation in liver cancer cells (63). Also, when glioblastoma cells were stimulated by EGF, the phosphorylated molecules including GAB1, SHC1, EIF4EBP1, RAF1 and RPS6 in mTOR signaling were shown to increase by more than 1.5 fold. These might play role in the regulation of cell proliferation (61). Wee1 inhibition led to a decrease of CDK1 Y15 phosphorylation and increased DNA damage and apoptosis in glioblastoma (64).

Since glioblastoma is known as the most aggressive tumor with poor prognosis, it is essential to understand the molecular mechanisms underlying the aberrant signalings in the cancer cells in order to develop potential therapeutic targets for glioblastoma cells. As reversible phosphorylation-dephosphorylation signaling events in cancer cells are known to play a crucial role in transmitting signals from receptors to the nucleus, our goal is to use high-resolution mass spectrometry-based proteomics technology to figure out global phosphoproteome dynamics in glioblastoma cells. The phosphoproteome data will help identify novel molecular markers and their regulatory sites in GBM whose phosphorylation levels can be changed upon the signaling cues. Thus, we plan to perform quantitative phosphoproteomic analysis of glioblastoma cells under various conditions regarding mTOR activity using high-resolution nanoflow LC-MS/MS system in combination with labeling technique and phosphopeptide enrichment. We would also like to clarify which proteins with altered phosphorylation patterns are involved with mTORC2 functions in glioblastoma cells. The ultimate goal of the project is to identify new potential downstream molecules of the mTORC2 signaling pathway that might confer more aggressive properties to glioblastoma

CHAPTER III

METHODOLOGY

3.1 Cell culture

U87-Glioblastoma multiforme (GBM) cell line was obtained from ATCC. U87 cells were maintained in DMEM low glucose, supplemented with 10% Fetal Bovine Serum (FBS), and 1% Antibiotic-Antimycotic.

For activation and treatment experiments, cells were starved in DMEM low glucose without 10% FBS for 24 hours. Cells were grown in DMEM low glucose for activation, supplemented with 10% Fetal Bovine Serum (FBS). In contrast, in treatment, cells were grown in DMEM low glucose, supplemented with 10% Fetal Bovine Serum (FBS) and 2 μ m AZD for 1 and 24 hours, respectively.

3.2 Quantitative Phosphoproteome sample preparation

3.2.1 Protein Extraction and Tryptic Digestion

The U87 cells were lysed with 8 M urea, 100 mM TEAB, 1x protease inhibitor, and 1x phosphatase inhibitor and homogenized for 5 min. Lysates were centrifuged at 13,000 g for 5 min at 4 °C. The BCA assay measured protein concentrations. Protein concentration was adjusted to 10 mg/ml with lysis buffer. Proteins were reduced with 10 mM dithiothreitol for 30 min at 37°C. It was alkylated in the dark with 40 mM iodoacetamide for 45 min at 25 °C and quenched with 10 mM dithiothreitol for 15 min at 25 °C. Samples were diluted to 0.6 M urea with 100 mM TEAB and digested with sequencing grade modified trypsin (Promega) at 1:150 Enzyme-to-substrate ratio at 37 °C for 16 h. The digested samples were then acidified with 100% trifluoroacetic acid (TFA) at the final sample solution of 0.5% TFA. Tryptic peptides were further cleaned up with reversed-phase C18 SPE columns. A Quantitative Fluorometric Peptide assay determines peptide concentrations. Finally, peptides were dried using Speed-Vac for long-term storage at -20 °C.

3.2.2 Dimethyl labeling

Digested samples were reconstituted with 100 μl of 100 mM TEAB. Peptides are reacted with 15 μl of 4% (vol/vol) in each formaldehyde isotope labeling (Light CH_2O 37%, Medium CD_2O 20%, Heavy $^{13}\text{CD}_2\text{O}$ 20%), and 15 μl of 0.6 M sodium cyanoborohydride (NaBH_3CN) for Light and Medium labeling samples, 15 μl of 0.6 M sodium cyanoborodeuteride (NaD_3CN) for Heavy labeling samples. Labeled samples were incubated at 25 $^\circ\text{C}$ in a fume hood with shaking for 1 hour. Labeled peptides were quenched with 30 μl of 1% (vol/vol) ammonia solution on ice. Samples were then acidified with 15 μl 100% formic acid and dried using Speed-Vacuum.

3.2.3 Phosphopeptide Enrichment

High-Select™ TiO_2 Phosphopeptide Enrichment Kit was used in this experiment. Labeled peptide samples are suspended in 150 μl of Binding/Equilibration buffer. To prepare column, Centrifuge Column Adaptor was placed in a 2 ml collection tube and inserted a TiO_2 Spin Tip into the adaptor. TiO_2 Spin Tip was equilibrated with 20 μl of Wash buffer, then centrifuged at $3000 \times g$ for 2 minutes and 20 μl of Binding/Equilibration buffer and centrifuged at $3000 \times g$ for 2 minutes. TiO_2 Spin Tip and adaptor were transferred into a new 2 ml microcentrifuge tube, samples were placed into the spin tip and centrifuge at $1000 \times g$ for 5 minutes. Samples were reapplied in the microcentrifuge tube to the spin tip and centrifuged at $1000 \times g$ for 5 minutes. TiO_2 Spin Tip was washed with 20 μl of Binding/Equilibration buffer, Wash buffer and LC-MS grade water. Samples were eluted with 50 μl of Phosphopeptide Elution buffer. Samples were dried immediately by using Speed Vacuum.

3.2.4 Peptide Fractionation

High pH Reversed-Phase Peptide Fractionation Kit was used. Prepare solutions in 2.0 ml tubes following the table below.

Fraction No.	%ACN	.ACN (ul)	Triethylamine 0.1% (ul)
1	5	50	950
2	7.5	75	925
3	10	100	900
4	11	110	890
5	12	120	880
6	13	130	870
7	14	140	860
8	14.5	145	855
9	15	150	850
10	15.5	155	845
11	16	160	840
12	16.5	165	835
13	18	180	820
14	19	190	810
15	22	220	780
16	23	230	770
17	25	250	750
18	27	270	730
19	30	300	700
20	50	500	500

The spin Column was placed into a 2.0 ml sample tube and centrifuged at 5000 × g for 2 minutes. The spin column was loaded with 300 µl of acetonitrile and centrifuged at 5000 × g for 2 minutes. This step was repeated. The spin column was washed twice with 0.1% TFA solution. Samples were dissolved with 300 µl of 0.1% TFA solution. Then samples were loaded into the column and centrifuge at 3000 × g for 2 minutes. The spin column was washed with 300µl of water. Samples were eluted with 300µl of the appropriate elution solution and centrifuge at 3000 × g for 2 minutes to collect the fraction. Repeat this step using the appropriate elution solutions gradient. Samples were dried by using Speed Vacuum. Before LC-MS analysis, samples were resuspended in appropriate volume with 0.1% formic acid (FA).

3.3 LC-MS/MS Analysis

The phosphoproteomic fractions were analyzed using the quadrupole orbitrap Q-Exactive Plus mass spectrometer (Thermo Scientific) with reversed-phase EASY nano-LC 1000 using a 25 cm EASY-Spray C18 column, 75 µm internal diameter. The analytical column was equilibrated with Mobile Phase A (0.1% formic acid in LCMS grade water) and Mobile Phase B (0.1% formic acid in acetonitrile). The column was maintained at a constant flow of 300 nL/min. Peptides were injected at 300 ng and eluted by the 90-minute gradient (0 to 5% B in 0 min, 5 to 20% B in 60 min, 20 to 40% B in 20 min, 40 to 98% B in 2 min, 98 to 100% B in 8 min). The electrospray voltage 2.0 kV was applied, and the ion transfer tube was set at 275 °C. Orbitrap precursor spectra were collected from 350-1400 m/z for 90 min at a resolution of 70,000 with AGC target at 3x10⁶ ions and a maximum IT 250 ms. The top 10 most abundant precursors with 2+ to 4+ charge states were selected and fragmented by N(CE) 27 to generate MS/MS data. Data-dependent MS/MS spectra were obtained at a resolution of 17500, AGC target of 5x10⁴ ions, and max ion injection time of 100 ms. Signals with unknown charge states were excluded from fragmentation. The dynamic exclusion option was enabled at 30 seconds. Raw MS data were processed using MaxQuant V1.6.2.10, and Data analysis was performed using Perseus V1.5.5.3

3.4 Immunofluorescence analysis

Briefly, the U87 cells grown on an 8-well chamber are fixed with 4% paraformaldehyde in phosphate-buffered saline (PBS) for 10 minutes. Subsequently, the cells are permeabilized by 0.2% Triton X-100 for 15 minutes and blocked with PBS containing 1% bovine serum albumin for 1 hour. Anti-Rap80 (Rabbit mAb #14466, Cell Signaling Technology) was incubated at RT for 1h, then conjugated to Alexa Fluor-488 at RT for 1h. Anti-BABAM1 (Rabbit mAb #12711, Cell Signaling Technology) was conjugated to Zenon® Alexa Fluor® 588, and Anti- Phospho-Histone H2A.X (Ser139) (Rabbit mAb #9718, Cell Signaling Technology) was conjugated to Zenon® Alexa Fluor® 647. Incubated for 1 hour. Nuclear DNA is stained with 4', 6'-diamidino-2-phenylindole (DAPI). Images are captured either with a fluorescence microscope or a confocal microscope.

3.5 Co-immunoprecipitation and immunoblotting

The Pierce™ Crosslink Magnetic IP/Co-IP Kit (Cat No. 88805) was used in this experiment. Beads were prewashed with 1X Coupling Buffer, and protein was incubated with Rap80 or BABAM1 antibody to A/G magnetic beads for 15 minutes. Beads were washed three times with 1X Coupling Buffer. Then, beads were cross-linked antibody with DSS for 30 minutes. Beads were washed three times with Elution Buffer and then with IP Lysis/Wash Buffer twice. The cell lysate was incubated with prepared beads for 1 hour at room temperature. Beads were collected and washed twice with IP Lysis/Wash Buffer and then once with purified water. Beads were eluted bound antigen. IP-eluted proteins were separated by SDS-polyacrylamide gel electrophoresis (SDS-PAGE) and immunoblotted with anti-RAP80 (Rabbit mAb #14466, Cell Signaling Technology), Anti-BABAM1 (Rabbit mAb #12711, Cell Signaling Technology), Anti- Phospho-Histone H2A.X (Ser139) (Rabbit mAb #9718, Cell Signaling Technology), and Anti-RICTOR antibody (ab104838, Abcam).

For immunoblotting, cells were washed with PBS and lysed on ice in buffer C supplemented with protease inhibitor cocktail and phosphatase inhibitor cocktail. Proteins were separated by SDS-PAGE and detected by immunoblotting with Phospho-BABAM1 (Ser29) Rabbit mAb, Phospho-Akt (Ser473) Rabbit mAb, Phospho-S6

Ribosomal Protein (Ser235/236) Rabbit mAb, Phospho-Histone H2A.X (Ser139) Rabbit mAb, BABAM1 Rabbit mAb, Akt Rabbit mAb S6 Ribosomal Protein Rabbit mAb, Histone H2A.X Rabbit mAb, and GAPDH Rabbit mAb from Cell Signaling Technology.

3.6 Cell viability assay

Cells were seeded onto a 96-well plate at a density of 5×10^3 per well with 100 μ l complete medium and cultured for 0 h to 24 h. Then 20 μ l of CellTiter 96® Aqueous One Solution Reagent was added to each well and incubated the plate at 37°C for 1–4 hours in a humidified, 5% CO₂ atmosphere. Cell viability was detected by the absorbance reading at 490nm using a 96-well plate reader.



3.7 Apoptosis assay

Cells were cultured in 6-well plates until about 50% confluence. Then the media was replaced by a 10% FBS medium with or without AZD8055 to induce apoptosis. After 24 h, cells were harvested, washed with PBS, and resuspended. About 1×10^5 cells were resuspended in a mixture of 200 μ l of Assay Buffer, 2 μ l of Apopxin Green Indicator, 1 μ l of 7-AAD, and 1 μ l of CytoCalcein 450 (Apoptosis/Necrosis Detection Kit; #ab176749; Abcam Co., Ltd.) as manual instructions. After 30–60 min incubation at room temperature, protected from light. Cell apoptotic status was measured via flow cytometry and analyzed by IDEAS software.

CHULALONGKORN UNIVERSITY

3.8 *RICTOR* knockdown by siRNA and CRISPR-Cas9-mediated *RICTOR* knockdown stable cell line generation

U87MG cells were cultured in DMEM low glucose supplemented with 10% (v/v) FBS and 1% Antibiotic-Antimycotic at 37°C under 5% CO₂ condition. For *RICTOR* knockdown by siRNA experiment, human *RICTOR* Accell siRNA (Dharmacon™) were incubated with the cells for 72 hours (siRNA) following the recommended Accell Delivery protocol.

For the generation of a stable *RICTOR* knockdown GBM cell line, four pairs of CRISPR-Cas9 single-guide RNA (sgRNA) against human *RICTOR* gene were constructed in pSpCas9n(BB)-2A-Puro (PX462) V2.0 plasmid. An empty vector without sgRNA

sequence was used to create negative control cells. The plasmids were transfected into U87MG cells using Lipofectamine 3000 (ThermoFisher). The transfected cells were then selected by puromycin (5 µg/ml) for 72 hours. The selected population was recovered and maintained in regular media (DMEM with 10% FBS). *RICTOR* gene expression was determined to confirm the gene knockdown compared to wild-type cells before other experiments were performed using the *RICTOR* knockdown U87MG cell line.

3.9 RICTOR overexpression

Myc-Rictor plasmid was purchased from Addgene (Addgene 11367). The plasmid was transformed into *E. coli* Stbl3 strain in LB broth with ampicillin at 37°C (100 µg/mL). Purification of plasmid DNA was performed using QIAprep Spin Miniprep Kit (QIAGEN). The plasmid DNA was transfected into U87MG cells using Lipofectamine 3000 (ThermoFisher) and incubated for 48 hours before cells were harvested, and immunoblotting experiments were performed.

3.10 Site-directed mutagenesis of BABAM1 (S29A mutation)

GFP-BABAM1(S29A)-P2A-Blast was cloned using Gibson assembly. Briefly, the vector was prepared by digesting EF1a-Cas13a-msfGFP-P2A-Blast plasmid (Addgene 91924) using AgeI-HF and BamHI-HF. EGFP fragment was PCR-amplified by using Q5 High-Fidelity DNA polymerase and GFP-APEX2-NIK3x plasmid (Addgene 129274) as the template. N and C terminal fragments of BABAM1 (S29A) were PCR-amplified using cDNA from U87MG cells as the template. All the fragments and vectors were assembled by NEBuilder HiFi DNA Assembly and transformed into *E. coli* Stbl3 strain. The sequence was confirmed by next-generation sequencing-based BT sequencing (U2Bio Thailand). To investigate the effect of BABAM1 phosphorylation (Ser29) on cancer cell apoptosis induction, the transient overexpression of *BABAM1*, both wild-type and mutant plasmid, was performed in U87MG cells. The plasmid DNA was transfected into U87MG cells using Lipofectamine 3000 (ThermoFisher) and incubated for 48 hours before related experiments were performed.

CHAPTER IV

RESULTS AND DISCUSSION

4.1 Results

4.1.1 The characteristics of quantitative proteomics

Total proteins	Peptides	PSMs
4887	57024	193726

Figure 9 Summary of proteomic quantification

We applied the quantitative proteomics approaches to characterize the mTOR signaling pathway using dimethyl labeling and phosphopeptide enrichment (TiO₂), followed by fractionation. We identified 4887 total proteins and acquired 57024 peptides in U87 cells line, and 193726 PSMs. After that we characterized protein ratio of ACT/N (Activated/Normal) and AZD/N (Treated/Normal) involved in mTOR signaling pathway at 24 h.

We found 17 proteins that were associated with mTOR signaling such as Rheb and BRAF were downregulated in the glioblastoma cells after treated with AZD8055 mTOR inhibitor. There were reduced migration, invasion, cell growth and protein synthesis. Whereas IRS1, MAPK3 were upregulated, mean that cancer might avoid the drugs to survive via activated other pathway as MAPK to increase the proliferation.

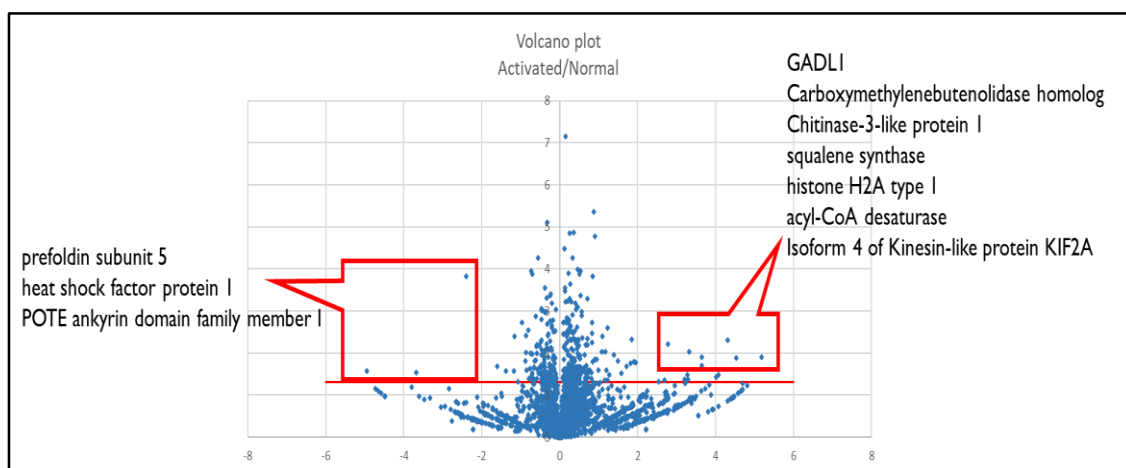
Accession	Description	ACT/N Raio	AZD/N Raio	ACT/N P-value	AZD/N P-value
Q13131-2	Isoform 2 of 5'-AMP-activated protein kinase catalytic subunit alpha-1	-1.0535	-1.0681	0.4973	0.4845
Q96B36-3	Isoform 3 of Proline-rich AKT1 substrate 1	-1.0077	-1.3867	0.6509	0.5201
P23588	eukaryotic translation initiation factor 4B	-0.6948	-0.5489	0.0108	0.2040
P06730-2	Isoform 2 of Eukaryotic translation initiation factor 4E	-0.2795	-0.3378	0.0625	0.0024

P62753	40S RIBOSOMAL PROTEIN S6	-0.2277	-0.2754	0.2018	0.1500
P28482	mitogen-activated protein kinase 1	-0.2035	0.0613	0.1700	0.4894
P17252	Protein kinase C alpha type	-0.1034	-0.0853	0.5011	0.5322
Q15382	GTP-binding protein rheb	0.0236	-0.3392	0.7866	0.0902
Q9Y376	Calcium-binding protein 39	0.1034	0.2374	0.3934	0.4266
Q9NQL2-1	Ras-related GTP-binding protein D	0.1733	0.2541	0.5789	0.3374
P35568	Insulin receptor substrate 1	0.1878	1.8260	0.7328	0.0085
P51812	Ribosomal protein S6 kinase alpha-3	0.2530	0.5004	0.9073	0.8186
Q5VZM2-2	Isoform 2 of Ras-related GTP-binding protein B	0.2601	0.9270	0.2850	0.0678
P27361-1	mitogen-activated protein kinase 3	0.5454	1.0021	0.1202	0.1499
P42345	Serine/threonine-protein kinase mTOR	1.1023	1.5986	0.4550	0.0664
Q13541	Eukaryotic translation initiation factor 4E-binding protein 1	1.7609	2.3508	0.5124	0.3400
P15056	serine/threonine-protein kinase B-raf	3.8401	0.7582	0.0560	0.0588

*The ratio reported in this table is an average log 2 ratio.

Table 2 The characteristics of the protein ratio between Activated/Normal and Treated/Normal in mTOR signaling

Volcano plot showing the distributions of protein ratio and p-value of ACT/N (Activated/Normal) as shown in blue dot and AZD/N (Treated/Normal) as shown in purple dot at 24h. Identical protein with fold changes were shown in red frame. Proteins in left side were significantly downregulated, and right side were significantly upregulated.



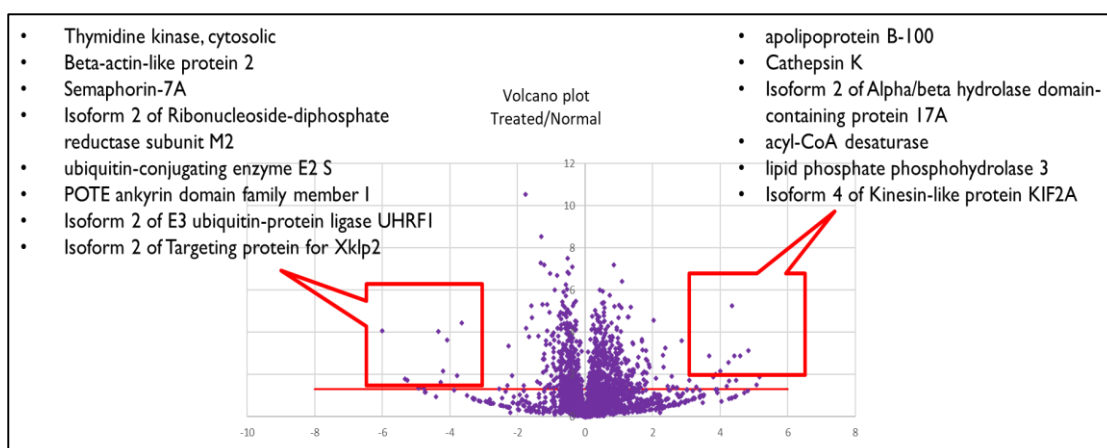


Figure 10 Volcano plot of Activated/Normal and Treated/Normal

4.1.2 Development of phosphoproteomic techniques

We performed phosphopeptide enrichment using High-Select™ TiO2 Phosphopeptide Enrichment Kit compare with IMAC technique. TiO2 kit were presented more than 70% of phosphopeptide enrichment efficiency while IMAC were presented 0.8%. Therefore, in this study we were enriched phosphopeptides by using High-Select™ TiO2 Kit

TiO2 Kit	Total protein	Phosphopeptide	Phospho site	PSM	% enrich phospho efficiency
1	541	2738/2986	3604	6168	91.69
2	716	3024/4041	4079	8030	74.8

IMAC	Total protein	Phosphopeptide	Phospho site	PSM	% enrich phospho efficiency
1	1290	67/8008	78	11180	0.8

Table 3 phosphopeptide enrichment efficiency

Venn diagram showing numbers of different percentage of peptide and phosphopeptides between TiO2 and IMAC techniques from a U87MG cell line.

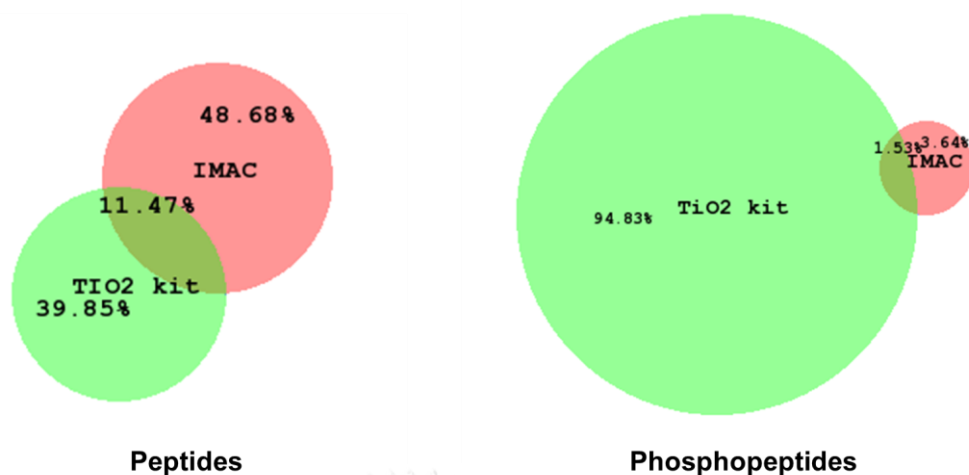


Figure 11 Venn diagram of TiO2 compared with IMAC

4.1.3 Development of phosphopeptide fractionation

Peptides were fractionated into 20 fractions per sample using Peptide Fractionation by High pH Reversed-Phase Peptide Fractionation Kit (Pierce™). Then we compared with difference of 3 set. Set1 was 20 fractions, set2 and set3 were concatenated from 20 fractions into 6 fractions and 10 fractions, respectively.

Set1 : U87_20 fractions				
Fraction No.	Protein	Peptide	PSM	MS/MS
F1	308	398	473	16242
F2	1253	2200	2713	25923
F3	2291	5288	6773	28423
F4	2481	5927	7645	27761
F5	2426	5869	7462	28343
F6	2479	6507	8456	27554
F7	2526	6813	9062	27255
F8	1742	4052	5178	23175
F9	2382	6272	8202	26104
F10	2536	6655	8742	26635
F11	2234	5371	6868	23889
F12	2031	4673	6053	22850
F13	2233	5484	6782	25391

F14	2184	5140	6364	25505	
F15	2255	5696	7129	27290	
F16	2119	4596	5833	21992	
F17	2109	4219	5375	24403	
F18	1816	3311	4352	23943	
F19	1773	3174	4107	25018	
F20	303	425	750	19171	
Set 2 : U87_6 pool fraction					
Fraction No.	Protein	Peptide	PSM	MS/MS	Concatenated fraction No.
P1	2052	5891	7222	24337	1+7+13+18
P2	2056	5863	6973	24115	2+8+14+19
P3	2227	7413	8729	21729	3+9+15+20
P4	2135	5761	6901	22545	4+11+16
P5	1954	4739	5692	20572	5+10
P6	2188	6533	8060	21945	6+12+17
Set 3 : U87_10 pool fraction					
Fraction no.	Protein	Peptide	PSM	MS/MS	Concatenated fraction No.
P1	533	731	853	9137	1+11
P2	1249	2197	2584	14649	2+12
P3	1925	4191	4893	15991	3+13
P4	1817	4185	4818	15212	4+14
P5	2319	6601	7855	21519	5+15
P6	2067	4723	5665	17181	6
P7	2119	4718	5736	17906	7
P8	2011	4764	5715	17940	8+9
P9	2039	4626	5837	19335	10
P10	1933	4927	5830	21080	16+17+18+19+20

Table 4 The 3 set difference of phosphopeptide fractionation

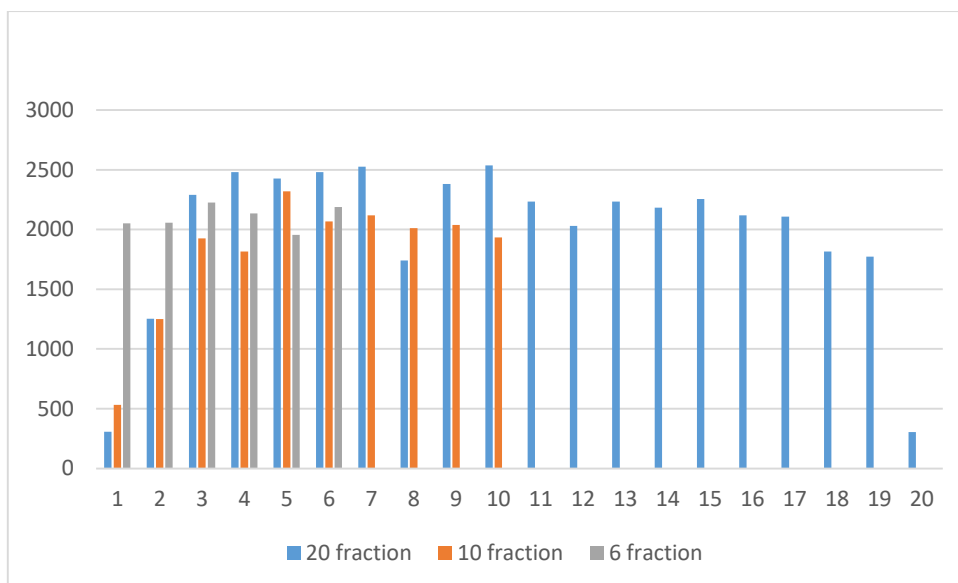


Figure 12 The Number of peptides in each fraction

We compared the number of protein and peptide with 3 different set. The result shown that Set1 were enhanced the highest total proteins and total peptides.

No.	Fraction	Total proteins	Peptides
Set1	20	5816	49074
Set2	6	3865	21565
Set3	10	4531	24694

Table 5 The Number of protein and peptide in 3 difference set

4.1.4 Quantitative phosphoproteome profiling by mTORC1 and mTORC1/2 and inhibitor

we applied the quantitative phosphoproteomics approaches to characterize the mTOR pathway using dimethyl labeling, phosphopeptide enrichment (TiO₂), and fractionation. Five replicates were performed for all MS experiments. In the experiments, we used two kinase inhibitors targeting only

mTORC1 (Rapamycin) and mTORC1/mTORC2 (AZD8055) at different time points (1 and 24 hours). Furthermore, we analyzed 20 phosphopeptide-enriched fractions to achieve high phosphoproteome coverage. We achieved more than 5,000 total proteins and 10,000 phosphosites, resulting in 15984 phosphosites quantified in AZD 1h, 18076 phosphosites in AZD 24h, 19860 phosphosites in RAP 1h, and 17431 phosphosites in RAP 24h.

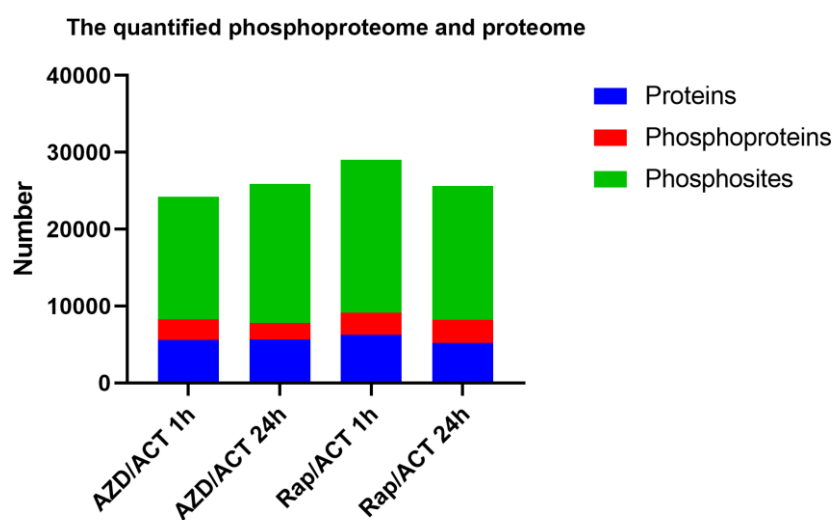
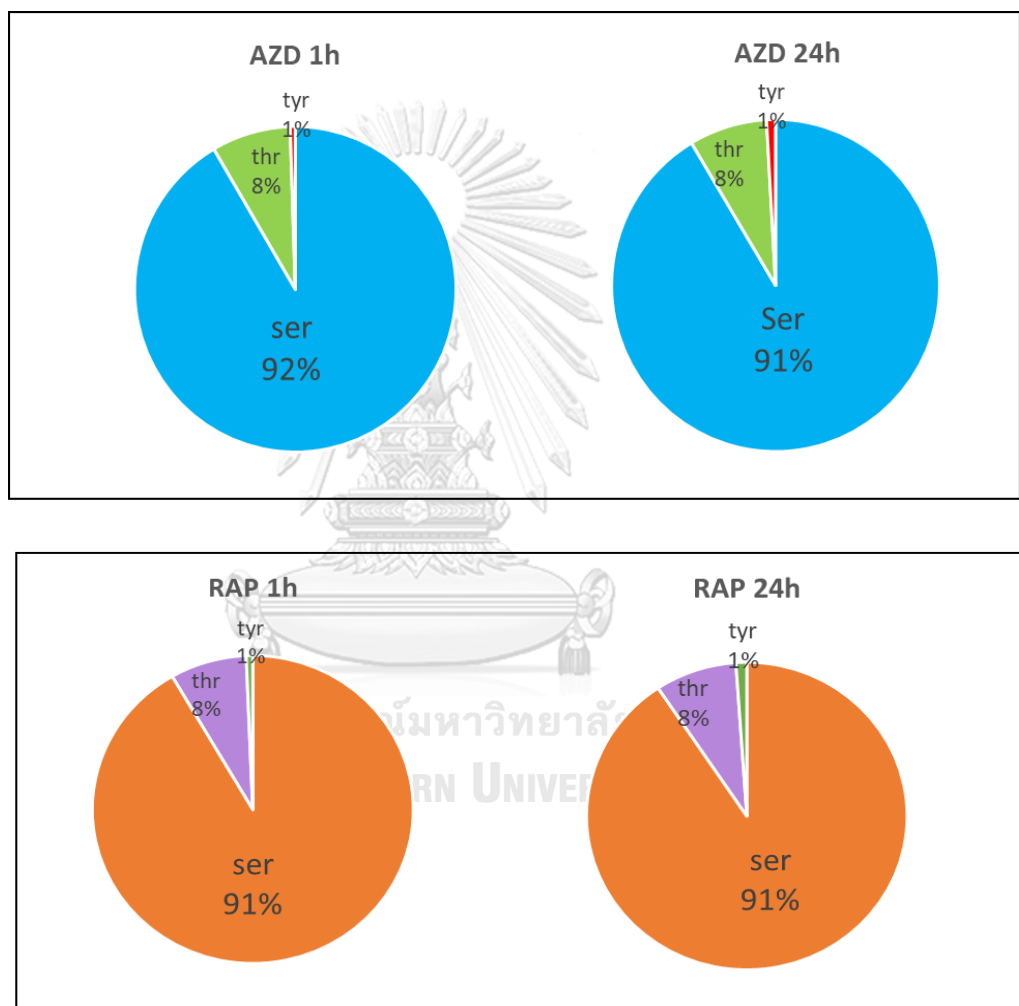


Figure 13 The number of proteins, phosphopeptides, and phosphosites.

Condition	Proteins	phosphoprotein	Phosphopeptides	Phospho-site
AZD 1 h	5633	2619	10094	15984
AZD 24 h	5695	2108	9803	18076
Rap 1 h	6241	2918	10062	19860
Rap 24 h	5230	2977	11952	17431

Table 6. Summary of the quantified phosphoproteome and proteome

We displayed the number of individual phosphopeptides containing phosphorylated serine, threonine, and tyrosine residues identified in the U87MG cells treated with AZD8055 or rapamycin for 1 hour, and 24 hours. From the results, we could determine that our drug treatment conditions did not affect the overall global phosphorylation pattern.



*RAP = Rapamycin, AZD = AZD8055

Figure 14 The phosphorylation site expression in the phosphoproteomic dataset

The Venn diagram of the phosphopeptides proportion differed in the U87 cells between AZD8055 and Rapamycin treatment for 1 and 24 h. we found 435 and 797 phosphopeptides in AZD8055 treatment, not rapamycin for 1 h and 24 h, respectively. These phosphopeptides might be mTORC2 substrates. In contrast, 704 and 689 phosphopeptides were found in Rapamycin treatment, not AZD8055 for 1 h and 24 h, respectively. These phosphopeptides might be mTORC1 substrates.

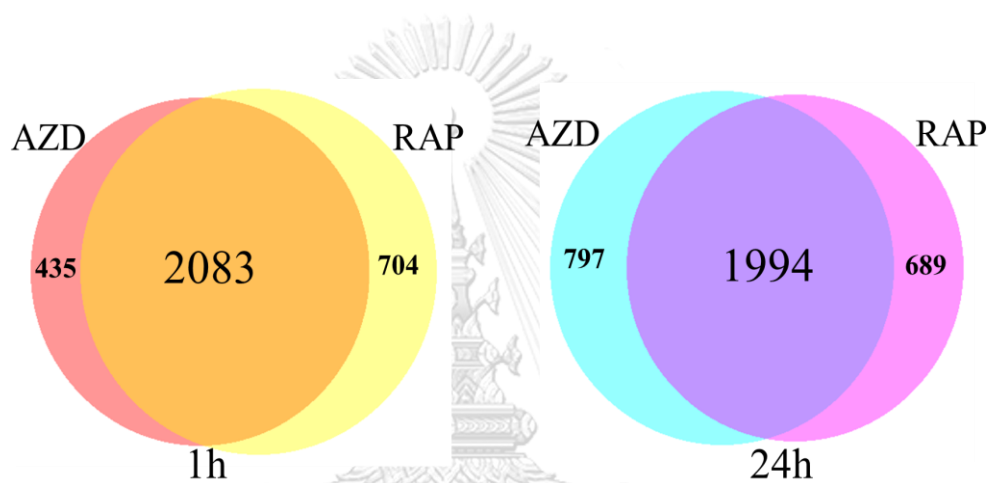


Figure 15 The overlap of phosphopeptides in the phosphoproteomic dataset

Heatmaps showing the log₂ ratio of representative phosphosites of phosphoproteomic data set in five replicate. The phosphopeptides were performed different cluster profiling in RAP/ACT and AZD/ACT at 1 and 24 hours. The upregulated phosphopeptides were shown in blue pattern and downregulated were shown in red pattern. A ratio of 1 means no change, > 1 means up-regulated, and < 1 means down-regulated. The log₂ ratio of abundance of RAP/ACT 1h is almost more reduced than AZD/ACT 1h, while AZD/ACT 24h is more reduced than RAP/ACT 24h.

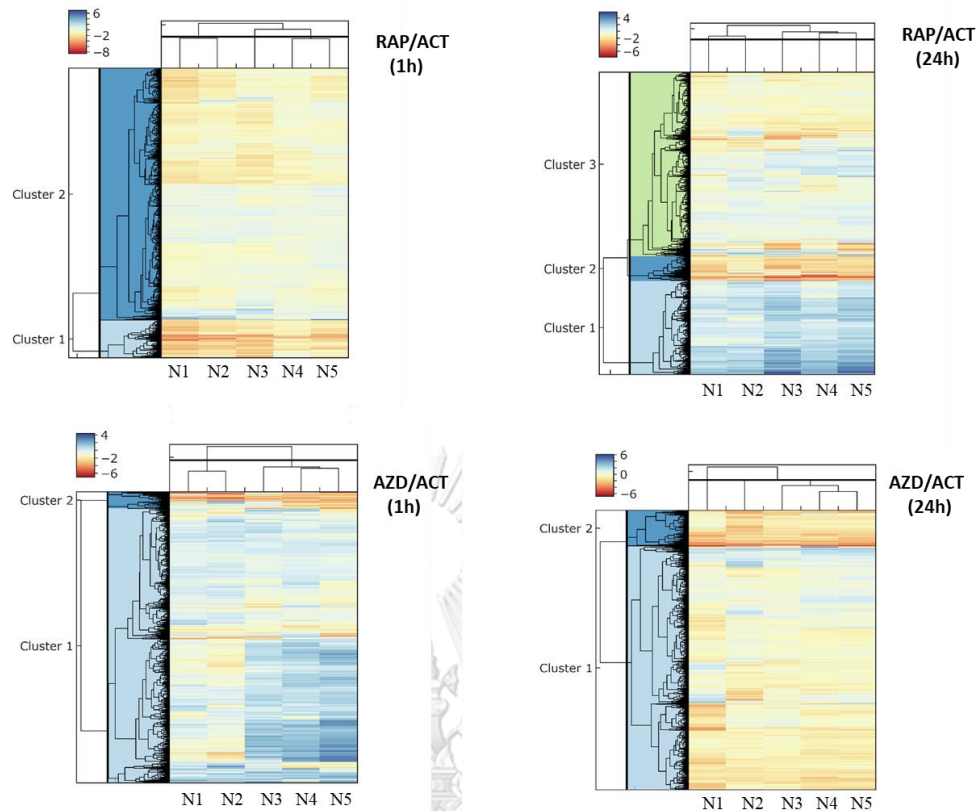


Figure 16 Phosphopeptides profiling in RAP/ ACT and AZD/ACT

Volcano plot showing the distributions of phosphopeptide ratio and p-value of AZD/ACT group (1-hour inhibition) in five biological replicates. We found 230 phosphopeptides were significantly downregulated (p-value <0.05) more than 2folds such as EEF2K, MAP4, EIF4EBP1, HNRNPA1, RTN4, LARP1, HMGA1, ULK1. And 57 phosphopeptides were significantly upregulated (p-value <0.05) such as PLEC, POXK1, ATF2, PATL1, and PCYT1A. As shown in figure 17.

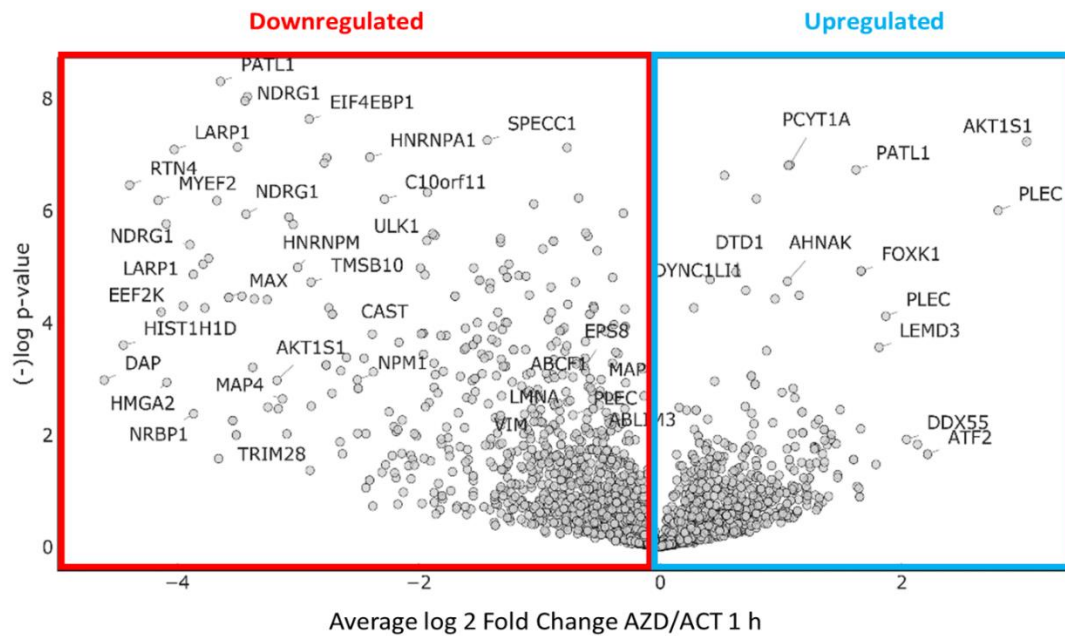


Figure 17 The distributions of phosphopeptide ratio and p-value of AZD/ACT group (1-hour inhibition)

Volcano plot showing the distributions of phosphopeptide ratio and p-value of RAP/ACT group (1-hour inhibition) in five biological replicates. We found 1096 phosphopeptides were significantly downregulated (p -value < 0.05) more than 2 folds such as TOP2A, RTN4, TMX1, PCBP1, MARCKS, TRAF2, LARP1, PHAX, MYO5A. Including H1FX were reduced up to 12 folds. And 37 phosphopeptides were significantly upregulated (p -value < 0.05) such as STK4, SRRM1, AHNAK, LMNA, LMNB, MAP2K2, and PCYT1A. As shown in figure 18.

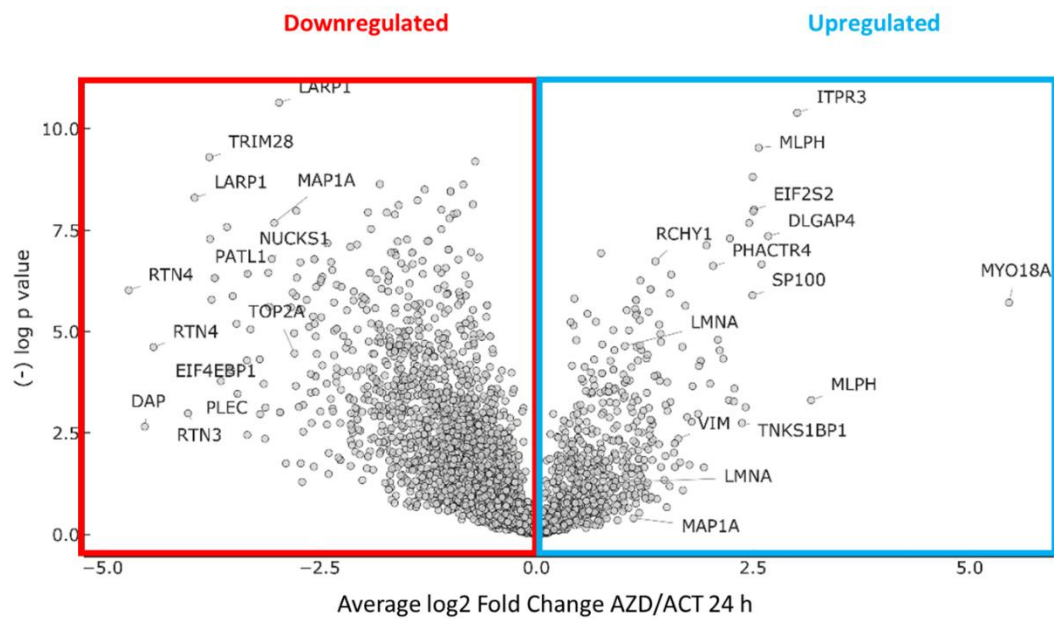


Figure 19 The distributions of phosphopeptide ratio and p-value of AZD/ACT group (24-hour inhibition)

Volcano plot showing the distributions of phosphopeptide ratio and p-value of RAP/ACT group (24-hour inhibition) in five biological replicates. We found 530 phosphopeptides were significantly downregulated (p-value <0.05) more than 2 folds such as AAK1, RTN4, TBX2, SCAMP1, MAX, ACIN1, H1-10, EIF4G1, and DAP. And 771 phosphopeptides were significantly upregulated (p-value <0.05) such as VIM, MAP15, PLEC, TNKS1BP1, HACD3, and R3HDM2. As shown in figure 20.

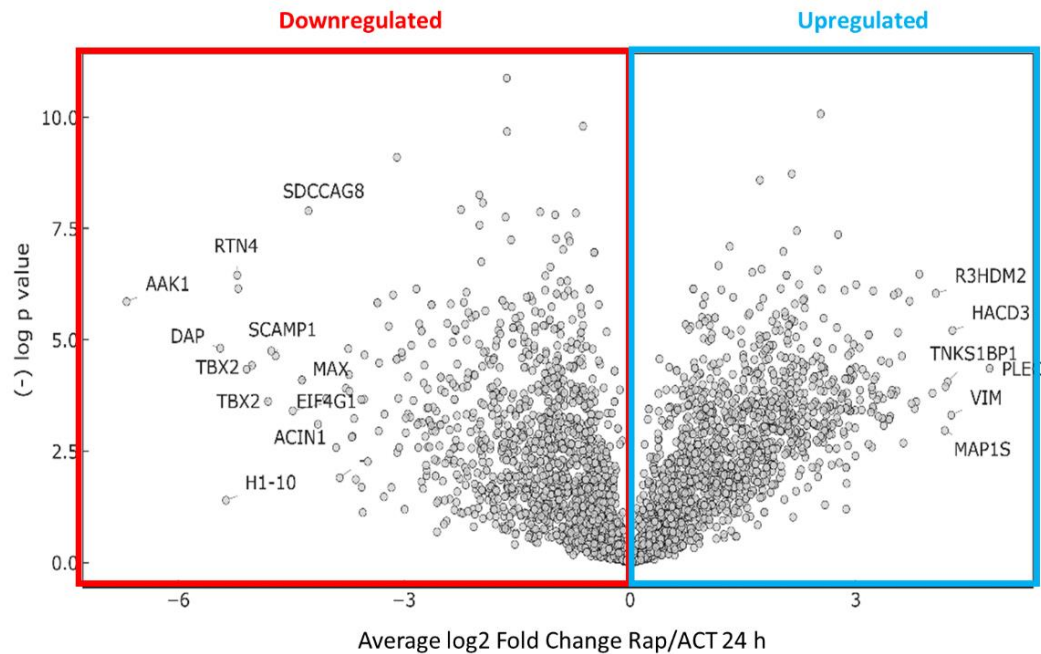


Figure 20 The distributions of phosphopeptide ratio and p-value of RAP/ACT group (24-hour inhibition)

We uploaded protein lists from phosphoproteomic data with human database into DAVID analysis (<https://david.ncifcrf.gov/>). The mTOR upstream and downstream target proteins are involved in the mTOR signaling pathway were explored via KEGG pathway analysis. Red star was presented mTOR targeted proteins in AZD inhibition at 1 hour and yellow star was presented mTOR targeted proteins in AZD inhibition at 24 hours. Moreover, IRS1 and RSK was expressed which was related to insulin signaling pathway and MAPK signaling pathway, respectively.

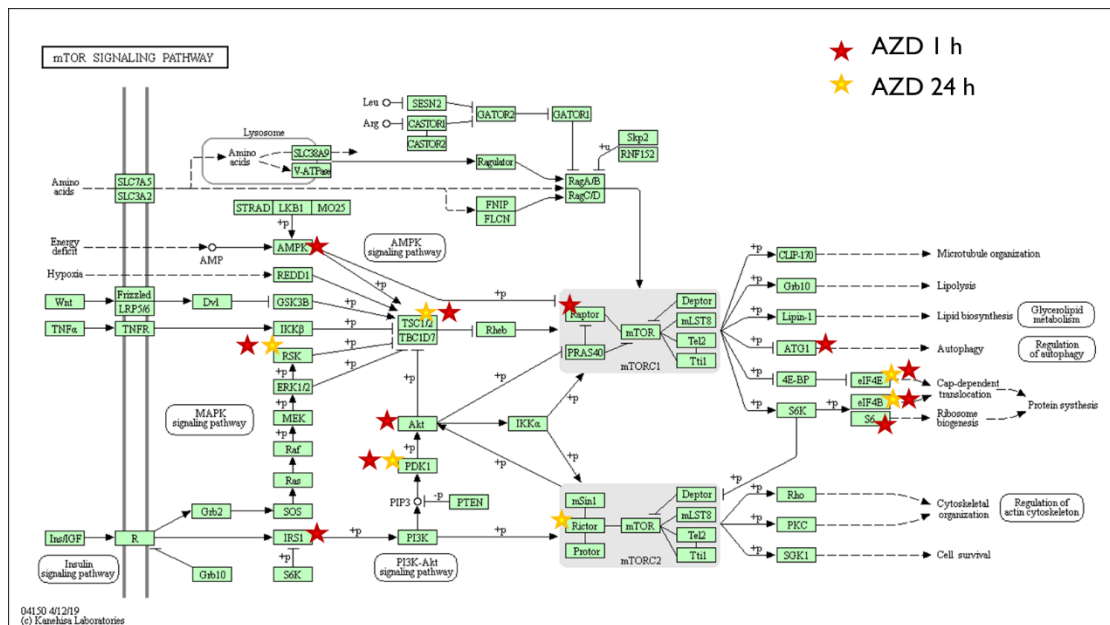


Figure 21 Upstream and downstream target of mTOR signaling pathway

The characteristics of phosphorylation sites that difference of the ratio between AZD/ACT group and RAP/ACT group for 1 h. was 2 fold at least. The ratio reported in this table is an average log 2 ratio and significant ($p < 0.05$).

Accession	Gene names	Amino acid	Position	Sequence	RAP/ACT 1h	AZD/ACT 1h	differ
Q2M218-2	AAK1	T	620	TTPPPAVQGQKVGSLTPPSSPKTORAGHRRI	-0.72055	-2.45487	1.734318
Q09666	AHNAK	S	5749	ASISGSKGDLKSSKASLGSLEGEAEAEASSP	-0.81107	-3.57546	2.764383
Q8IVF2	AHNAK2	S	280	QSIKSRGPGPQRSHSSSEAYEPRDAHVDVSP	-0.54274	-2.50833	1.965588
Q96B36-3	AKT1S1	T	266	EDTQVFGDLPRPRLNTSDFQKLKRKY	-0.75172	-2.64632	1.894593
Q9NWW8-3	BABAM1	S	29	EEEEHSAEPRPRTRSNPGEAEDRAVGAQAS	-1.18511	-3.57546	2.390348
P51397	DAP	S	2	MSSPPEGKLETKAGHPP	-0.38099	-1.47954	1.098557
Q9BTC0	DIDO1	S	805	KKTAPRQEAIPDLEDSPVSDSEEQQESARA	0.415048	-1.55139	1.966441
O00418	EEF2K	S	74	YYSNLTKSERYSSSGSPANSFHFKEAWKHAI	0.212085	-1.01045	1.222538
O75822-2	EIF3J	S	11	MAAAAAAGDSDSDWDADAFSVEDPVR	0.087	-2.20877	2.295769
Q13541	EIF4EBP1	T	37	VLGDGVQLPPGDYSTTPGGTLFSTTPGGTRI	-1.80127	-2.90932	1.108046
Q6PJG2	ELMSAN1	T	704	KSAHRTLRLTNSAEVTPPVLSVMGEATPVSI	-0.45079	-1.72354	1.27275
O43768	ENSA	S	67	DFLMKRLQKGQKYFDSGDYDMAKAKMKNKQL	-2.4234	-4.13465	1.711249
P15408-3	FOSL2	S	191	SVGAVVVKQEPLEEDSPSSSSAGLDKAQRSV	0.746682	-1.61257	2.359248
Q9BW71	HIRIP3	S	196	APGKASVSRKQAREESEAEAPVQRTAKKV	-0.5308	-1.59807	1.067272
P38646	HSPA9	S	200	TAKNAVITVPAYFNDSQRQATKDAGQISGLN	0.652521	-1.10177	1.754288

P10809	HSPD1	S	398	SEYEKEKLNERLAKLSDGVAVLKVGGTSDVE	-0.06291	-1.12442	1.061507
Q16666-3	IFI16	S	168	SPAGAGMSTAMGRSPSPKTSLSAPPNSSTE	-0.84525	-1.87484	1.029588
Q9P206	KIAA1522	S	858	ALGPSAQKPLRRALSGRASVPVAPSSGLHA	0.200747	-1.1453	1.346051
Q9P206	KIAA1522	S	862	SAPQKPLRRALSGRASVPVAPSSGLHAAVRL	-1.70421	-3.17676	1.472555
Q9H0B6-2	KLC2	S	505	GTPQEPPNPRMKRASSLNFLNKSVEEPTQPG	0.312472	-1.31139	1.623861
Q6PKG0	LARP1	S	766	ANKLFGAPEPSTIARSLPTTVPESPNYRNR	-0.70786	-1.75813	1.050275
Q6PKG0	LARP1	S	774	EPSTIARSLPTTVPESPNYRNRTRTPRTP	0.973517	-2.24754	3.22106
Q6PKG0	LARP1	S	850	VMDSREHRPRTASISSPSEGTPVGSYGCT	-0.12421	-1.27082	1.146616
Q4G0J3	LARP7	S	300	SSLPEVRTGKRKRSSSEDAESLAPRSKVKKI	0.349004	-1.27082	1.619827
Q4G0J3	LARP7	S	299	ASSLPEVRTGKRKRSSSEDAESLAPRSKVKK	-0.63486	-1.65991	1.025056
P61244-2	MAX	S	2	MSDNDDIEVESDADKRA	-0.19324	-1.53242	1.339189
P61244-2	MAX	S	11	MSDNDDIEVESDADKRAHHNALERKR	0.248587	-1.67395	1.922533
P55196-3	MLLT4	S	215	EYKDMPETSFTRTISNPEVWMKRRRQKLE	0.110617	-2.76818	2.878799
P06748-2	NPM1	S	225	KGPSVEDIKAKMQASIEKGGSLPKVEAKFI	1.148606	-1.53749	2.686092
Q86TB9-2	PATL1	S	34	PEDDRDLSERALPRRSTSPIIGSPPVRAVPI	0.366997	-1.53749	1.904483
P48634	PRRC2A	S	759	YPPGVHPSGLVPRERSDSGGSSSEPFDRHAP	-2.12247	-3.25777	1.135302
P48634	PRRC2A	S	761	PGVHPSGLVPRERSDSGGSSSEPFDRHAPAM	-0.10691	-3.46836	3.361446
P28066	PSMA5	S	16	MFLTRSEYDRGVNTFSPEGRLFQVEYAIEAI	0.664446	-1.04744	1.711887
P20962	PTMS	S	5	MSEKSVEAAAELSAKDLKEK	-0.79766	-3.78705	2.989391
Q9UQ35	SRRM2	T	1003	SHSGSISPYPKVKAQTPPGPSLSGSKSPCPQ	-0.1487	-1.21541	1.066709
Q9Y6A5	TACC3	S	317	TAPTNIHLVAGRAMTSLPQEEVAAGQMASSSR	-0.1487	-1.21541	1.066709
P19532	TFE3	S	556	LSPLRAASDLLSSVPAVSKASSRRSSFSM	0.46104	-1.51689	1.977932
P11388	TOP2A	S	1471	DPAKTKNRRKRKPSTSDSDSNFEKIVSKAV	0.194185	-1.2695	1.463681
P11388	TOP2A	S	1474	KTKNRRKRKPSTSDSDSNFEKIVSKAVTSK	0.241579	-1.4148	1.656378
P08670	VIM	S	293	SIAAKNLQEAEEWYKSKYADLSDAANRNHEA	0.241579	-1.4148	1.656378

Table 7 Characteristics of phosphorylation sites of AZD/ACT and RAP/ACT group at 1 h.

The characteristics of phosphorylation sites that difference of the ratio between AZD/ACT decreased more than 2 fold and RAP/ACT increased more than 2 fold for 24 h. The ratio reported in this table is an average log 2 ratio and significant ($p < 0.05$).

accession	Gene names	Amino acid	Position	Sequence	RAP/ACT 24h	AZD/ACT 24h	Differ
P21333-2	FLNA	S	1084	KVKAFGPGLOGGSAGSPARFTIDTKGAGTGG	1.628154	-1.166329	2.794482
Q9UNZ2-4	NSFL1C	S	114	SERSGQQIVGPPRKKSPNELVDDLFGAKEH	1.826375	-1.175865	3.002239
Q6P5R6	RPL22L1	S	118	TYELRYFQISQDEDESESED_____	1.335245	-1.617332	2.952577
P46821	MAP1B	S	1433	DKASGRGAESPFEKSGKQGSPOQVSPVSEM	1.50152	-1.762377	3.263896
P46821	MAP1B	S	1438	RGAESPFEKSGKQGSPOQVSPVSEMTSTSL	2.008337	-1.040196	3.048532
Q13283	G3BP1	S	149	QDEVFGGFVTEPQEESEEEVEEPEERQQTPE	3.30312	-1.128871	4.431991
P78559	MAP1A	S	1675	PAGEQKELAPAWEDTSPEQDNRYWRGREDVA	1.911952	-1.398001	3.309953
P16949	STMN1	S	16	MASSDIQVKELEKCRASGQAFELILSPRSKES	3.17388	-1.290156	4.464036
Q09666	AHNAK	S	177	VDVTGREGAKDIDISSPEFKIKIPRHELTEI	1.038346	-1.107779	2.146125
Q9NVP2	ASF1B	S	198	GLGLPGCIPGLLPENSMDCI_____	1.994132	-1.164443	3.158575
Q8NEF9	SRFBP1	S	203	IAKMEHGPKAVTIANSPSKPSEKDSVVSLES	1.96663	-1.874598	3.841228
P78559	MAP1A	S	2106	PSPKESGRSHWDDSTSDSELEKGAREQPEKE	1.002825	-1.693435	2.69626
Q13283	G3BP1	S	232	PVLEETAPEDAQKSSSPAPADIAQTVQEDLR	3.28416	-1.152506	4.436666
Q09666	AHNAK	S	2397	KAPKISMPDLDLHLKSPKAKGEVDVDVPKLE	1.279968	-1.578303	2.858272
Q96AY4	TTC28	S	2398	GTMTSKRDVLSLLNLSRPHNKKEEGVDKLEL	1.852319	-1.14659	2.998909
O00303	EIF3F	S	258	DTERIGVDLIMKTCFSPNRVIGLSSDLQQVG	2.040943	-1.503568	3.544511
O14745	SLC9A3R1	S	280	QKENSREALAEAALESPPALVRSASSDTSE	1.663134	-1.172733	2.835867
P20810-9	CAST	S	285	PDDAIDALSSDFTCGSPTAAGKKEEESTE	2.5935	-1.898682	4.492182
Q9NTJ3-2	SMC4	S	28	RREEGPPPPSPDGASSDAEPEPPSGRTESPA	1.022217	-1.532663	2.55488
P20810-5	CAST	S	291	PDDAIDALSSDFTCGSPTAAGKKEEESTE	1.193377	-2.093943	3.28732
Q8NHW5	RPLP0P6	S	304	PAAAAAPAKVEAKEESESEDEDMGFGLFD__	1.625265	-1.250848	2.876113
Q8NHW5	RPLP0P6	S	307	AAAPAKVEAKEESESEDEDMGFGLFD_____	1.625265	-1.250848	2.876113
P49023	PXN	S	322	LSDFKFMAOQKTGSSSPPGGPPKPGSQLDSM	1.219648	-1.583984	2.803632
O75970-5	MPDZ	S	354	EERTAPTALGITLSSSPTSTPELRVDASTQK	1.28689	-1.749532	3.036422
Q9BV36-3	MLPH	S	364	RDKSVGLPQADPEVSDIESRIIAALRAAGLT	1.462087	-1.144568	2.606655
Q6NZI2	PTRF	S	366	GGAERGEAGDLRRGSSPDVHALLEITEESDA	2.1529	-1.789344	3.942244
P17096	HMGA1	S	36	TEKRGRGRPRKQPPVSPGTALVGSQKEPSEV	1.28611	-1.460015	2.746125
Q13541	EIF4EBP1	T	37	VLGDGVQLPPGDYSTTPGGTLFSTTPGGTRI	2.142278	-3.6374	5.779678
O14545	TRAFD1	S	415	VTEGIPRLDSQPQETSPELPRRRVRHQDLS	1.582264	-1.079679	2.661943
Q09666	AHNAK	S	41	AQRDDGVFVQEVTONSPAARTGVVKEGDQIV	1.149056	-1.58713	2.736186
Q13541	EIF4EBP1	T	46	PGDYSTTPGGTLFSTTPGGTRIIYDRKFLME	2.189824	-2.54235	4.732174
O96013	PAK4	S	474	FGFCAQVSKEVPRRKLVLGTPYWMAPELISR	2.695122	-1.055355	3.750477
Q09666	AHNAK	S	511	QKPKISMQVDVLSLGSPLKGDIVSAPGVQ	1.401113	-1.117034	2.518148
Q86VM9	ZC3H18	S	532	DPWRRSKSPKKLGVSVSPSRARRRRKTSAS	1.029526	-1.034734	2.06426
Q86VM9	ZC3H18	S	534	WRRSKSPKKLGVSVSPSRARRRRKTSASSA	1.122181	-1.287491	2.409672
P27816	MAP4	S	624	SLQDVGQSAAPTFMISPETVGTGKCKSLPA	1.00589	-1.051216	2.057106
Q8TEQ0	SNX29	T	641	ELIDLRGVPGDLSQTSQSDQSLSDFEISNRA	2.443813	-1.135504	3.579317
Q8TEQ0	SNX29	S	642	LIDLRGVPGDLSQTSQSDQSLSDFEISNRAL	2.443813	-1.448421	3.892235

Q9BZQ8	FAM129A	S	646	PSSLAKGESLSLPGSPPPDGTQVIISRVD	2.93784	-1.521739	4.459579
Q96TA1-2	FAM129B	S	652	VTEIRGLLAQGLRPESPPPAGPLLNGAPAGE	1.162397	-1.800216	2.962613
P42166	TMPO	S	66	PPLPAGTNSKGPPDFSSDEEREPTVVGSGA	1.90468	-1.214748	3.119428
P42166	TMPO	S	67	PLPAGTNSKGPPDFSSDEEREPTVVGSGAA	1.90468	-1.214748	3.119428
Q96TA1-2	FAM129B	S	683	SPQPKAAPEASSPPASPLQHLLPGKAVDLGP	1.161094	-1.038778	2.199872
P51812	RPS6KA3	S	715	KGAMAATYSALNRNOSPVLPEVGRSTLAQRR	1.541853	-1.134799	2.676652
Q6PKG0	LARP1	S	766	ANKLFGAPEPSTIARSLPTTVPEPNYRNR	2.355126	-2.52911	4.884236
Q9Y5U2-2	TSSC4	S	82	RSPVEGLGRAHRSPASPRVPPVPDYVAHPER	1.065252	-1.982778	3.04803
Q96RS0	TGS1	S	85	GTAESHDSKIGLDESELDSEAEMLRSMGLP	2.304693	-1.431903	3.736597
Q96RS0	TGS1	S	89	SHDSKIGLDESELDSEAEMLRSMGLPLQFG	1.698778	-1.313553	3.01233

Table 8 Characteristics of phosphorylation sites of AZD/ACT and RAP/ACT group at 24 h

4.1.5 Functional analysis of phosphoproteome reveals phosphoprotein clustering related in mTOR signaling.

The phosphorylation profile was examined for downregulated phosphopeptides in AZD/ACT group and RAP/ACT group for 1 and 24 hours using Gene Ontology Annotations from DAVID tools analysis. Top 5 enriched annotation clusters in each GO term, Molecular function (MF), Cellular Component (CC), and Biological Process (BP) of downregulated phosphoprotein more than 2 fold with P values of 0.05. The downregulated phosphopeptides in AZD/ACT group (1h) revealed that there was a highly associated with nucleosomal DNA binding, Chromosome condensation, and Chromatin silencing. In AZD/ACT group (24h), it was still associated with Chromosome condensation, including eukaryotic initiation factor 4E binding and regulation of DNA repair.

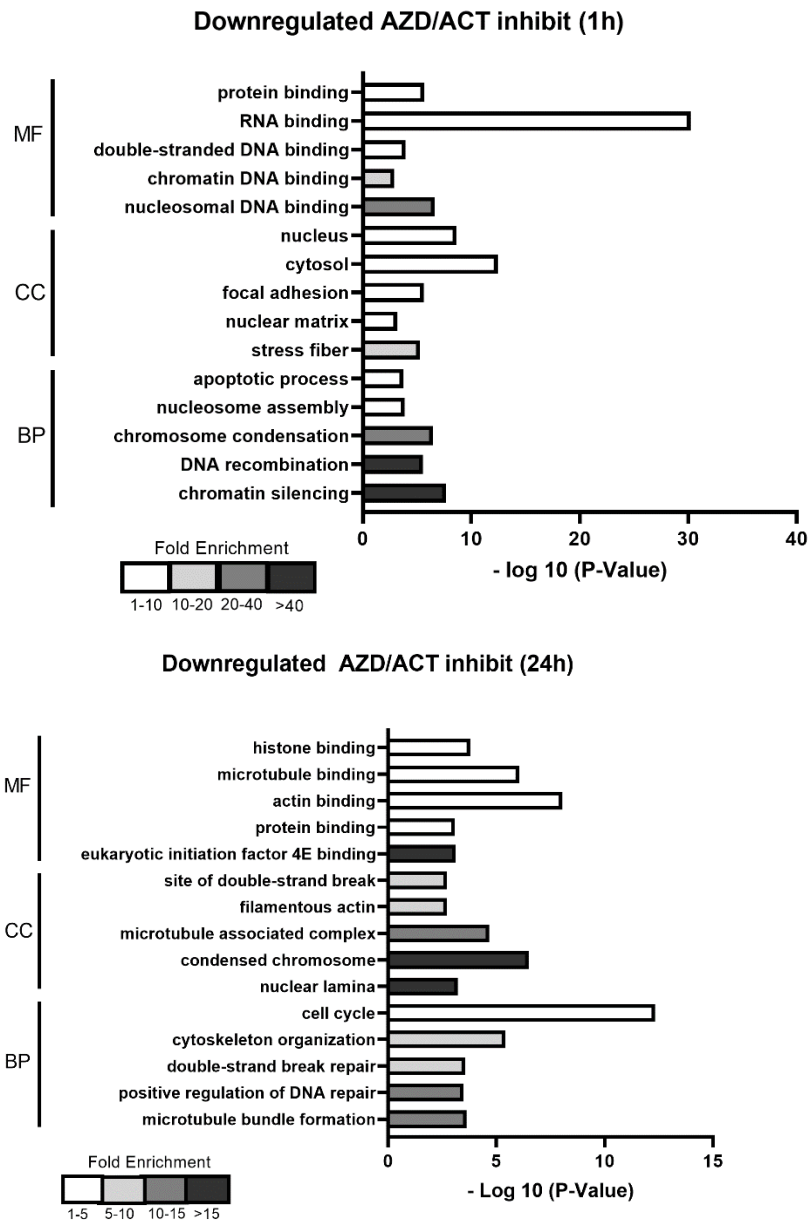


Figure 22 the downregulated phosphopeptides in AZD/ACT group for 1 and 24 hours

Top 5 enriched annotation clusters in each GO term, Molecular function (MF), Cellular Component (CC), and Biological Process (BP) of downregulated phosphoprotein more than 2 fold with P values of 0.05. in RAP/ACT group (1h) correspond to cell-cell adhesion, glycolytic process, and translational elongation. As well as RAP/ACT group (24h) presented, stress fiber, DNA recombination, and chromatin silencing.

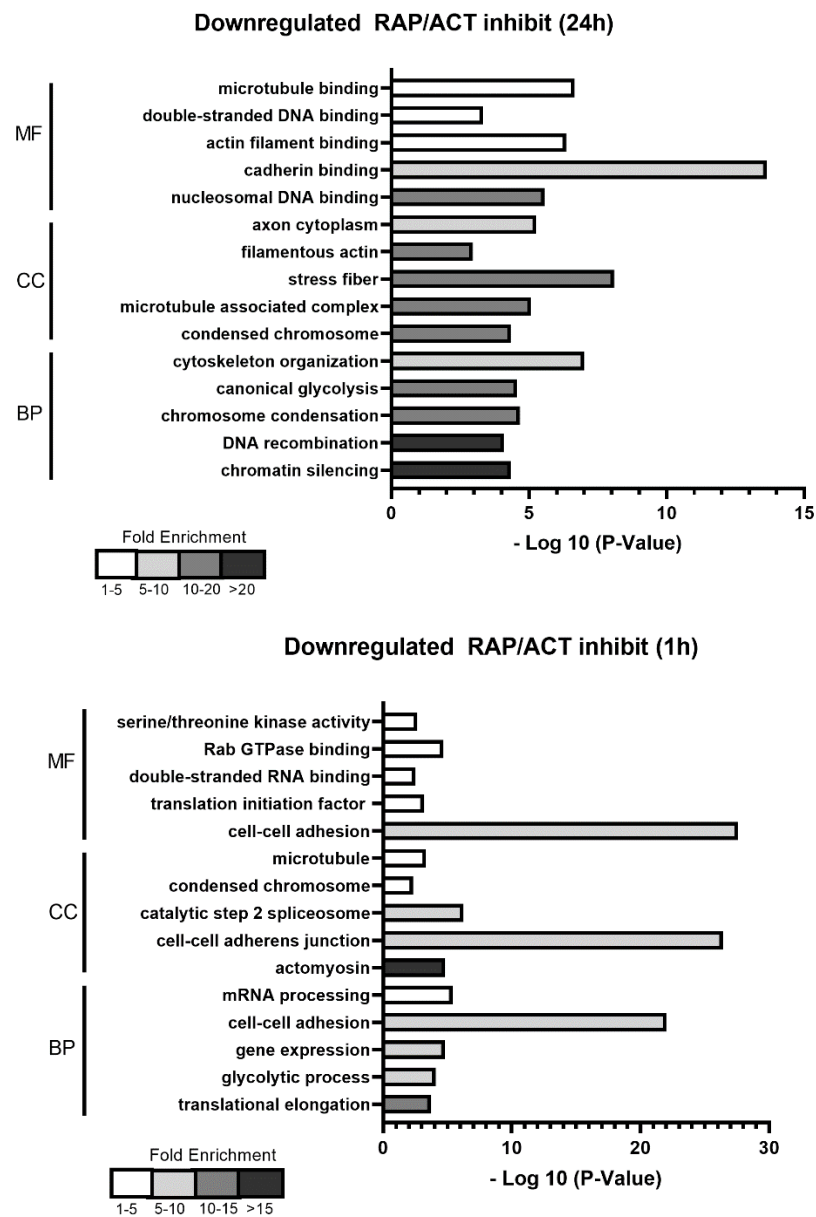


Figure 23 The downregulated phosphopeptides in RAP/ACT group for 1 and 24 hours

The characteristics of phosphorylation sites of the difference ratio more than 2 folds between AZD/ACT decreased and RAP/ACT decreased for 1h and 24 h. The ratio reported in this table is an average log 2 ratio and significant ($p < 0.05$).

Accession	Gene names	Protein names	Amino acid	Position	RAP/ACT 24h	AZD/ACT 24h	Differ
Q96GM8	TOE1	Target of EGR1 protein 1	S	5	-1.05509	0.756777	-1.81187
P06493-2	CDK1	Cyclin-dependent kinase 1	Y	15	-0.66596	1.283062	-1.94902
Q86TB9-2	PATL1	Protein PAT1 homolog 1	S	36	-2.36482	1.619806	-3.98463
O43818	RRP9	U3 small nucleolar RNA-interacting protein 2	S	50	-0.93425	1.180582	-2.11483
O43818	RRP9	U3 small nucleolar RNA-interacting protein 2	S	51	-0.93425	1.180582	-2.11483
P15336-5	ATF2	Cyclic AMP-dependent transcription factor ATF-2	T	51	-0.09284	2.213109	-2.30595
O43818	RRP9	U3 small nucleolar RNA-interacting protein 2	S	53	-0.93425	1.180582	-2.11483
P15336-5	ATF2	Cyclic AMP-dependent transcription factor ATF-2	T	53	-0.09284	2.213109	-2.30595
Q9BVV8	C19orf24	Uncharacterized membrane protein C19orf24	S	120	-0.87654	0.696163	-1.57271
O76021-2	RSL1D1	Ribosomal L1 domain-containing protein 1	S	141	-0.67618	0.463584	-1.13977
Q9Y2U8	LEMD3	Inner nuclear membrane protein Man1	S	144	-0.25318	1.81277	-2.06595
Q15365	PCBP1	Poly(rC)-binding protein 1	S	173	-0.03749	1.236328	-1.27382
Q8TEA8	DTD1	D-tyrosyl-tRNA(Tyr) deacylase 1	S	197	-0.46207	0.625619	-1.08769
Q8NHQ9-2	DDX55	ATP-dependent RNA helicase DDX55	S	201	-0.2595	2.039374	-2.29888
Q6ZTN6-2	ANKRD13D	Ankyrin repeat domain-containing protein 13D	S	202	-0.03387	1.274892	-1.30877
Q8N573-5	OXR1	Oxidation resistance protein 1	S	203	-0.8983	0.511098	-1.4094
Q6ZTN6-2	ANKRD13D	Ankyrin repeat domain-containing protein 13D	T	206	-0.03387	1.274892	-1.30877
Q09666	AHNAK	Neuroblast differentiation-associated protein AHNAK	S	210	-0.37862	0.703519	-1.08214
Q9Y5J1	UTP18	U3 small nucleolar RNA-associated protein 18 homolog	S	210	-0.45159	1.049082	-1.50067
Q5JTV8-2	TOR1AIP1	Torsin-1A-interacting protein 1	S	216	-0.99814	0.798163	-1.7963
Q5JTV8-2	TOR1AIP1	Torsin-1A-interacting protein 1	T	221	-0.69897	0.798163	-1.49713
Q86TY3-3	C14orf37	Uncharacterized protein C14orf37	S	227	-0.5993	0.732937	-1.33224
Q86TY3-3	C14orf37	Uncharacterized protein C14orf37	S	228	-0.5993	0.732937	-1.33224
P85037-2	FOXK1	Forkhead box protein K1	S	253	-0.86722	1.787172	-2.65439
P08559-3	PDHA1	Pyruvate dehydrogenase E1 component subunit alpha	S	262	-0.74015	1.109932	-1.85008
Q9H788-2	SH2D4A	SH2 domain-containing protein 4A	S	270	-0.65382	1.066285	-1.7201
P85037-2	FOXK1	Forkhead box protein K1	T	273	-1.09535	1.66294	-2.75829

P60709	ACTB	Actin, cytoplasmic 1	S	323	-1.55094	1.006689	-2.55762
P49768-7	PSEN1	Presenilin-1	S	333	-1.80242	1.661127	-3.46355
Q9Y606-2	PUS1	tRNA pseudouridine synthase A, mitochondrial	S	392	-0.73938	1.277578	-2.01696
Q9Y606-2	PUS1	tRNA pseudouridine synthase A, mitochondrial	T	398	-0.60218	1.277578	-1.87976
Q8WX93-4	PALLD	Palladin	S	407	-1.2787	0.387616	-1.66632
Q9BYX2-6	TBC1D2	TBC1 domain family member 2A	S	460	-0.88331	1.417475	-2.30078
Q96D46	NMD3	60S ribosomal export protein NMD3	S	468	-0.63686	1.410205	-2.04706
Q96D46	NMD3	60S ribosomal export protein NMD3	T	470	-0.44159	1.360383	-1.80197
Q08J23-3	NSUN2	tRNA (cytosine(34)-C(5))-methyltransferase	S	515	-0.63706	0.70845	-1.34551
Q08J23-3	NSUN2	tRNA (cytosine(34)-C(5))-methyltransferase	S	507	-0.02902	1.176116	-1.20514
Q9NRF8	CTPS2	CTP synthase 2	S	571	-0.29135	1.17081	-1.46216
Q96N67-2	DOCK7	Dedicator of cytokinesis protein 7	S	900	-1.17092	1.2913	-2.46222

*A ratio of 1 means no change, > 1 means upregulated, and < 1 means downregulated.

Table 9 The upregulated phosphopeptides in AZD/ACT compared with downregulated RAP/ACT group (1h)

Accession	Gene names	Protein names	Amino acid	Position	RAP/ACT 24h	AZD/ACT 24h	Differ
P20042	EIF2S2	Eukaryotic translation initiation factor 2 subunit 2	S	2	-0.18222	2.50904	-2.69126
Q92522	H1FX	Histone H1x	S	2	-5.36558	1.545899	-6.91148
O00193	SMAP	Small acidic protein	S	15	-0.26946	0.890133	-1.15959
P08670	VIM	Vimentin	T	37	-0.7145	0.306609	-1.02111
P04075	ALDOA	Fructose-bisphosphate aldolase A	S	39	-1.42117	0.40744	-1.82861
P08670	VIM	Vimentin	S	39	-0.30381	1.635659	-1.93947
P06733	ENO1	Alpha-enolase;Beta-enolase	T	41	-0.78935	0.880078	-1.66943
P08670	VIM	Vimentin	S	42	-0.35104	0.736914	-1.08795
Q13610-2	PWP1	Periodic tryptophan protein 1 homolog	S	50	-2.15945	0.644046	-2.8035
P06733	ENO1	Alpha-enolase	T	55	-1.08156	1.027306	-2.10887
Q6QNY0	BLOC1S3	Biogenesis of lysosome-related organelles complex 1 subunit 3	S	65	-1.77523	0.923982	-2.69921
P07437	TUBB	Tubulin beta chain;Tubulin beta-2B chain;Tubulin beta-2A chain;Tubulin beta-3 chain	S	75	-0.89783	0.470544	-1.36838
P08670	VIM	Vimentin	S	83	-0.5014	1.066506	-1.5679
P17096	HMG1	High mobility group protein HMG-I/HMG-Y	S	103	-0.53043	0.476064	-1.00649
P31323	PRKAR2B	cAMP-dependent protein kinase type II-beta regulatory subunit	S	114	-1.98344	0.607532	-2.59097
Q8IZ21	PHACTR4	Phosphatase and actin regulator 4	S	118	-2.94936	2.03693	-4.98629
P06576	ATP5B	ATP synthase subunit beta, mitochondrial	S	128	-0.9495	1.173953	-2.12345

Q09666	AHNAK	Neuroblast differentiation-associated protein AHNAK	S	135	-0.69315	0.34868	-1.04183
Q5JTV8-2	TOR1AIP1	Torsin-1A-interacting protein 1	S	154	-0.96395	1.197147	-2.1611
O95208-3	EPN2	Epsin-2	S	156	-0.74921	0.469079	-1.21829
Q5JTV8-2	TOR1AIP1	Torsin-1A-interacting protein 1	S	156	-2.08797	1.197147	-3.28511
Q5JTV8-2	TOR1AIP1	Torsin-1A-interacting protein 1	S	157	-2.08797	1.197147	-3.28511
P56181-2	NDUV3	NADH dehydrogenase [ubiquinone] flavoprotein 3	S	164	-0.72421	0.601556	-1.32577
Q659C4-4	LARP1B	La-related protein 1B	S	169	-0.2405	0.773089	-1.01358
P02794	FTH1	Ferritin heavy chain; Ferritin heavy chain, N-terminally processed	S	179	-0.62933	0.620956	-1.25028
O60841	EIF5B	Eukaryotic translation initiation factor 5B	S	182	-0.01165	1.766129	-1.77778
P38646	HSPA9	Stress-70 protein, mitochondrial	S	200	-0.37941	1.16545	-1.54486
Q4G0J3	LARP7	La-related protein 7	S	261	-0.06642	1.336683	-1.4031
P55081	MFAP1	Microfibrillar-associated protein 1	T	267	-0.75057	0.541512	-1.29208
P85037-2	FOKK1	Forkhead box protein K1	T	273	-1.76276	1.021027	-2.78379
Q8IVF2	AHNAK2	Protein AHNAK2	S	280	-0.69182	0.927556	-1.61937
O94880	PHF14	PHD finger protein 14	T	287	-1.69709	1.183133	-2.88022
O94880	PHF14	PHD finger protein 14	S	290	-1.69709	1.183133	-2.88022
Q4G0J3	LARP7	La-related protein 7	S	300	-0.77761	1.43098	-2.20859
O94929-2	ABLIM3	Actin-binding LIM protein 3	S	311	-0.30998	1.156361	-1.46634
P22626-2	HNRNPA2B1	Heterogeneous nuclear ribonucleoproteins A2/B1	S	332	-0.60212	0.407476	-1.0096
O94763	URI1	Unconventional prefoldin RPB5 interactor 1	S	372	-2.39351	0.371269	-2.76478
P06576	ATP5B	ATP synthase subunit beta, mitochondrial	Y	395	-0.20812	1.045708	-1.25383
P06576	ATP5B	ATP synthase subunit beta, mitochondrial	S	403	-0.56808	1.188588	-1.75667
P55072	VCP	Transitional endoplasmic reticulum ATPase	S	581	-0.13429	0.983614	-1.1179
P02545-3	LMNA	Prelamin-A/C; Lamin-A/C	S	598	-0.00016	1.020456	-1.02062
P49959-2	MRE11A	Double-strand break repair protein MRE11A	S	621	-0.51529	0.546019	-1.06131
Q9UHB6-4	LIMA1	LIM domain and actin-binding protein 1	S	687	-0.94635	0.402866	-1.34921
Q8N9B5-2	JMY	Junction-mediating and -regulatory protein	S	962	-0.4948	0.575259	-1.07006
Q641Q2-2	FAM21A	WASH complex subunit FAM21A	S	1066	-0.62151	0.837692	-1.4592
Q55W79	CEP170	Centrosomal protein of 170 kDa	S	1165	-0.36515	0.889785	-1.25493
Q14160	SCRIB	Protein scribble homolog	S	1306	-2.31054	0.103247	-2.41378
Q15149	PLEC	Plectin	S	4252	-0.23054	0.918507	-1.14904
Q09666	AHNAK	Neuroblast differentiation-associated protein AHNAK	S	5749	-2.0626	0.628868	-2.69147
Q09666	AHNAK	Neuroblast differentiation-associated protein AHNAK	S	5752	-1.54719	1.160984	-2.70818

*A ratio of 1 means no change, > 1 means upregulated, and < 1 means downregulated.

Table 10 The upregulated phosphopeptides in AZD/ACT compared with downregulated RAP/ACT group (1h)

Top 5 enriched annotation clusters in each GO term, Molecular function (MF), Cellular Component (CC), and Biological Process (BP) of downregulated phosphoprotein more than 2 fold with P values of 0.05. in RAP/ACT group for 1h and 24h.

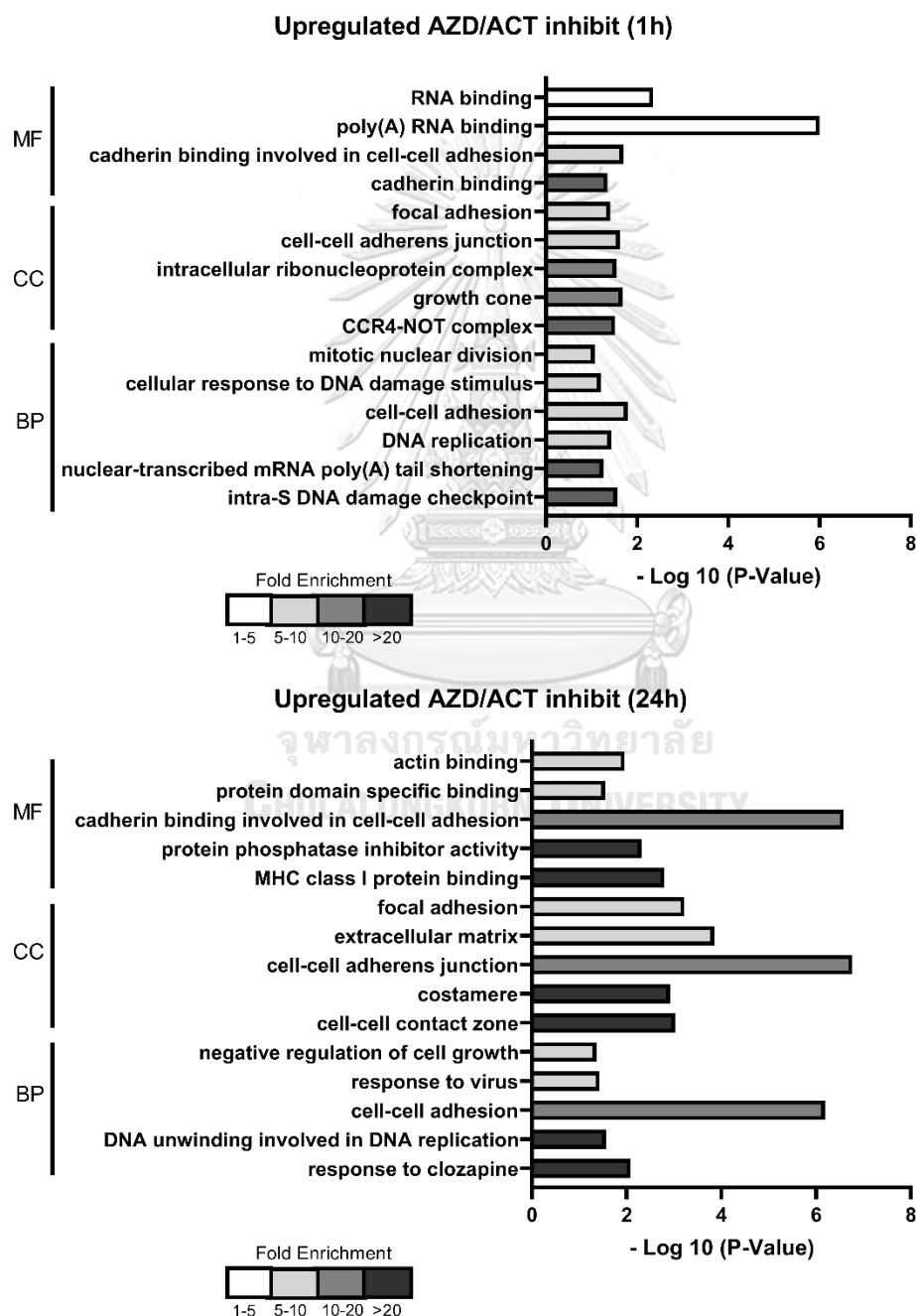


Figure 24 The upregulated phosphopeptides in AZD/ACT group

for 1 and 24 hours

The Cytoscape platform provided and indicated protein-protein interactions. We loaded the phosphoproteome dataset and found that the phosphorylation of AZD/ACT groupion decreased more than 2-fold after 1 h. We detected 70 interactions related to the mTOR signaling pathway. These interactions revealed the related proteins and classified into 6 clusters: cell-cell adhesion, cytoskeleton, autophagy, RNA binding, chromatin organization, DNA repair, transcription factor, and translation.

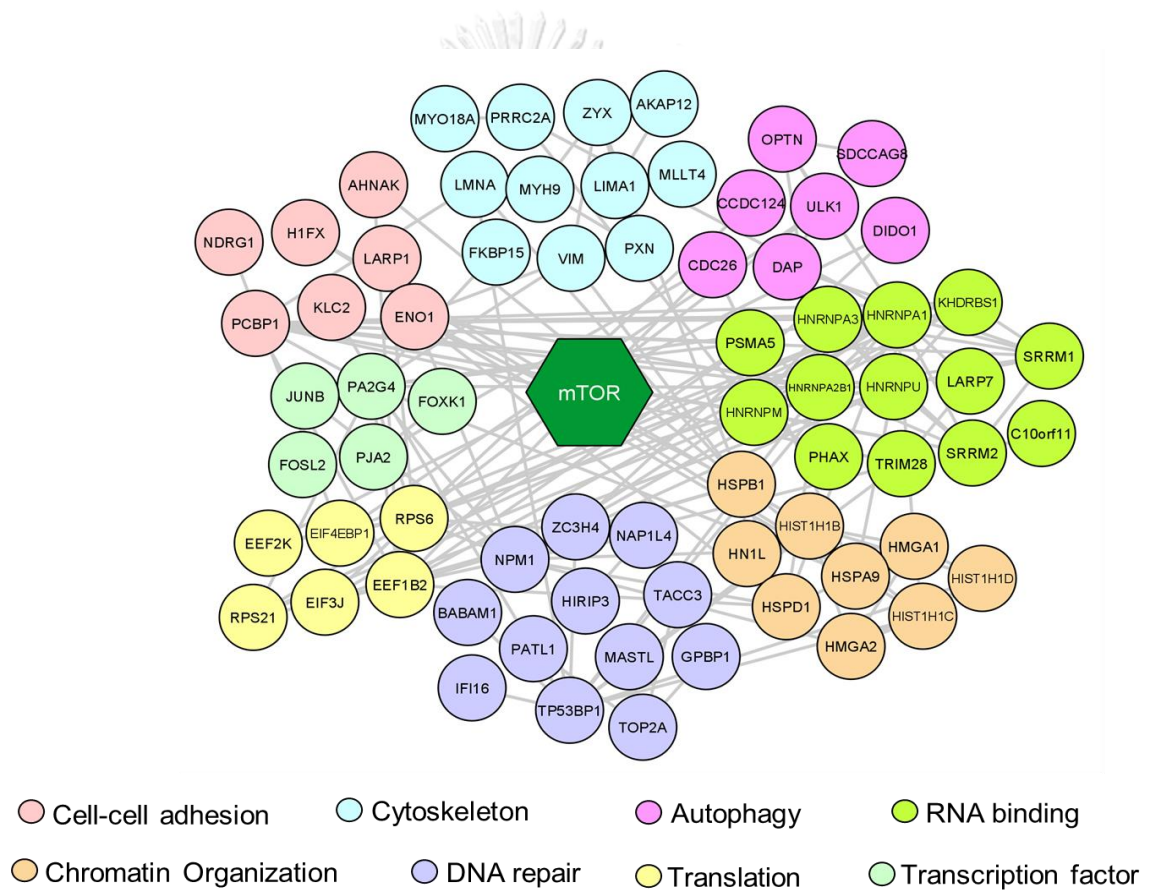
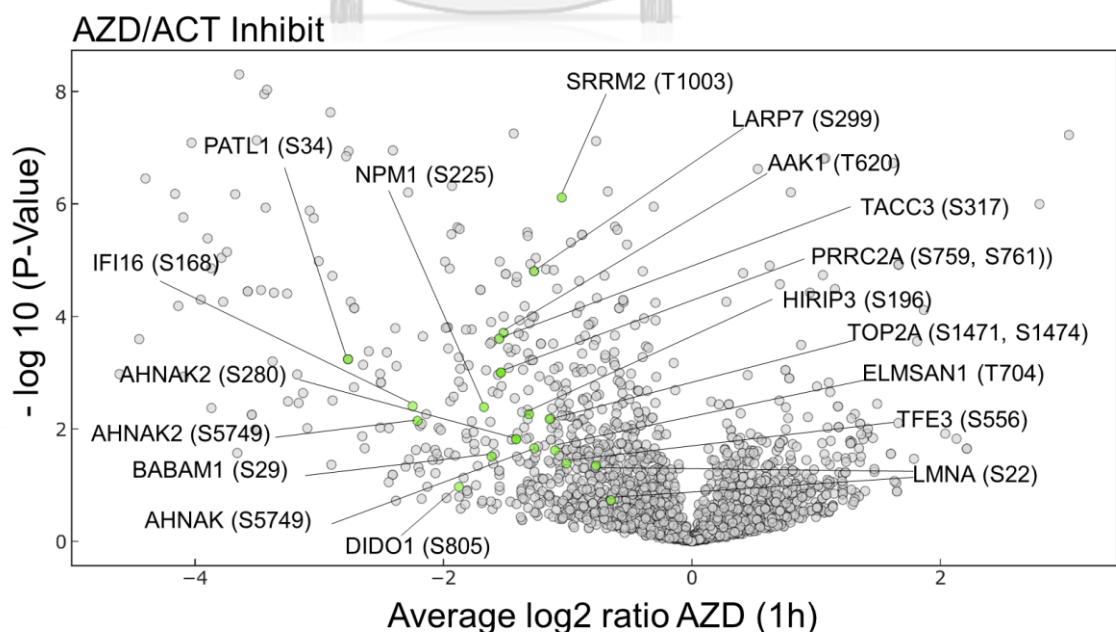


Figure 25 the Classification of the functionally related phosphopeptides and phosphoprotein interactions involved in the mTOR pathway.

4.1.6 The potential targets in the mTORC2 signaling pathway.

For bioinformatics analysis, we need to find out whether proteins with altered phosphorylation patterns are involved in mTORC2 functions in glioblastoma cells. We filtered out the same phosphosites between AZD/ACT and RAP /ACT, where phosphorylation changed differently and significantly ($p < 0.05$). We selected the average log₂ ratio of AZD/ACT that contained less than -1, indicating that phosphosites were down-regulated by more than 2-fold after AZD8055 treatment. Then, we selected the average log₂ ratio of RAP /ACT that contained more than 1, indicating upregulated phosphosites after treatment with Rapamycin. When inhibited after 1 h, we discovered that 18 phosphosites downregulated by AZD/ACT (green dot) and upregulated by RAP /ACT (red dot) could be direct downstream targets of mTORC2, such as AAK1 (T620), AHNAK (S5749), DIDO1 (S805), EIF3J (S11), EIF4EBP1 (T37), ELMSAN1 (T704), HIRIP3 (S196), KLC2 (S505), LARP1 (S766), LARP1 (S774), LARP1 (S850), LARP7 (S299), LARP7 (S300), MAX (S11), MAX (S2), PRRC2A (S761), and SRRM2 (T1003). Interestingly, this study identified several phosphosites whose function via the mTORC2 pathway in glioblastoma is much less elucidated.



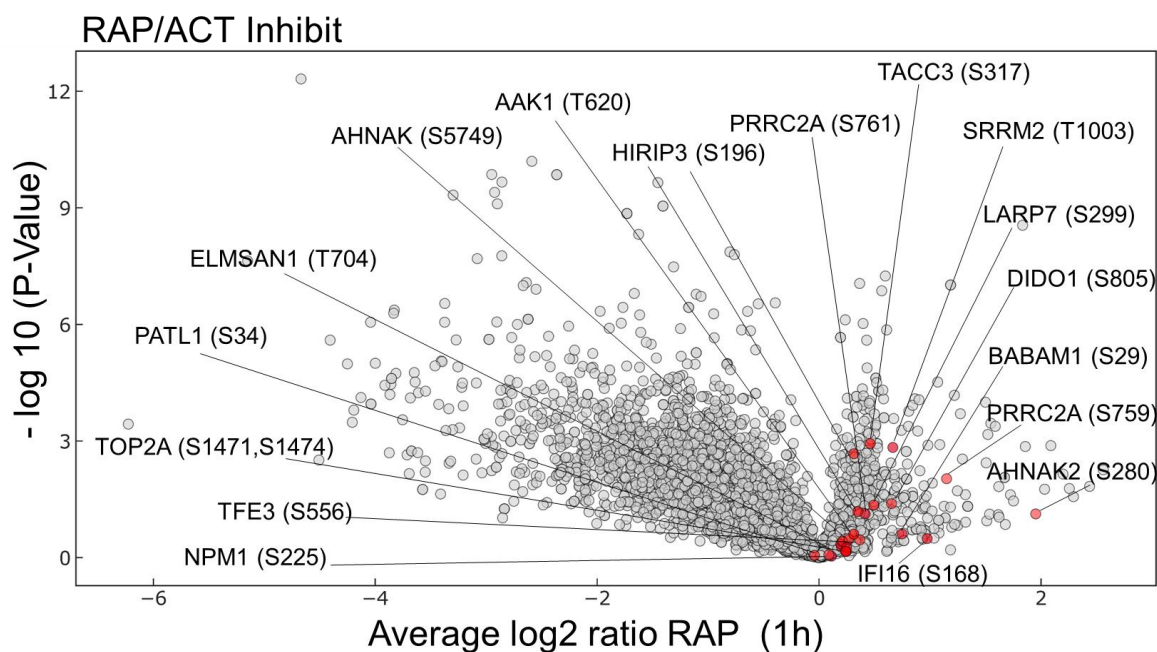


Figure 26 The distributions of phosphosite ratio and p-value of AZD/ACT group and RAP/ACT group for 1h.

The Heatmap of the representative log₂ ratio of phosphosites significant (p-value < 0.05). The log₂ ratio of phosphopeptide abundance of RAP/ACT and AZD/ACT showed different cluster profiles. RAP/ACT is upregulated (red bar), and AZD/ACT is downregulated (green bar) at 1h and 24h, respectively. A ratio of 1 means no change, > 1 means up-regulated, and < 1 means down-regulated. The top 18 changed phosphorylations of AZD8055 compared to Rapamycin inhibition at 1 hour in glioblastoma cell lines. These phosphorylated proteins were significantly decreased after AZD8055 treatment.

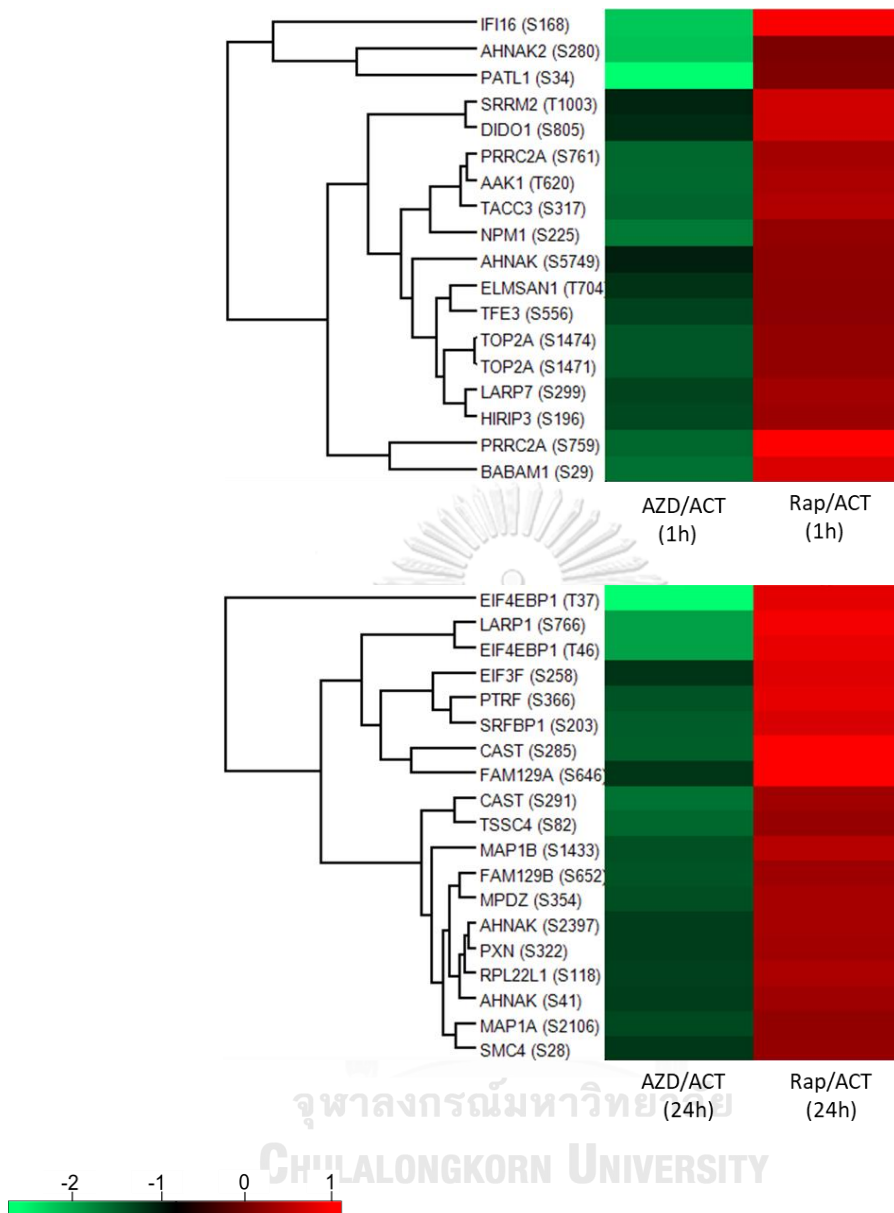


Figure 27 Heatmap of log₂ ratio of phosphosites significant (p-value < 0.05).

The top 18 changed phosphorylations at all 4 time points (1, 6, 24, 48 h.) of AZD8055 in glioblastoma cell lines. The ratio is an average log₂ ratio and significant (p < 0.05). Almost all phosphorylated proteins were significantly decreased after AZD8055 treatment and greatly decreased after 6 hours, as shown in Figure 14 and Table 5. Excitingly, phosphorylation of BABAM1 at serine 29 was reduced by more than 2-fold and was so much reduced after 6 hours

with AZD8055 treatment that it disappeared. Furthermore, the phosphorylation of PRRC2A on serine 761, SRRM2 on threonine 1003, and ELMSAN1 on threonine 704 are poorly known to have a biological function in the mTORC2 pathway. In addition, we discovered a novel site of KLC2 on serine 505 that has not yet been investigated.

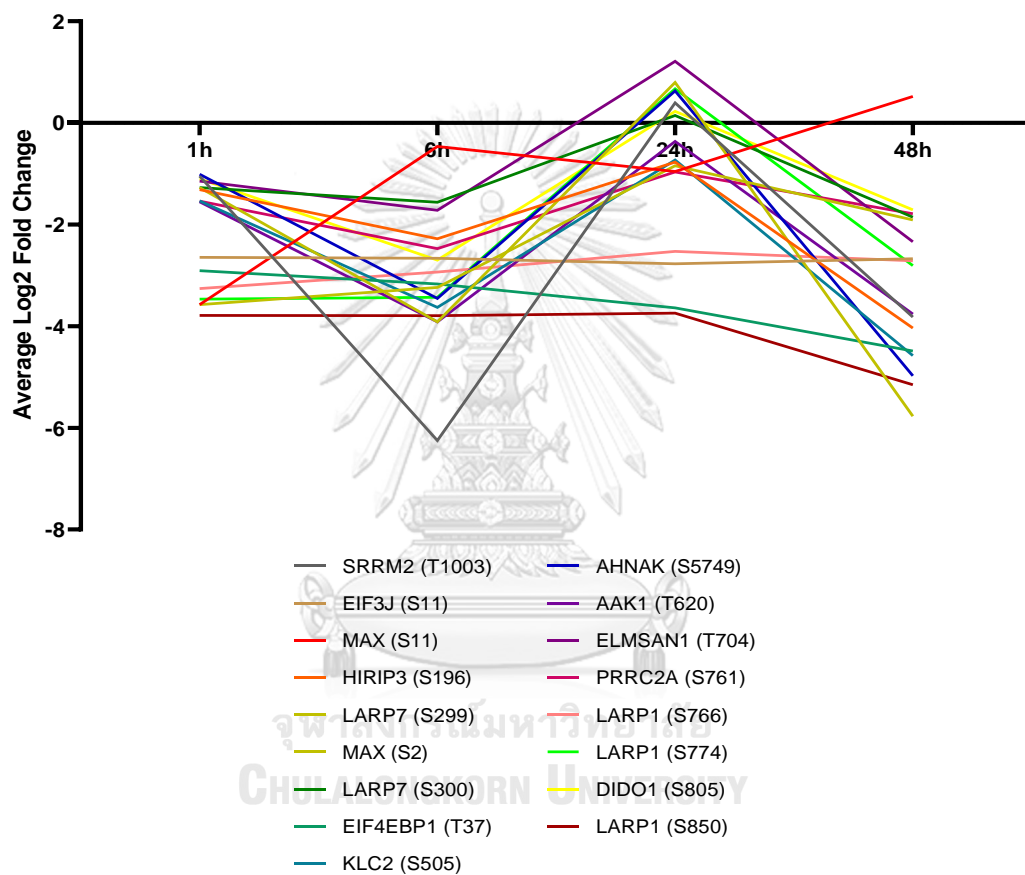


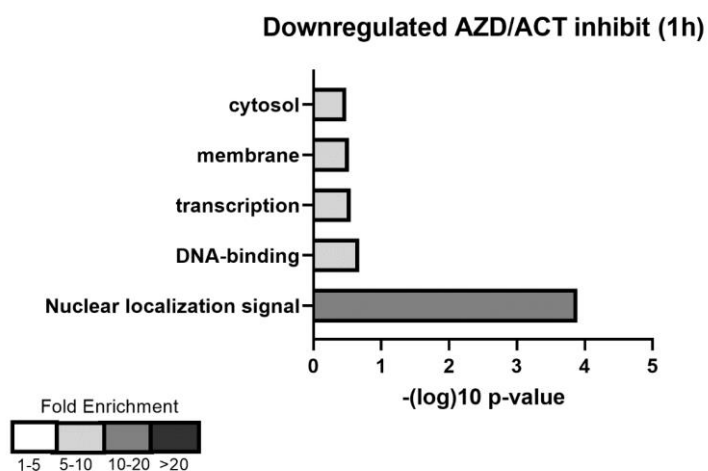
Figure 28 Average Log₂ fold change of the phosphorylation sites in AZD8055 inhibition at 4 time points.

gene name	amino acid	position	sequence	Ratio AZD/ACT 1h	Ratio AZD/ACT 6h	Ratio AZD/ACT 24h	Ratio AZD/ACT 48h
AAK1	T	620	TTPPPAVQGQKVGSLTPP SSPKTQRAGHRRRI	-1.55139	-3.91433	-0.36581	-3.76328
AHNAK	S	5749	ASISGSKGDLKSSKASLGS LEGEAEAEASSP	-1.01045	-3.45369	0.628868	-4.97755
BABAM1	S	29	EEEEHSAEPRPRTRSNPE GAEDRAVGAQAS	-1.612566	-	-1.323823	-1.703824
DIDO1	S	805	KKTAPRQEAIPLDLESDPPV SDSEEQQESARA	-1.10177	-2.69773	0.227299	-1.71081
EIF3J	S	11	MAAAAAAAGDSDSWDA DAFSVEDPVR	-2.64632	-2.66335	-2.77195	-2.67214
EIF4EBP1	T	37	VLGDGVQLPPGDYSTTPG GTLFSTTPGGTRI	-2.90932	-3.17118	-3.6374	-4.48682
ELMSAN1	T	704	KSAHRTLRLTNSAEVTPP VLSVMGEATPVSII	-1.1453	-1.71994	1.211249	-2.338
HIRIP3	S	196	APGKASVSRKQAREESEES EAEPVQRTAKKV	-1.31139	-2.27876	-0.77241	-4.03475
KLC2	S	505	GTPQEPPNPRMKRASSLN FLNKSVEEPTQPG	-1.53242	-3.63183	-0.72935	-4.5786
LARP1	S	766	ANKLFGAPEPSTIARSLPT TVPESPNYRNTR	-3.25777	-2.93284	-2.52911	-2.7148
LARP1	S	774	EPSTIARSLPTTVPESPNYR NTRTPRTPRTP	-3.46836	-3.43136	0.670993	-2.80772
LARP1	S	850	VMDSREHRPRTASISSSPS EGTPTVGSYGCT	-3.78705	-3.79118	-3.74285	-5.15163
LARP7	S	299	ASSLPEVRTGKRKRSSSED AESLAPRSKVKK	-1.27082	-3.91665	0.797496	-5.76895
LARP7	S	300	SSLPEVRTGKRKRSSSEDA ESLAPRSKVKKI	-1.27082	-1.56318	0.144155	-1.85524

MAX	S	11	MSDNDDIEVESDADKRAH HNALERKR	-3.57546	-0.46597	-0.95778	0.518629
MAX	S	2	MSDNDDIEVESDADKRA	-3.57546	-3.2351	-0.84106	-1.90719
PRRC2A	S	761	PGVHPSGLVPRERSDSGG SSSEPFDRHAPAM	-1.53749	-2.47501	-0.96673	-1.78904
SRRM2	T	1003	SHSGSISPYPKVKAQTPPG PSLSGSKSPCPQ	-1.04744	-6.24928	0.395787	-3.81843

Table 11 Characteristics of the 18 major phosphorylation sites in AZD8055 inhibition at 4 time points.

In the functional analysis, we used more than 2 fold of downregulated AZD/ACT data to upregulated Rap/ACT at 1 h and 24h, respectively. The most strongly enriched the nuclear localization signal ($P = 1.30E-04$). After DNA binding, transcription, membrane, and cytosol for AZD/ACT (1h), Inversely, the cytoskeleton was the most enriched ($P = 9.50E-07$). The AZD/ACT groupion was downregulated for 24 h, followed by cell-cell adhesion, cytoplasmic translation, microtubule association, and cell cycle. We hypothesized that downregulation of nuclear localization signaling and cytoskeleton phosphorylation should characterize mTORC2 functions in glioblastoma cells.



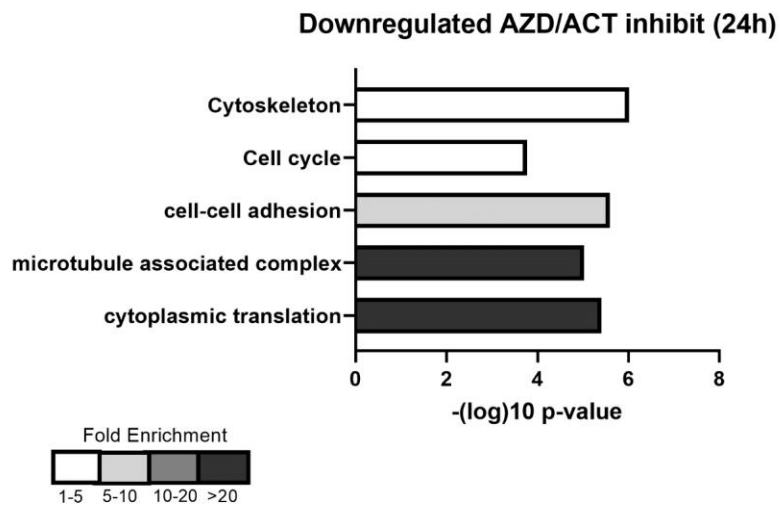


Figure 29 Functional annotations of more than 2 fold of downregulated AZD/ACT with upregulated Rap/ACT at 1 h and 24h.

We found a change in phosphorylation upon AZD8055 treatment for all of these phosphopeptides, which could be a potential target in mTORC2 signaling. Moreover, we discovered their multiple molecular functions and potential targets in the mTORC2 signaling pathway in GBM.

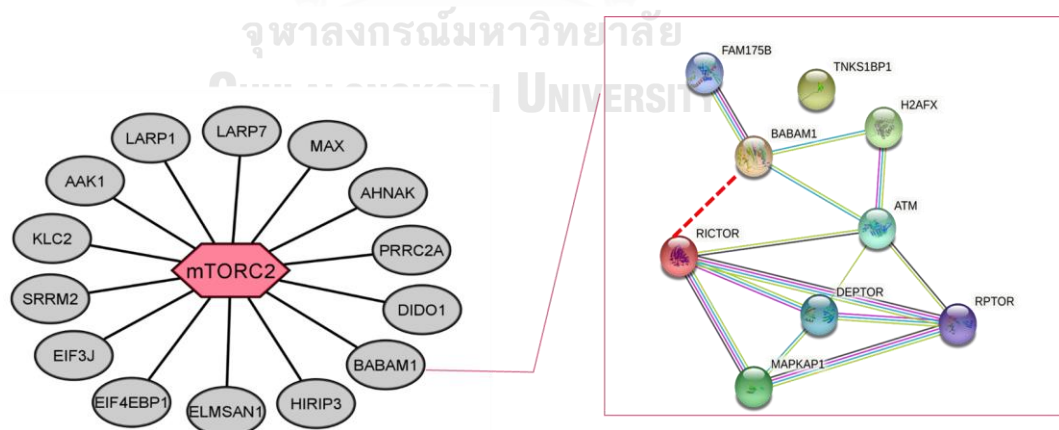
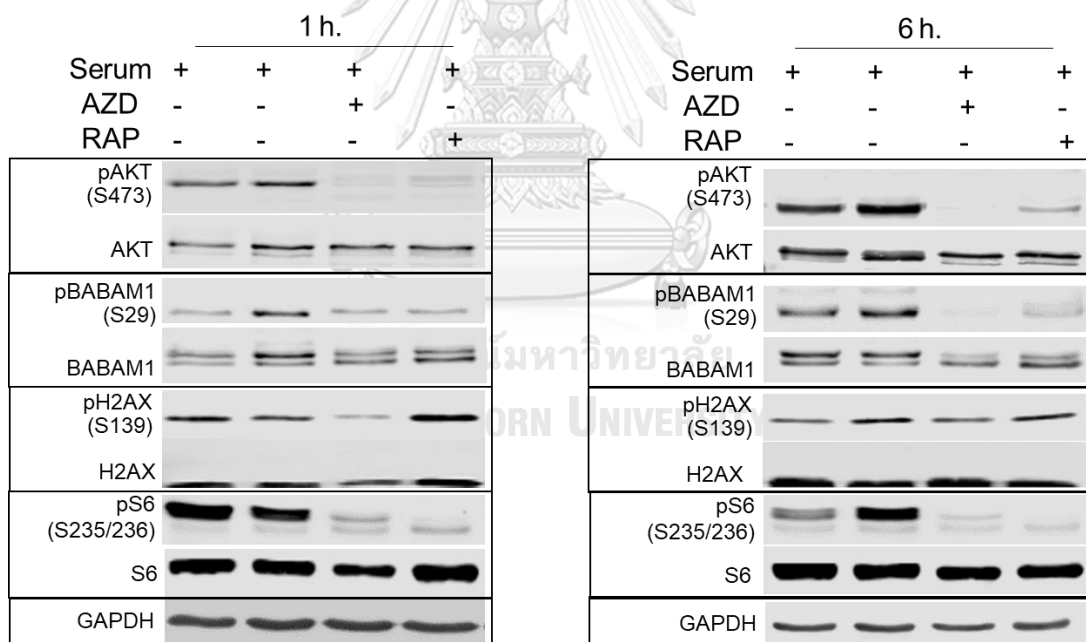


Figure 30 The classification of phosphoprotein interactions involved in mTORC2.

4.1.7 Effect of mTOR inhibitors on BABAM1 activity

AZD8055 is an mTORC1/2 inhibitor that directly affects Akt activation by decreasing phosphorylation at Ser473 in U87 glioblastoma cells. The results show that AZD8055 is able to significantly reduce the phosphorylation of BABAM1 at Ser29, also in parallel with the phosphorylation of histone H2A.X, a marker of DNA damage and genomic instability. Surprisingly, phosphorylation at Ser29 of BABAM1 is directly involved in downstream mTORC2 signaling. Inhibition of mTORC1/2 with AZD8055 is more effective than that of mTORC1 with Rapamycin, suggesting that mTORC2 plays a critical role in regulating DNA damage and repair. Additionally, specific knockdown of RICTOR (designed by Dharmacon™ Accell siRNA delivery) able to inhibit phosphorylation of BABAM1 at Ser29 and phosphorylation of histone H2A.X at Ser139.



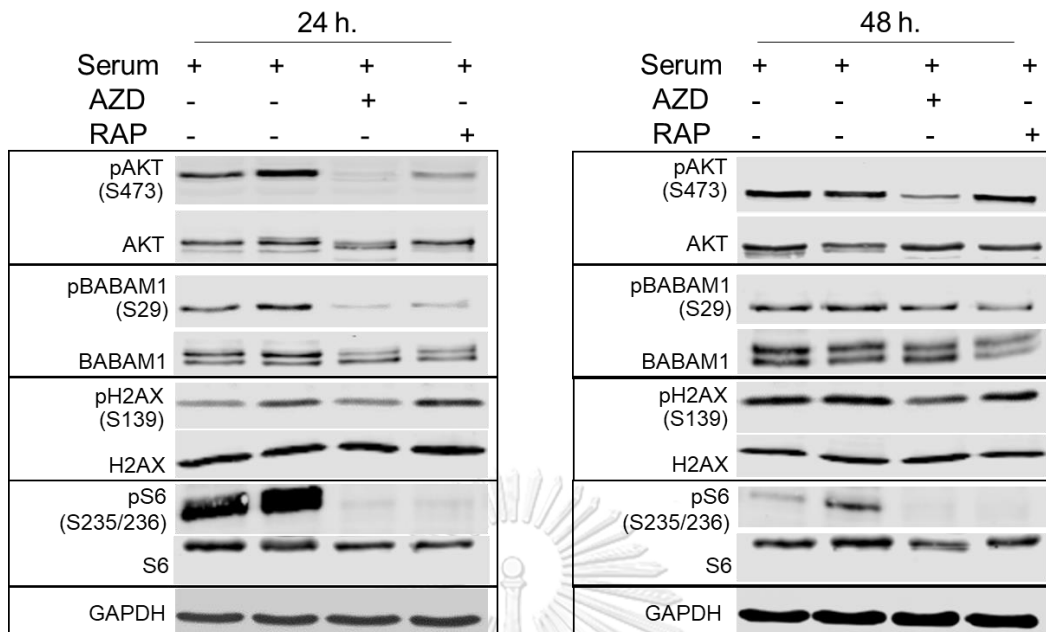


Figure 31 U87 cells were activated with 10% FBS, treated with 2 μ M AZD8055 and 0.1 μ M Rapamycin for 1, 6, 24 and 48 hours, respectively.

Additionally, specific knockdown of RICTOR (designed by Dhamacon™ Accell siRNA delivery) able to inhibit phosphorylation of BABAM1 at Ser29 and phosphorylation of histone H2A.X at Ser139. And confirm that mTORC2 could induce BABAM1 phosphorylation on S29 residue, the transient overexpression of the RICTOR gene was performed in U87MG cells. RICTOR overexpression able to significantly activated phosphorylation of AKT at Ser473 and BABAM1 at Ser29. Interestingly, BABAM1 is an mTORC2 downstream target phosphorylated via mTORC2 signaling recruit DNA damage, suggesting that mTORC2 is mainly involved in DNA damage and repair.

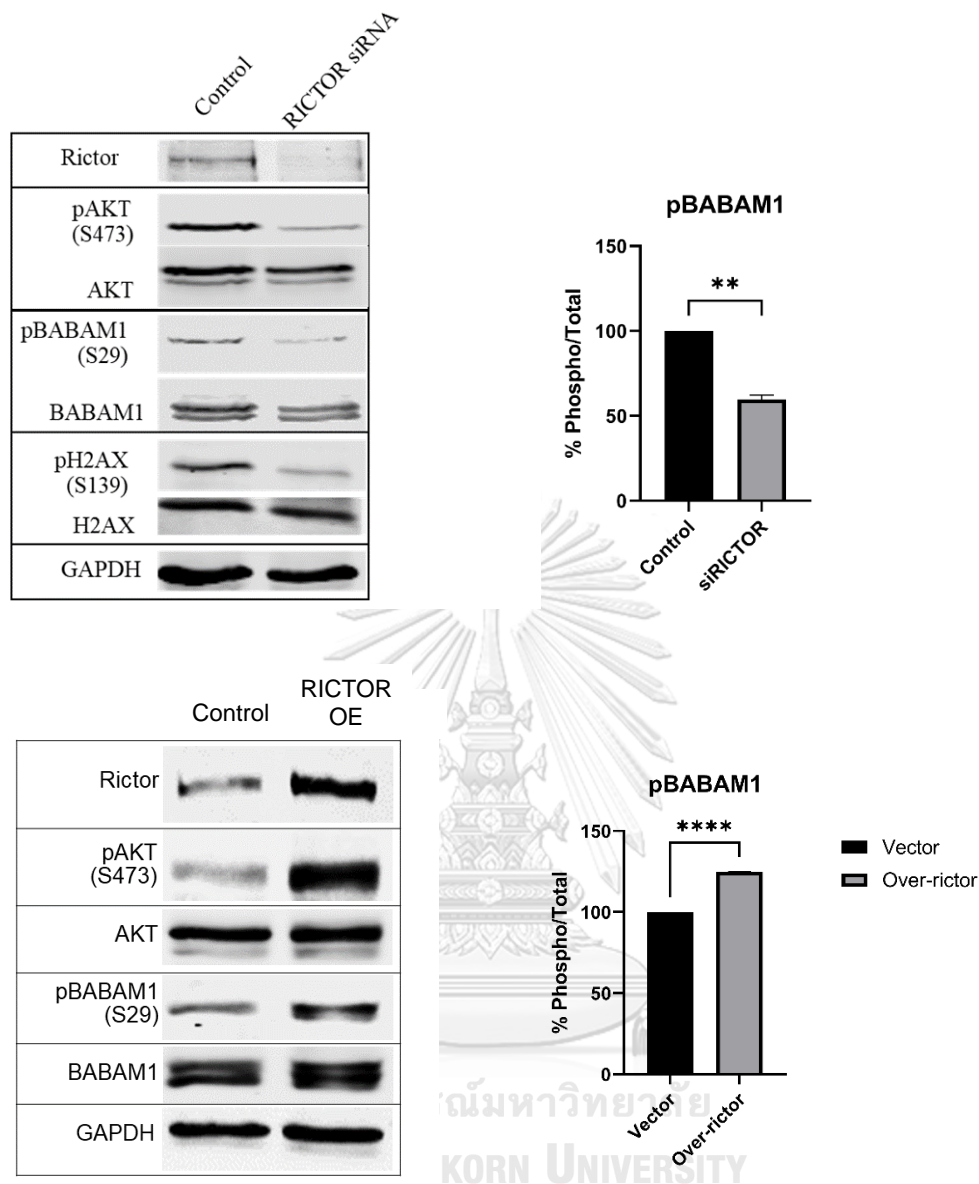


Figure 32 RICTOR siRNA and RICTOR overexpression

Previously, Brown et al. (2015) reported that purified recombinant Akt1, Akt2, or Akt3 can phosphorylate BABAM1 directly at Ser29 and that IGF-1 stimulation promoted phosphorylation of MERIT40, which was blocked in cells with BKM120, MK2206, and Torin1, but not with the mTORC1 inhibitor rapamycin. Remarkably, this was related to our quantitative phosphoproteomics data, which revealed that BABAM1 was dephosphorylated for 1 hour to 24 hours after treatment with the mTORC1/2 inhibitor AZD8055. The average log₂ fold change of AZD8055 to activation ratio (AZD/ACT) for 1 hour from BABAM1 to Ser29 was significantly decreased (p-value

< 0.05). Nevertheless, Rapamycin to activation (RAP /ACT) was increased almost 2-fold. At the same time, the intensity of phosphorylation of BABAM1 on Ser29 by AZD8055 inhibitor was decreased. In contrast, the intensity of total BABAM1 protein was increased when treated with AZD8055. Consequently, mTORC2 is the kinase associated with BABAM1 phosphorylation at Ser29 of the mTORC2 pathway in GBM.

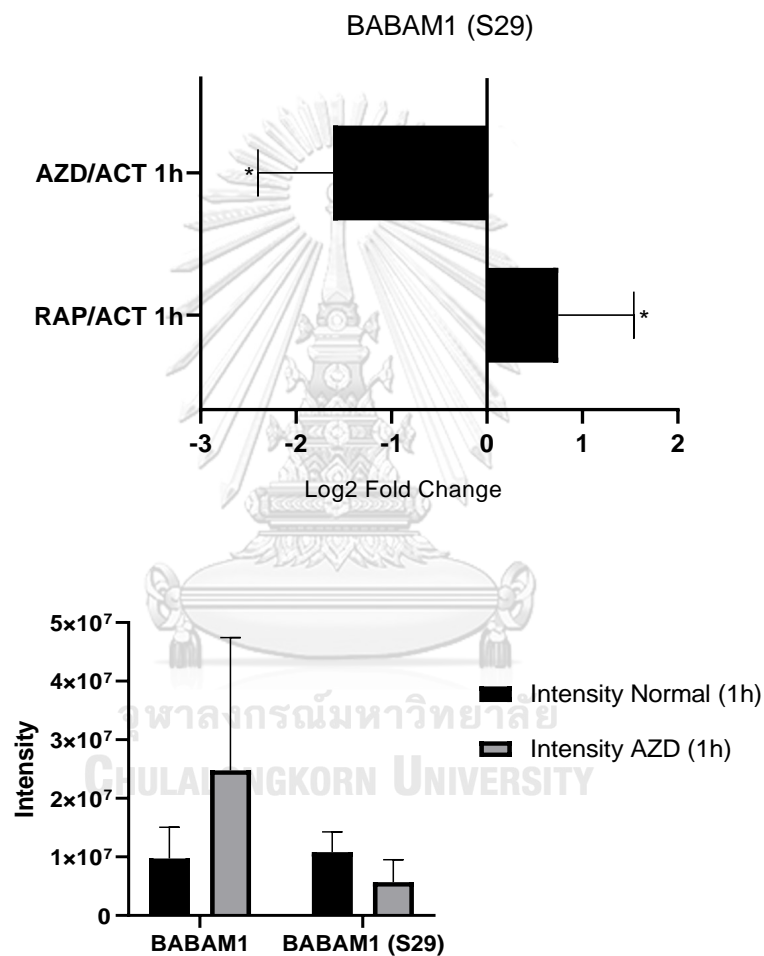


Figure 33 The log₂ fold change of pBABAM1 and The intensity of pBABAM1 and BABAM1

4.1.8 mTORC2 reveals the cellular response to DNA damage

We employed MTS assays to determine the effects of mTORC1/2 activity on cell survival after AZD8055 and Rapamycin exposure. Bar graphs showed the percentage of cell viability when U87 cells were activated with 10% FBS, treated with 2 μM AZD8055 and 0.1 μM Rapamycin after 24 h. Control was set at 100%. U87 cells growth was significantly increased (p-value <0.05) in activated with 10% FBS and treated with 0.1 μM Rapamycin, while U87 cells sustained in AZD8055 treatment indicated that AZD8055 stronger affected cells growth than Rapamycin. Inhibition of AZD8055 might be induced apoptosis in GBM.

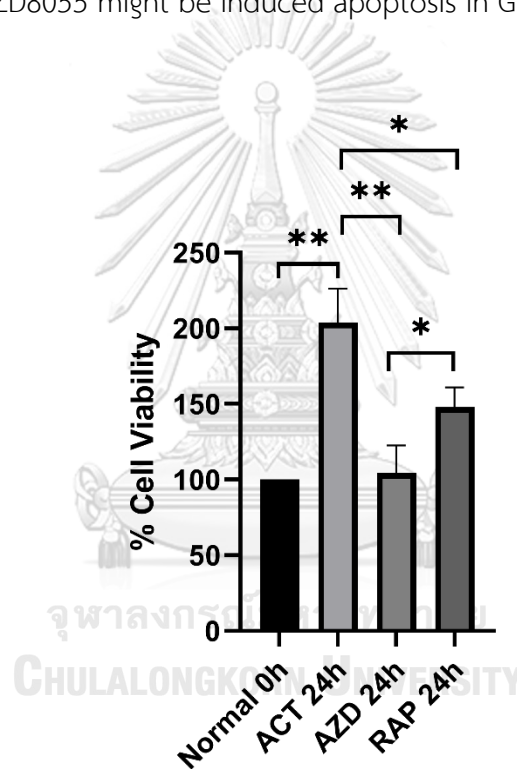


Figure 34 The percentage of Cell viability in different condition

We detected apoptosis using the Apoptosis/ Necrosis Detection Kit (ab176749) and measurement with a flow cytometer. U87 single cell was observed with an evidently different morphology of living cell (violet-stained), early apoptosis (green-stained), and late apoptosis (green- and red-stained).

Interestingly, in 2 μM AZD8055, U87 cells showed a higher rate of early apoptosis than control and raised late phase of apoptosis. We considered it

irreversible and critical to apoptotic cells' morphological changes, including membrane exposure, which Apopxin Green detected. The characteristic dot plots indicated the flow cytometric valuation of apoptosis compared to the control. This evidence fulfilled that mTORC2 inhibition leads to apoptosis and DNA damage response.

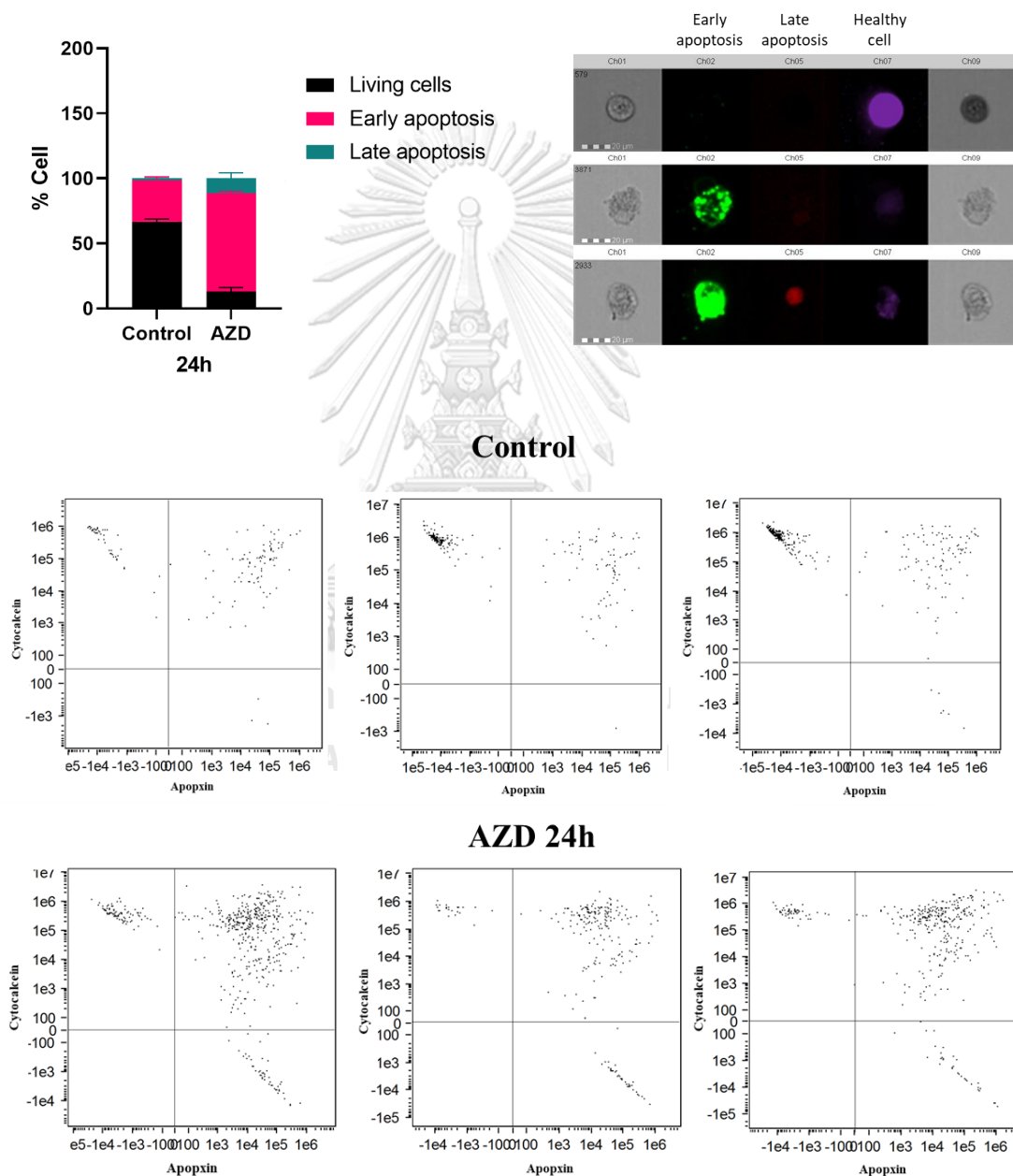


Figure 35 The flow cytometry measurement of apoptosis in AZD 24h

To determine whether BABAM1 phosphorylation at Ser29 residue promotes DNA repair in GBM cells and the loss of pBABAM1 (Ser29) would lead to cell apoptosis, we transiently overexpressed BABAM1 S29A mutant in U87MG cells in comparison to wild-type BABAM1 and the control cells. We found that the proliferation of GBM cells was significantly affected in the mutant group when observed at 48h after plasmid transfection. However, overexpression of wild-type BABAM1 did not induce cell proliferation in the GBM cells.

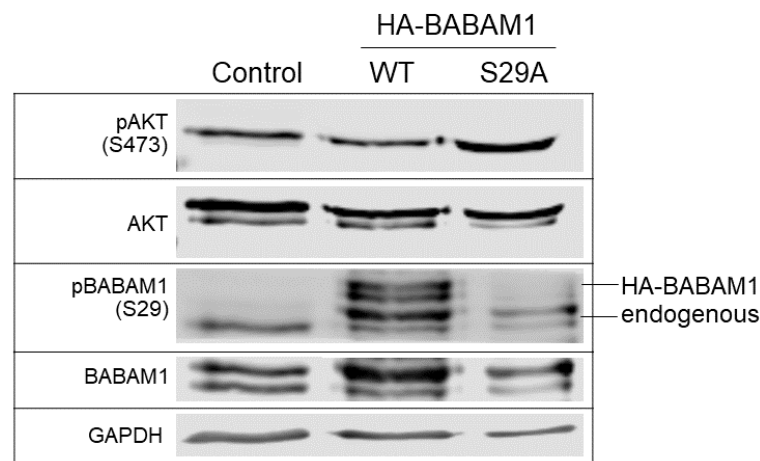


Figure 36 Western blotting analysis of BABAM1 overexpression in U87MG cells

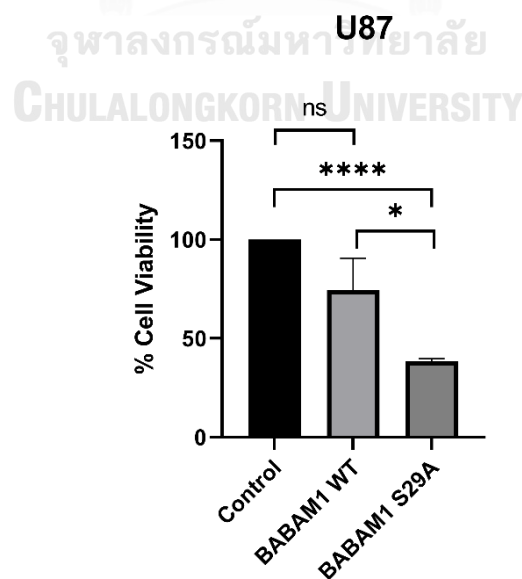
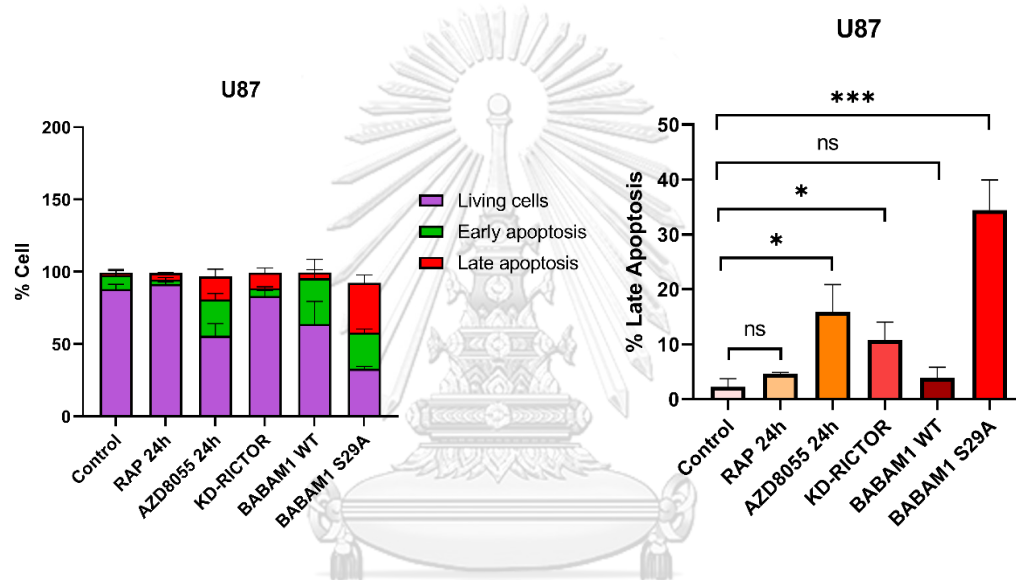


Figure 37 Cell viability of U87MG-overexpressing BABAM1

Next, we performed apoptosis assays and analyzed for percentages of late apoptotic cells in the samples from various conditions. As expected, GBM cells from mTORC2-inactivating conditions (AZD8055 and *RICTOR* knockdown) showed high late apoptosis rates as well as BABAM1 (S29A)-expressing cells while cells treated with rapamycin or overexpressing wild-type BABAM1 did not significantly promote apoptosis in GBM



Statistical significance was calculated using unpaired two-sided Student's *t*-test. All data are mean \pm SD: * $p < 0.05$, ** $p < 0.01$, *** $p < 0.001$, **** $p < 0.0001$, ns = not significant.

Figure 38 Percentages of early and late apoptotic cells in U87MG

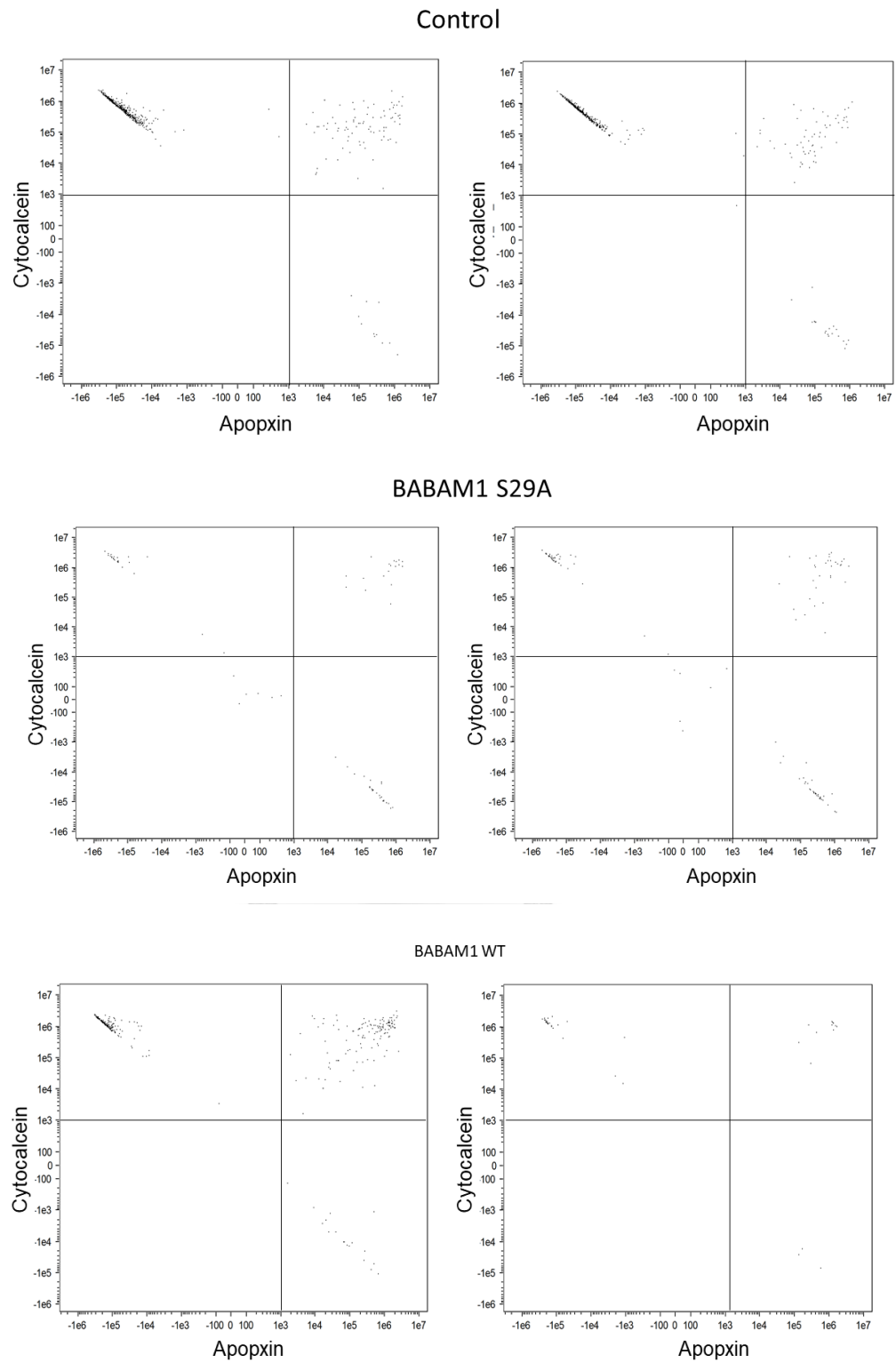


Figure 39 The flow cytometry measurement of apoptosis in BABAM1

We examined the localization of BABAM1. Colocalization of BABAM1, BRCA1-A complex subunit RAP80, and γ H2AX, the marker for DNA damage, in serum-activated and AZD8055-treated U87MG cells was observed by immunofluorescence staining. BABAM1 colocalized with γ H2AX and RAP80 in the nucleus and cytosol in mTORC2-activating conditions in both 1 and 24h groups (shown in orange). At the same time, AZD8055-treated cells demonstrated colocalization of BABAM1 and γ H2AX, particularly around the perinuclear region and cytosol but not in the nucleus. After 24-hour drug treatment, the aggregation of BABAM1 and γ H2AX outside the nucleus was clearly observed. The results suggested that the colocalization of BABAM1 and γ H2AX might be associated with mTORC2 inhibition and responsible for reducing the DNA repair machinery assembly in the nucleus.

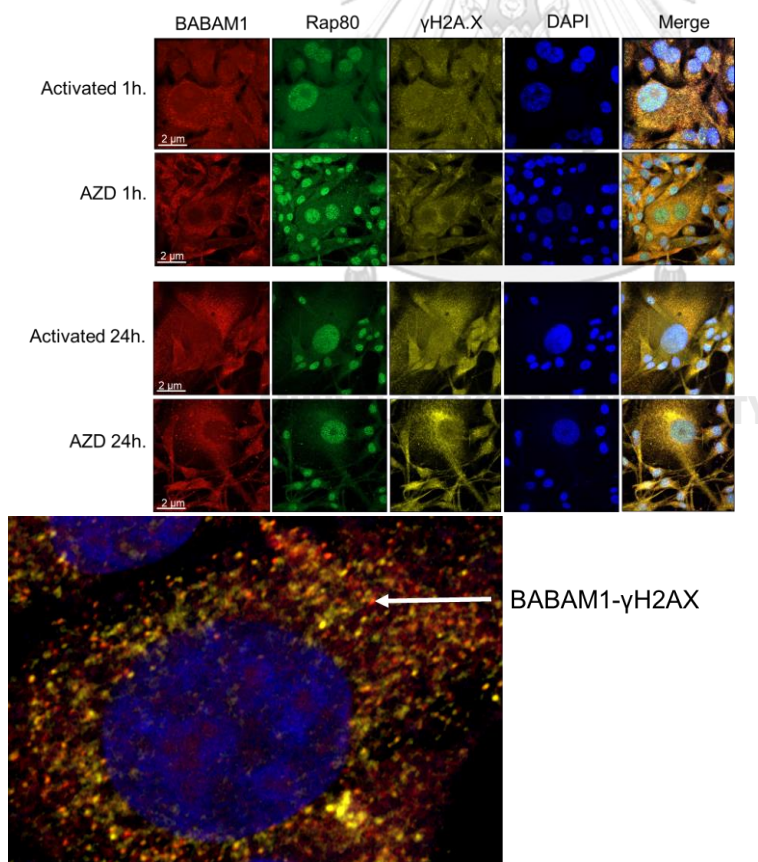


Figure 40 The co-localization of BABAM1, Rap80, and γ H2AX in serum activated and AZD8055 treatment for 1 and 24h.

We further validated the association between phosphorylated BABAM1 (Ser29) and its key interacting partner, BRCA1, under mTORC2-inhibiting conditions by immunofluorescence staining. The colocalization of BRCA1 and pBABAM1 in the nucleus was observed in an activation condition. In contrast, when pBABAM1 (Ser29) was inhibited by AZD8055 treatment, the nuclear localization of BABAM1 protein and the formation of BRCA1-A complex would be strongly affected, while U87MG cells under rapamycin treatment showed similar results as the activated cells.

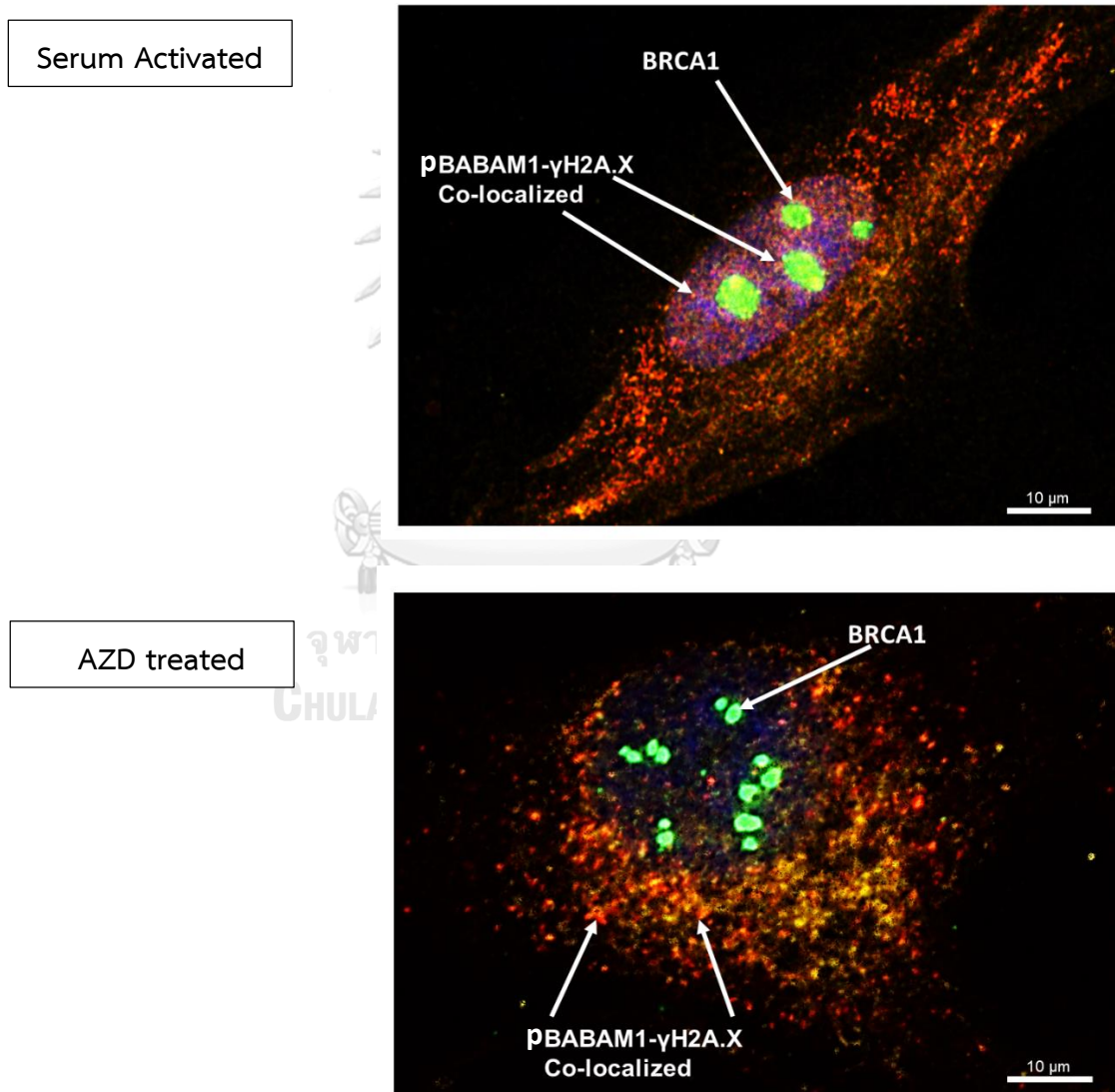


Figure 41 The co-localization of pBABAM1 (s29), BRCA1, and γH2AX in serum activated and AZD8055 treatment

4.1.9 mTORC2 phosphorylated BABAM1 on ser29 to promotes DNA repair

We studied co-immunoprecipitation to confirm that BABAM1 is a downstream target of mTORC2 signaling in immunoblotting and mass spectrometry analysis of BABAM1 pulldown protein. We found the components involved in DNA damage response (DDR), a tankyrase-1 binding protein (TNKS1BP1), and γ H2AX, including Rictor, a major component of mTORC2.

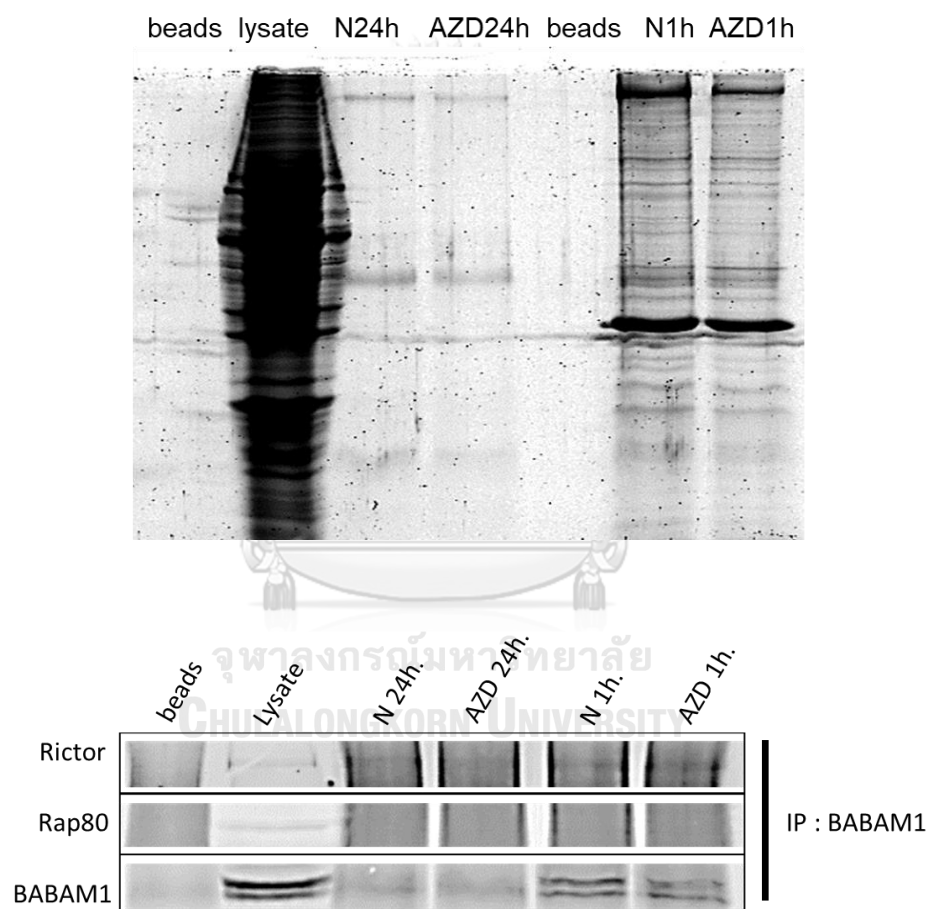


Figure 42 Co-immunoprecipitation of BABAM1

Accession	Protein names	Gene name	Unique Peptides	Coverage	Sum PEP Score	Score Sequest HT
P12956	X-ray repair cross-complementing protein 6	XRCC6	27	49.58949097	191.193	500.69
P78527	DNA-dependent protein kinase catalytic subunit	PRKDC	39	10.02906977	131.659	161.3
P62805	Histone H4	HIST1H4A	12	64.0776699	127.917	794.41
P55072	Transitional endoplasmic reticulum ATPase	VCP	22	34.73945409	117.708	334.99
P23396	40S ribosomal protein S3	RPS3	15	62.96296296	88.994	481.73
P13010	X-ray repair cross-complementing protein 5	XRCC5	17	27.04918033	83.87	172.81
P33993	DNA replication licensing factor MCM7	MCM7	13	25.17385257	57.163	89.72
P16104	Histone H2AX	H2AFX	1	54.54545455	44.606	189.48
Q16531	DNA damage-binding protein 1	DDB1	10	11.14035088	40.866	48.6
Q9NWW8	BRISC and BRCA1-A complex member 1	BABAM1	6	36.17021277	33.52	66.79
P52292	Importin subunit alpha-1	KPNA2	7	16.25708885	32.398	73.04
P31689	DnaJ homolog subfamily A member 1	DNAJA1	6	22.92191436	29.032	99.22
P09874	Poly [ADP-ribose] polymerase 1	PARP1	8	10.35502959	28.867	36.37
P33992	DNA replication licensing factor MCM5	MCM5	7	12.39782016	24.148	14.89
P82933	28S ribosomal protein S9, mitochondrial	MRPS9	4	14.8989899	23.811	30.45
Q9C0C2	182 kDa tankyrase-1-binding protein	TNKS1BP1	6	5.725853094	22.036	37.24
Q14566	DNA replication licensing factor MCM6	MCM6	6	7.795371498	21.877	22.21
Q9UMS4	Pre-mRNA-processing factor 19	PRPF19	5	16.46825397	20.566	42.56

P49736	DNA replication licensing factor MCM2	MCM2	5	7.411504425	20.297	18.08
Q92499	ATP-dependent RNA helicase DDX1	DDX1	5	10.40540541	17.307	25.26
P40937	Replication factor C subunit 5	RFC5	5	20.58823529	17.222	34.38
Q9NXR7-1	Isoform 1 of BRISC and BRCA1-A complex member 2	BABAM2	4	11.56626506	15.71	14.59
P27694	Replication protein A 70 kDa DNA- binding subunit	RPA1	4	9.253246753	15.207	4.71
O00487	26S proteasome non-ATPase regulatory subunit 14	PSMD14	3	13.87096774	14.86	26.13
P40938	Replication factor C subunit 3	RFC3	3	8.707865169	12.238	12.14
P09429	High mobility group protein B1	HMGB1	3	13.48837209	9.988	5.76
P35249	Replication factor C subunit 4	RFC4	2	8.26446281	9.593	16.64
P12004	Proliferating cell nuclear antigen	PCNA	2	12.2605364	8.463	17.22
Q6R327-3	Isoform 3 of Rapamycin-insensitive companion of mTOR	RICT	4	2.251732102	8.388	2.07
P33991	DNA replication licensing factor MCM4	MCM4	4	4.982618772	7.596	6.82
P35244	Replication protein A 14 kDa subunit	RPA3	2	22.31404959	7.381	16.73
P82912	28S ribosomal protein S11, mitochondrial	MRPS11	2	8.762886598	7.309	15.43
P35250	Replication factor C subunit 2	RFC2	3	12.71186441	7.023	8.55
Q15645	Pachytene checkpoint protein 2 homolog	TRIP13	2	5.787037037	6.85	20.44
P43246	DNA mismatch repair protein Msh2	MSH2	2	2.676659529	6.385	5.13
Q13620	Cullin-4B	CUL4B	2	2.73822563	6.368	14.58
P39748	Flap endonuclease 1	FEN1	2	8.157894737	5.454	10.79
P25205-2	Isoform 2 of DNA replication licensing factor MCM3	MCM3	2	2.227432591	4.974	8.59

Table 12 The associated proteins from BABAM1 IP to involved in DNA damage response and repair

We then confirmed the interaction of BABAM1 with mTORC2 complex with Rap80 pulldown protein for 1 and 6h. We added the 6h condition for this experiment because the global phosphoproteome dataset showed that the phosphorylation of BABAM1 at serine 29 was reduced by more than 2-fold for 1h and was highly reduced after 6 hours with AZD8055 treatment that it disappeared. In immunoblotting of Rap80 pulldown protein showed that BABAM1 and γ H2AX were reduced after AZD8055 treatment.

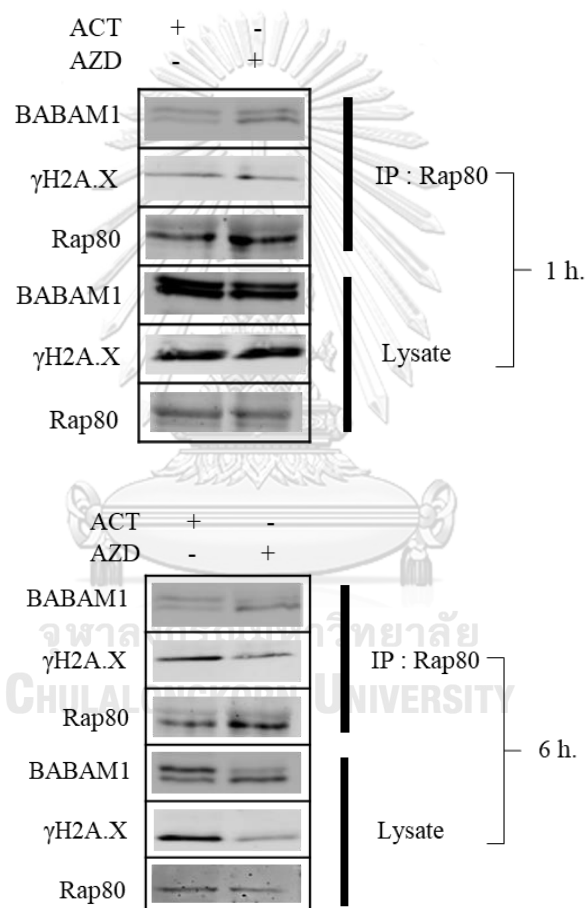


Figure 43 Co-immunoprecipitation of Rap80

In addition, Co-immunostaining of U87 cells was confirmed again for 6h with stable knockdown RICTOR, which RT-PCR confirmed to have a 2-fold lower RICTOR gene expression.

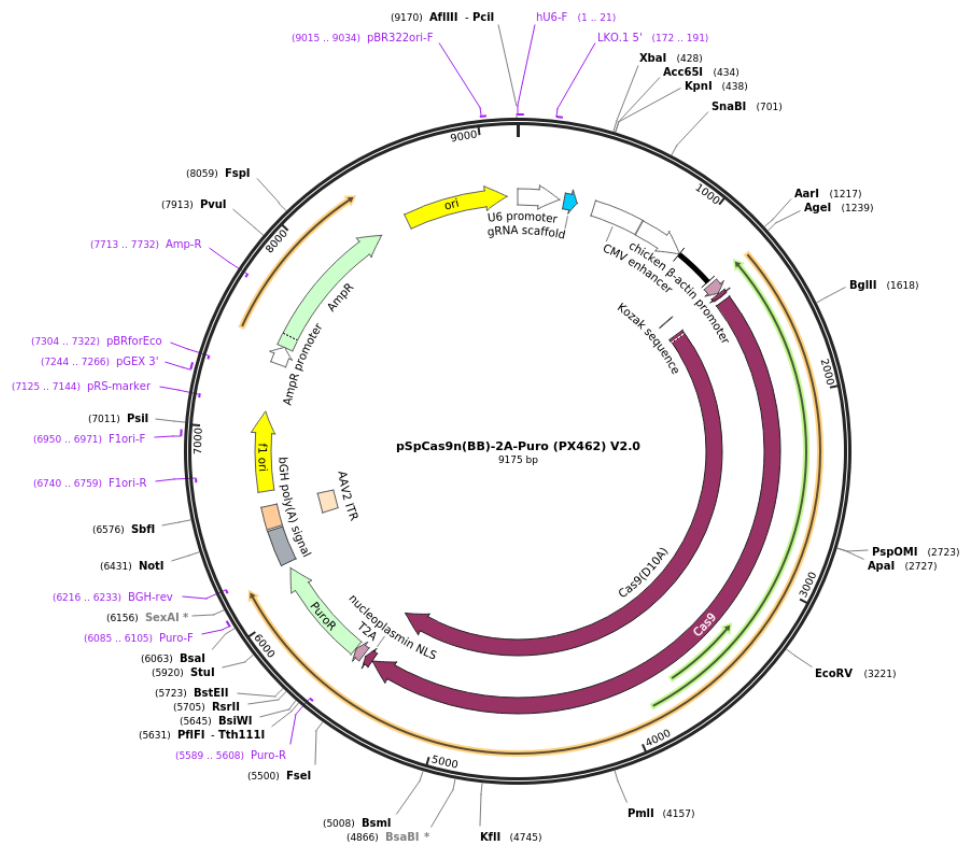


Figure 44 Figure Vectors of stable RICTOR knockdown gene.

For stable RICTOR knockdown cells, RICTOR gene were constructed in pSpCas9n(BB)-2A-Puro (PX462) V2.0. plasmids were transfected into U87 cells using lipofectamine P3000. The infected cells were then selected by puromycin 5µg/ml.

Oligo name	Sequence 5' → 3'
hsRICTOR_Start_Left_top	CACCGTGAAGAACCTCCGAGTACGAGG
hsRICTOR_start_Left_bottom	AAACCGGGTTTCAGTCACAACACCGGC
hsRICTOR_Start_Right_top	CACCGTGAAGAACCTCCGAGTACGAGG
hsRICTOR_Start_Right_bottom	AAACCCTCGTACTCGGAGGTTCTTCAC
hsRICTOR_g934_Left_top	CACCGCCAATCTTTTGAAAGAGTGAC
hsRICTOR_g934_Left_bottom	AAACGTCACTCTTTCAAAGATTTGGC
hsRICTOR_g934_Right_top	CACCGAAATATCGGCTCATCAAATTGG
hsRICTOR_g934_Right_bottom	AAACCCAATTTGATGAGCCGATATTC

Table 13 RICTOR gene sequence

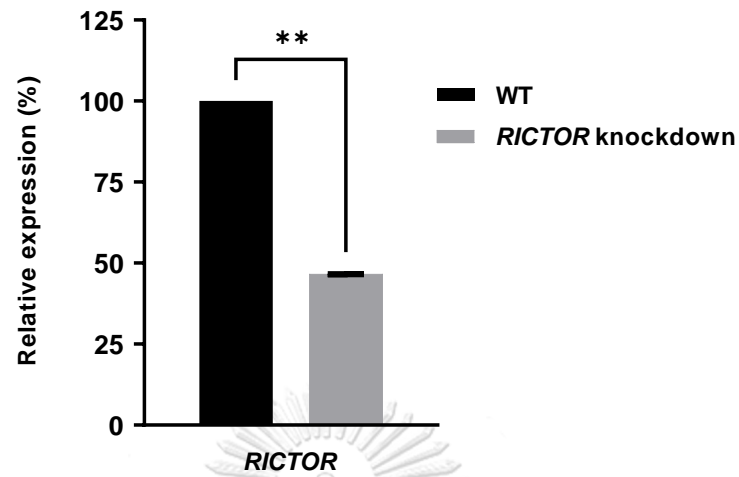


Figure 45 RICTOR gene expression.

Knockdown RICTOR and AZD8055 treatment appeared to co-localize BABAM1 and γ H2AX around the nuclear membrane and cytosol, whereas serum activated, BABAM1 co-localized with γ H2AX found in the nucleus and cytosol. Believable, BABAM1 interacts with the mTORC2 complex.

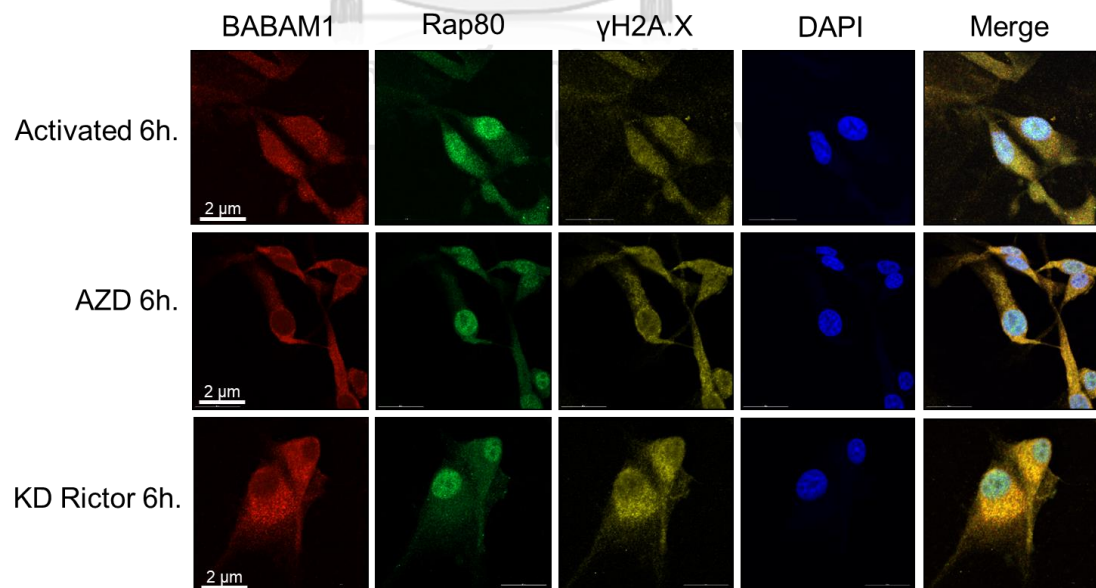


Figure 46 Immunofluorescence staining: U87 cells were Activated with serum, 2 μ M AZD8055, and knockdown Rictor for 6h

This result suggests that inhibition of the mTORC2 complex directly decreased the phosphorylation of BABAM1 on ser29, lead to reduce DNA repair signaling. This experiment confirmed that BABAM1 is a potential downstream target of mTORC2 signaling that plays a vital role in repairing DNA damage to DNA double-strand breaks (DSBs) in GBM.

4.2 Discussion

Most research on the mTOR pathway in GBM has historically focused on the use of Rapamycin, which mainly blocks mTORC1 activity but not mTORC2. Therefore, the resistance of mTORC2 downstream target phosphorylation to Rapamycin likely contributes to the low efficacy of Rapamycin in glioblastoma. The mTORC2 signaling is regulated in various processes of cancer cells, such as cell proliferation, apoptosis, cytoskeletal organization, metabolic reprogramming, and cellular stress response (65). Recently, phosphorylation events have been widely recognized as a central player in tumor growth of human glioblastoma (61). In a phosphoproteomics study, the authors reported no changes in stemness marker gene expression after therapy responsive and recurrence or resistance in GBM model (66). Phosphoproteomic analysis's potential helps identify targets for drug treatment in GBM patients (67). Although phosphorylation events in GBM have been studied in numerous biological backgrounds (68), it is essential to understand the molecular mechanisms underlying the aberrant signaling in order to develop potential therapeutic targets.

BABAM1 regulation and function in mTORC1/mTORC2 inhibitor in cancer

BABAM1 or MERIT40 are components of the BRCA1-A complex that direct DNA repair. The BRCA1-A complex, which includes BRCA1, BRE, BRCC36, Abraxas, Rap80, and BABAM1, forms at sites of DNA double-strand breaks (DSBs) and contributes to DNA damage repair by BRE and BABAM1 stabilizing this complex and maintaining the localization of the BRCA1-A complex at DSBs (69).

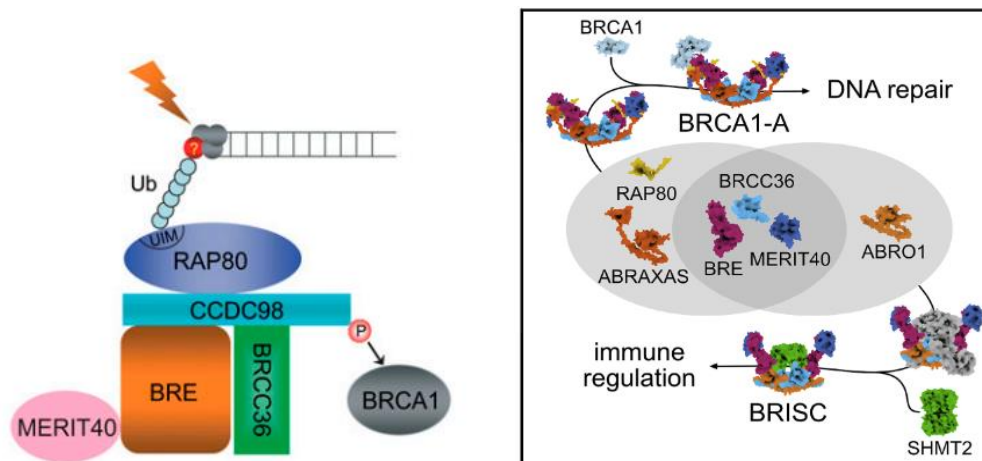


Figure 47 BRCA1-A complex in DNA repair

Inhibition of Akt signaling and BABAM1 phosphorylation has been reported to sensitize breast cancer cells to doxorubicin-induced DNA damage, execution of HRR, and survival (70). In addition, studies found that Akt phosphorylates a protein of the BRCA1 complex, the mediator of Rap80 interactions, and targets BABAM1 on Ser29. And BRCA1 co-localizes with γ H2AX to recruit the DNA damage response protein to repair double-strand breaks. These support our study; it is possible that mTORC2 phosphorylates BABAM1 via the mTOR signaling pathway. However, the role of mTORC2-associated phosphorylation of BABAM1 in cellular response and DNA damage repair in GBM has not been explored and remains elusive. Accordingly, we investigated whether mTORC1/2 signaling might play a role in the phosphorylation of BABAM1 in the repair of double-strand breaks in glioblastoma cells.

The BRCA1 complex is recruited to DNA double-strand breaks (DSBs) via the ubiquitin-binding motifs (UIMs) of RAP80 (71). In addition, tankyrase has been reported to associate directly with BABAM1 and form a complex with BABAM1-BRE-BRCC36. Inhibition of tankyrase-BABAM1 or tankyrase-PARP results in abnormal function in DNA repair (72). In the context of our LC-MS /MS analysis,

Rap80, BRCA1, and tankyrase were also identified. In addition, a recent study demonstrated that mTORC2, as an interaction partner with the tBRCT domain of BRCA1, leads to a DNA damage response (DDR) and that lack of expression of functional BRCA1 in breast cancer is more sensitive to mTOR inhibitors (73).

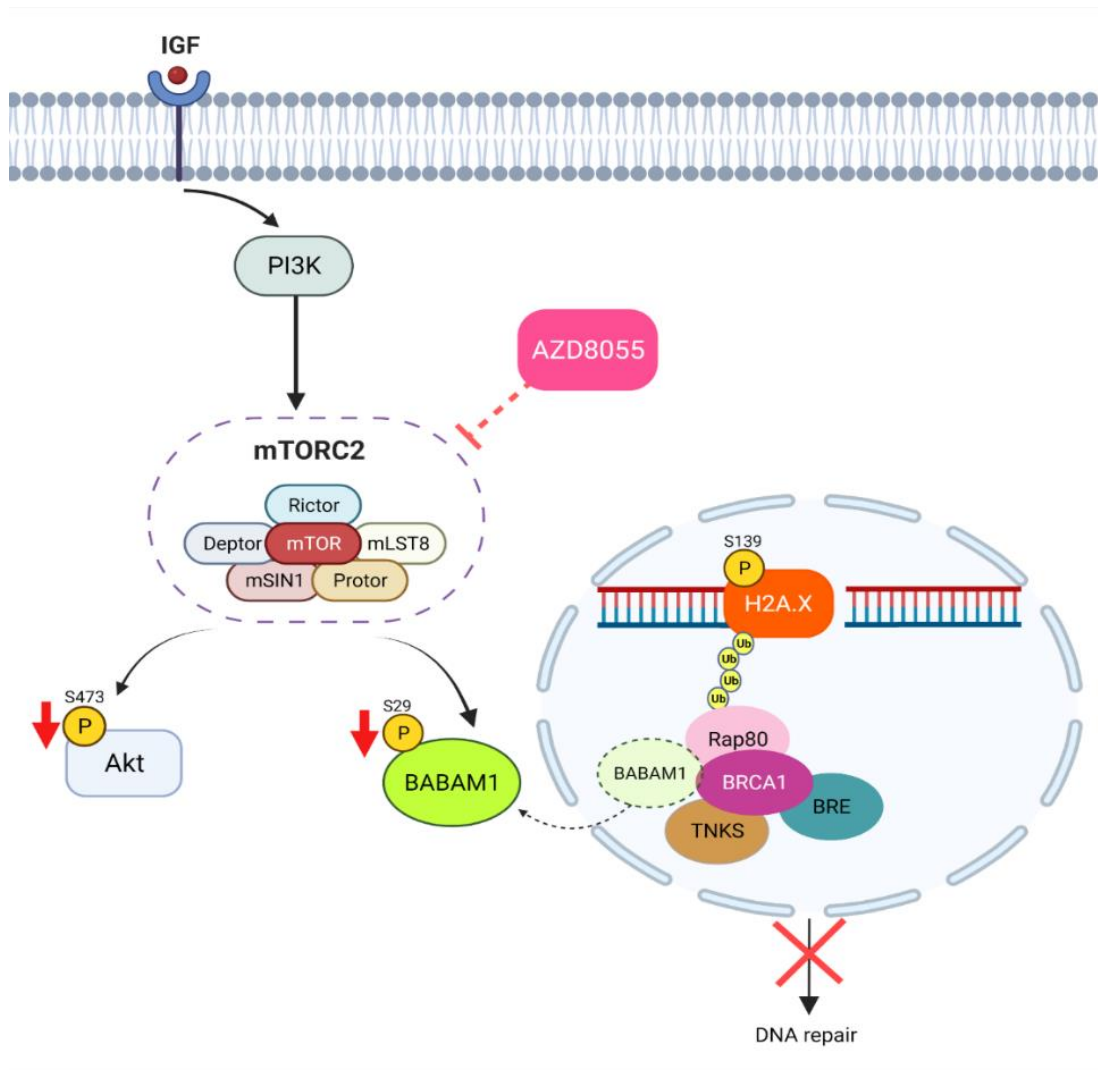


Figure 48 A schematic model of mTORC2 complex associated with DNA damage response by AZD80855 inhibitor

CHAPTER V

CONCLUSION

In this study, we investigated the phosphorylation of proteins in the U87MG glioblastoma cell line under mTOR conditions. The U87MG was treated with the mTORC1/mTORC2 inhibitor AZD8055 and the mTORC1 inhibitor rapamycin to elucidate which proteins with different phosphorylation changes are involved in mTORC2 functions. The stable isotope-labeled (dimethyl labeling) technique was used for comparative quantification. Phosphopeptides were enriched using the High-Select™ TiO₂ Phosphopeptide Enrichment Kit and fractionated into 20 fractions/sample to greatly enhance the number of phosphopeptides isolated from complex cell lysate. The phosphoproteomic fractions were analyzed using the orbitrap LCMS/MS. Massive data was computed with bioinformatics software. We observed the several phosphopeptides and phosphosites involved in mTORC2 signaling. The phosphorylation profile was looked at for downregulated phosphopeptides in AZD/ACT group (p-value <0.05). Compared with upregulated RAP/ACT group (p-value <0.05) at 1 and 24 hours by using Gene Ontology Annotations from DAVID tools analysis. We discovered the multiple molecular functions and potential downstream targets in the mTORC2 signaling pathway in GBM. One of them was BABAM1. So, we demonstrated the phosphorylation of BABAM1 at Ser29 to confirm the mTORC2-associated protein and its role in promoting aggressive characteristics of glioblastoma cells. We used siRNA-RICTOR knockdown; after presence treated with AZD8055, pBABAM1 on ser29 was dephosphorylated. Relatively, co-immunofluorescence in stable knockdown-RICTOR showed that BABAM1 was not present on nuclei, which affects DNA repair and causes apoptosis through the mTORC2. In addition, the novel associated phosphopeptides of mTORC2 were discovered, such as PRRC2A on ser761, SRRM2 on thr1003, ELMSAN1 on thr704, and novel phosphosite of KLC2 on ser505. In the mTORC2 pathway, these proteins are still poorly known to have a biological function. These might be investigated in further studies.

In conclusion, quantitative phosphoproteomics can determine changing phosphorylation patterns affected by the aberration of the mTOR signaling pathway and associated with brain cancer progression. And dysregulation of some phosphorylated proteins necessary for glioblastoma survival in the mTOR signaling pathway. Furthermore, this study helps to understand the mechanism and components of the mTOR pathway, which might be potential targets to inhibit the metastasis of glioblastoma.



REFERENCES

1. Lovely MP. Symptom management of brain tumor patients. *Semin Oncol Nurs.* 2004;20(4):273-83.
2. Li S. Mechanisms of cellular signal transduction. *Int J Biol Sci.* 2005;1(4):152.
3. Anagnostopoulos AK, Tsangaris GT. The proteomics of pediatric brain tumors. *Expert Rev Proteomics.* 2014;11(5):641-8.
4. Gilbert MR, Dignam JJ, Armstrong TS, Wefel JS, Blumenthal DT, Vogelbaum MA, et al. A randomized trial of bevacizumab for newly diagnosed glioblastoma. *N Engl J Med.* 2014;370(8):699-708.
5. Ohgaki H, Kleihues P. The definition of primary and secondary glioblastoma. *Clin Cancer Res.* 2013;19(4):764-72.
6. Ohgaki H, Kleihues P. Genetic pathways to primary and secondary glioblastoma. *Am J Pathol.* 2007;170(5):1445-53.
7. Sever R, Brugge JS. Signal transduction in cancer. *Cold Spring Harb Perspect Med.* 2015;5(4).
8. Chandrika G, Natesh K, Ranade D, Chugh A, Shastry P. Suppression of the invasive potential of Glioblastoma cells by mTOR inhibitors involves modulation of NFkappaB and PKC-alpha signaling. *Sci Rep.* 2016;6:22455.
9. Zou Z, Tao T, Li H, Zhu XJC, Bioscience. mTOR signaling pathway and mTOR inhibitors in cancer: Progress and challenges. 2020;10(1):1-11.
10. Ricoult SJ, Yecies JL, Ben-Sahra I, Manning BDO. Oncogenic PI3K and K-Ras stimulate de novo lipid synthesis through mTORC1 and SREBP. 2016;35(10):1250-60.
11. Wang B, Jie Z, Joo D, Ordureau A, Liu P, Gan W, et al. TRAF2 and OTUD7B govern a ubiquitin-dependent switch that regulates mTORC2 signalling. 2017;545(7654):365-9.
12. Xie X, Hu H, Tong X, Li L, Liu X, Chen M, et al. The mTOR-S6K pathway links growth signalling to DNA damage response by targeting RNF168. 2018;20(3):320-31.
13. Laplante M, Sabatini DM. mTOR signaling at a glance. *J Cell Sci.* 2009;122(Pt 20):3589-94.

14. Mecca C, Giambanco I, Bruscoli S, Bereshchenko O, Fioretti B, Riccardi C, et al. PP242 counteracts glioblastoma cell proliferation, migration, invasiveness and stemness properties by inhibiting mTORC2/AKT. 2018;12:99.
15. Masui K, Harachi M, Ikegami S, Yang H, Onizuka H, Yong WH, et al. mTORC2 links growth factor signaling with epigenetic regulation of iron metabolism in glioblastoma. 2019;294(51):19740-51.
16. Holmes B, Benavides-Serrato A, Saunders JT, Kumar S, Nishimura RN, Gera JJN. mTORC2-mediated direct phosphorylation regulates YAP activity promoting glioblastoma growth and invasive characteristics. 2021;23(9):951-65.
17. Oh WJ, Jacinto E. mTOR complex 2 signaling and functions. *Cell Cycle*. 2011;10(14):2305-16.
18. Fu W, Hall MNJG. Regulation of mTORC2 signaling. 2020;11(9):1045.
19. Chantaravisoot N, Wongkongkathep P, Loo JA, Mischel PS, Tamanoi FJMc. Significance of filamin A in mTORC2 function in glioblastoma. 2015;14(1):1-14.
20. Harsha HC, Pandey A. Phosphoproteomics in cancer. *Mol Oncol*. 2010;4(6):482-95.
21. Ramroop JR, Stein MN, Drake JM. Impact of Phosphoproteomics in the Era of Precision Medicine for Prostate Cancer. *Front Oncol*. 2018;8:28.
22. Martinez Calejman C, Trefely S, Entwisle SW, Luciano A, Jung SM, Hsiao W, et al. mTORC2-AKT signaling to ATP-citrate lyase drives brown adipogenesis and de novo lipogenesis. *Nat Commun*. 2020;11(1):575.
23. Aldape K, Brindle KM, Chesler L, Chopra R, Gajjar A, Gilbert MR, et al. Challenges to curing primary brain tumours. *Nat Rev Clin Oncol*. 2019;16(8):509-20.
24. Kramer I, Lipp HP. Bevacizumab, a humanized anti-angiogenic monoclonal antibody for the treatment of colorectal cancer. *J Clin Pharm Ther*. 2007;32(1):1-14.
25. Feugier P. A review of rituximab, the first anti-CD20 monoclonal antibody used in the treatment of B non-Hodgkin's lymphomas. *Future Oncol*. 2015;11(9):1327-42.
26. Wells A, Grahovac J, Wheeler S, Ma B, Lauffenburger D. Targeting tumor cell motility as a strategy against invasion and metastasis. *Trends Pharmacol Sci*. 2013;34(5):283-9.

27. Ardito F, Giuliani M, Perrone D, Troiano G, Lo Muzio L. The crucial role of protein phosphorylation in cell signaling and its use as targeted therapy. *Int J Mol Med.* 2017;40(2):271-80.
28. Louis DN, Ohgaki H, Wiestler OD, Cavenee WK, Burger PC, Jouvet A, et al. The 2007 WHO classification of tumours of the central nervous system. *Acta Neuropathol.* 2007;114(2):97-109.
29. Hanif F, Muzaffar K, Perveen K, Malhi SM, Simjee Sh U. Glioblastoma Multiforme: A Review of its Epidemiology and Pathogenesis through Clinical Presentation and Treatment. *Asian Pac J Cancer Prev.* 2017;18(1):3-9.
30. Swartling FJ, Hede SM, Weiss WA. What underlies the diversity of brain tumors? *Cancer Metastasis Rev.* 2013;32(1-2):5-24.
31. Laug D, Glasgow SM, Deneen B. A glial blueprint for gliomagenesis. *Nat Rev Neurosci.* 2018;19(7):393-403.
32. Ostrom QT, Cioffi G, Gittleman H, Patil N, Waite K, Kruchko C, et al. CBTRUS Statistical Report: Primary Brain and Other Central Nervous System Tumors Diagnosed in the United States in 2012-2016. *Neuro Oncol.* 2019;21(Supplement_5):v1-v100.
33. Veerasarn K, Yuthagovit S, Chailorrat A. Prevalence of Brain Tumor in Thailand from 2005 to 2014: Data from the National Health Security Office. *J Med Assoc Thai.* 2016;99 Suppl 3:S62-73.
34. Zoncu R, Efeyan A, Sabatini DM. mTOR: from growth signal integration to cancer, diabetes and ageing. *Nat Rev Mol Cell Biol.* 2011;12(1):21-35.
35. Mossmann D, Park S, Hall MN. mTOR signalling and cellular metabolism are mutual determinants in cancer. *Nat Rev Cancer.* 2018;18(12):744-57.
36. Yoon MS. The Role of Mammalian Target of Rapamycin (mTOR) in Insulin Signaling. *Nutrients.* 2017;9(11).
37. Populo H, Lopes JM, Soares P. The mTOR signalling pathway in human cancer. *Int J Mol Sci.* 2012;13(2):1886-918.
38. Tian T, Li X, Zhang J. mTOR Signaling in Cancer and mTOR Inhibitors in Solid Tumor Targeting Therapy. *Int J Mol Sci.* 2019;20(3).
39. Crespo S, Kind M, Arcaro AJCMT. The role of the PI3K/AKT/mTOR pathway in brain tumor metastasis. 2016;2(3):80-9.

40. Masui K, Cavenee WK, Mischel PS. mTORC2 in the center of cancer metabolic reprogramming. *Trends Endocrinol Metab.* 2014;25(7):364-73.
41. Johannessen TC, Bjerkvig R. Molecular mechanisms of temozolomide resistance in glioblastoma multiforme. *Expert Rev Anticancer Ther.* 2012;12(5):635-42.
42. Meng D, Frank AR, Jewell JL. mTOR signaling in stem and progenitor cells. *Development.* 2018;145(1).
43. Castellanos M, Gubern C, Kadar E. Chapter 7 - mTOR: Exploring a New Potential Therapeutic Target for Stroke. In: Maiese K, editor. *Molecules to Medicine with mTOR.* Boston: Academic Press; 2016. p. 105-22.
44. Xie J, Wang X, Proud CG. mTOR inhibitors in cancer therapy. *F1000Res.* 2016;5.
45. Li X, Wu C, Chen N, Gu H, Yen A, Cao L, et al. PI3K/Akt/mTOR signaling pathway and targeted therapy for glioblastoma. *Oncotarget.* 2016;7(22):33440-50.
46. Lamm N, Rogers S, Cesare AJ, Pib, biology m. The mTOR pathway: Implications for DNA replication. 2019;147:17-25.
47. Del Alcazar CRG, Hardebeck MC, Mukherjee B, Tomimatsu N, Gao X, Yan J, et al. Inhibition of DNA double-strand break repair by the dual PI3K/mTOR inhibitor NVP-BEZ235 as a strategy for radiosensitization of glioblastoma. 2014;20(5):1235-48.
48. Toulany M, Kasten-Pisula U, Brammer I, Wang S, Chen J, Dittmann K, et al. Blockage of epidermal growth factor receptor-phosphatidylinositol 3-kinase-AKT signaling increases radiosensitivity of K-RAS mutated human tumor cells in vitro by affecting DNA repair. 2006;12(13):4119-26.
49. Toulany M, Lee K-J, Fattah KR, Lin Y-F, Fehrenbacher B, Schaller M, et al. Akt promotes post-irradiation survival of human tumor cells through initiation, progression, and termination of DNA-PKcs-dependent DNA double-strand break repair. 2012;10(7):945-57.
50. Götting I, Jendrossek V, Matschke J. A New Twist in Protein Kinase B/Akt Signaling: Role of Altered Cancer Cell Metabolism in Akt-Mediated Therapy Resistance. *International Journal of Molecular Sciences.* 2020;21(22).
51. Shimada K, Filipuzzi I, Stahl M, Helliwell SB, Studer C, Hoepfner D, et al. TORC2 signaling pathway guarantees genome stability in the face of DNA strand breaks. 2013;51(6):829-39.

52. Cam M, Bid HK, Xiao L, Zambetti GP, Houghton PJ, Cam HJJoBC. p53/TAp63 and AKT regulate mammalian target of rapamycin complex 1 (mTORC1) signaling through two independent parallel pathways in the presence of DNA damage. 2014;289(7):4083-94.
53. Bian Y-H, Xu J, Zhao W-Y, Zhang Z-Z, Tu L, Cao H, et al. Targeting mTORC2 component rictor inhibits cell proliferation and promotes apoptosis in gastric cancer. 2017;9(9):4317.
54. Li H, Lin J, Wang X, Yao G, Wang L, Zheng H, et al. Targeting of mTORC2 prevents cell migration and promotes apoptosis in breast cancer. *Breast Cancer Res Treat.* 2012;134(3):1057-66.
55. O'Connor MJMc. Targeting the DNA damage response in cancer. 2015;60(4):547-60.
56. Lawrence J, Nho R. The Role of the Mammalian Target of Rapamycin (mTOR) in Pulmonary Fibrosis. *Int J Mol Sci.* 2018;19(3).
57. Calejman CM, Trefely S, Entwisle S, Luciano A, Jung SM, Hsiao W, et al. mTORC2-AKT signaling to ATP-citrate lyase drives brown adipogenesis and de novo lipogenesis. 2020;11(1):1-16.
58. Lescarbeau RS, Lei L, Bakken KK, Sims PA, Sarkaria JN, Canoll P, et al. Quantitative phosphoproteomics reveals Wee1 kinase as a therapeutic target in a model of proneural glioblastoma. 2016;15(6):1332-43.
59. Bijnsdorp IV, Schelfhorst T, Luinenburg M, Rolfs F, Piersma SR, de Haas RR, et al. Feasibility of phosphoproteomics to uncover oncogenic signalling in secreted extracellular vesicles using glioblastoma-EGFRVIII cells as a model. 2021;232:104076.
60. Recasens A, Humphrey SJ, Ellis M, Hoque M, Abbassi RH, Chen B, et al. Global phosphoproteomics reveals DYRK1A regulates CDK1 activity in glioblastoma cells. 2021;7(1):1-16.
61. Kozuka-Hata H, Nasu-Nishimura Y, Koyama-Nasu R, Ao-Kondo H, Tsumoto K, Akiyama T, et al. Phosphoproteome of human glioblastoma initiating cells reveals novel signaling regulators encoded by the transcriptome. *PLoS One.* 2012;7(8):e43398.
62. Dunn JD, Reid GE, Bruening ML. Techniques for phosphopeptide enrichment prior to analysis by mass spectrometry. *Mass Spectrom Rev.* 2010;29(1):29-54.

63. Zhu B, He Q, Xiang J, Qi F, Cai H, Mao J, et al. Quantitative Phosphoproteomic Analysis Reveals Key Mechanisms of Cellular Proliferation in Liver Cancer Cells. *Sci Rep.* 2017;7(1):10908.
64. Lescarbeau RS, Lei L, Bakken KK, Sims PA, Sarkaria JN, Canoll P, et al. Quantitative Phosphoproteomics Reveals Wee1 Kinase as a Therapeutic Target in a Model of Proneural Glioblastoma. *Mol Cancer Ther.* 2016;15(6):1332-43.
65. Oh WJ, Jacinto EJ. mTOR complex 2 signaling and functions. *Cell.* 2011;10(14):2305-16.
66. Wei W, Shin YS, Xue M, Matsutani T, Masui K, Yang H, et al. Single-cell phosphoproteomics resolves adaptive signaling dynamics and informs targeted combination therapy in glioblastoma. *Nat Commun.* 2016;29(4):563-73.
67. van Linde ME, Labots M, Brahm CG, Hovinga KE, De Witt Hamer PC, Honeywell RJ, et al. Tumor Drug Concentration and Phosphoproteomic Profiles After Two Weeks of Treatment With Sunitinib in Patients with Newly Diagnosed Glioblastoma: Tumor Sunitinib Concentrations and Phosphoproteomics. *Front Oncol.* 2022:OF1-OF8.
68. Lubanska D, Porter LJ. Revisiting CDK inhibitors for treatment of glioblastoma multiforme. *Front Oncol.* 2017;17(2):255-63.
69. Feng L, Huang J, Chen JJ. Development of MERIT40 facilitates BRCA1 localization and DNA damage repair. *Mol Cell.* 2009;23(6):719-28.
70. Brown KK, Montaser-Kouhsari L, Beck AH, Toker AJ. MERIT40 is an Akt substrate that promotes resolution of DNA damage induced by chemotherapy. *Mol Cell.* 2015;11(9):1358-66.
71. Kim H, Chen J, Yu XJ. Ubiquitin-binding protein RAP80 mediates BRCA1-dependent DNA damage response. *Mol Cell.* 2007;316(5828):1202-5.
72. Okamoto K, Ohishi T, Kuroiwa M, Iemura S-i, Natsume T, Seimiya H. MERIT40-dependent recruitment of tankyrase to damaged DNA and its implication for cell sensitivity to DNA-damaging anticancer drugs. *Mol Cell.* 2018;9(88):35844.
73. Krieger KL, Hu W-F, Ripberger T, Woods NT. Functional impacts of the BRCA1-mTORC2 interaction in breast cancer. *Mol Cell.* 2019;20(23):5876.



จุฬาลงกรณ์มหาวิทยาลัย
CHULALONGKORN UNIVERSITY



จุฬาลงกรณ์มหาวิทยาลัย
CHULALONGKORN UNIVERSITY

VITA

NAME Nuttiya Kalpongkul

DATE OF BIRTH 13 October 1989

PLACE OF BIRTH Saraburi

INSTITUTIONS ATTENDED August 2017 - August 2022

HOME ADDRESS 614/487 A space asoke ratchada, G-building, Dindang, Bangkok 10400

PUBLICATION

1. Thasinas Dissayabutra, Nuttiya Kalpongkul, Jakkhaphan Rattanaphan, Chanchai Boonla, Monpichar Srisa-art, Wattanachai Ungchareonwattana, Piyaratana Tosukhowong. Proteinuria and oxidative stress in nephrolithiasis family members. *Nephrology*. 19:28, MAY (2014)
2. Thasinas Dissayabutra, Jakkapan Rattanapan, Nuttiya Kalpongkul, Supawadee Mingmongkol, Wattanachai Ungchareonwattana, Chanchai Boonla, Piyaratana Tosukhowong. Increased protein excretion, including albumin, by children of patients with urolithiasis. *Asian Biomedicine* Vol. 9 No.3 June; 401 – 408. (2015)
3. Nithidol Sakunrangsit, Nuttiya Kalpongkul, Trairak Pisitkun, Wannarasmi Ketchart. Plumbagin Enhances Tamoxifen Sensitivity and Inhibits Tumor Invasion in Endocrine Resistant Breast Cancer through EMT Regulation. *PHYTOTHERAPY RESEARCH* *Phytother. Res.* 30: 1968–1977 (2016)
4. Thasinas Dissayabutra, Nuttiya Kalpongkul, Jakkhaphan Rattanaphan, Chanchai Boonla, Monpichar Srisa-art, Wattanachai Ungchareonwattana, Piyaratana

Tosukhowong. Urinary risks of stone formation in descendants of nephrolithiasis. *Pediatric Nephrology*. (2017)

5. Piyaratana Tosukhowong, Pimsuda Kulpradit, Sakdithep Chaiyanit, Wattanachai Ungjareonwattana, Nuttiya Kalpongkukul, Supoj Ratchanon, Visith Thongboonkerd. Lime powder treatment reduces urinary excretion of total protein and transferrin but increases uromodulin excretion in patients with urolithiasis. *Urolithiasis*. (2017)

6. Thasinas Dissayabuttra, Nuttiya Kalpongkul, Jakkhaphan Rattanaphan, Chanchai Boonla, Monpichar Srisa-art, Wattanachai Ungchareonwattana, Piyaratana Tosukhowong. Urinary stone risk factors in the descendants of patients with kidney stone disease. *Pediatric Nephrology*, 33(7), 1173-1181. (2018)

7. Duangnapa Kovanich, Chonticha Saisawang, Potchaman Sittipaisankul, Suwipa Ramphan, Nuttiya Kalpongkukul, Poorichaya Somparn, Trairak Pisitkun, Duncan Smith. Analysis of the Zika and Japanese encephalitis virus NS5 interactomes. *J Proteome Res* 2;18(8):3203-3218 (2019)

8. Panchaprateep R, Pisitkun T, Kalpongkukul N. Quantitative proteomic analysis of dermal papilla from male androgenetic alopecia comparing before and after treatment with low-level laser therapy. *Lasers Surg Med*. Sep;51(7):600-608. (2019)

9. Jupatanakul N, Pengon J, Selisana SMG, Choksawangkarn W, Jaito N, Saeung A, Bunyong R, Posayapisit N, Thammatinna K, Kalpongkukul N, Aupalee K, Pisitkun T, Kamchonwongpaisan S. *Serratia marcescens* secretes proteases and chitinases with larvicidal activity against *Anopheles dirus*. *Acta Trop*. 2020 Dec;212:105686.

(2020)

10. Choksawangkar W, Sriswasdi S, Kalpongkukul N, Wongkongkathap P, Saethang T, Chanhome L, Laoungbua P, Khow O, Sumontha M, Chaiyabutr N, Sitprijia V, Pisitkun T.

Combined proteomic strategies for in-depth venom analysis of the beaked sea snake (*Hydrophis schistosus*) from Songkhla Lake, Thailand. *J Proteomics*.

15;259:104559. (2022)

AWARD RECEIVED

- The 100th Anniversary Chulalongkorn University for Doctoral Scholarship
- Ratchadapiseksompotch Funds, Faculty of Medicine, Chulalongkorn University, grant number RA62/075
- National Research Council of Thailand (NRCT)
- GRADUATE THESIS GRANT



จุฬาลงกรณ์มหาวิทยาลัย
CHULALONGKORN UNIVERSITY